Progress in Retinal and Eye Research xxx (xxxx) xxx

Contents lists available at ScienceDirect

Progress in Retinal and Eye Research

journal homepage: www.elsevier.com/locate/preteyeres

Quantitative approaches in multimodal fundus imaging: State of the art and future perspectives

Alessandro Arrigo *, Emanuela Aragona, Maurizio Battaglia Parodi, Francesco Bandello

Department of Ophthalmology, IRCCS San Raffaele Scientific Institute, via Olgettina 60, 20132, Milan, Italy

ARTICLE INFO

Keywords:
Multimodal fundus imaging
Optical coherence tomography
Optical coherence tomography angiography
Quantitative parameters
Imaging artifacts

ABSTRACT

When it first appeared, multimodal fundus imaging revolutionized the diagnostic workup and provided extremely useful new insights into the pathogenesis of fundus diseases. The recent addition of quantitative approaches has further expanded the amount of information that can be obtained. In spite of the growing interest in advanced quantitative metrics, the scientific community has not reached a stable consensus on repeatable, standardized quantitative techniques to process and analyze the images. Furthermore, imaging artifacts may considerably affect the processing and interpretation of quantitative data, potentially affecting their reliability. The aim of this survey is to provide a comprehensive summary of the main multimodal imaging techniques, covering their limitations as well as their strengths. We also offer a thorough analysis of current quantitative imaging metrics, looking into their technical features, limitations, and interpretation. In addition, we describe the main imaging artifacts and their potential impact on imaging quality and reliability. The prospect of increasing reliance on artificial intelligence-based analyses suggests there is a need to develop more sophisticated quantitative metrics and to improve imaging technologies, incorporating clear, standardized, post-processing procedures. These measures are becoming urgent if these analyses are to cross the threshold from a research context to real-life clinical practice.

1. Introduction

The need to capture, analyze and interpret retinal findings dates from the dawn of modern ophthalmology. The first picture of the human retina was obtained at the end of 19th century (Jackman and Webster, 1886). From that moment, the realization that retinal imaging could furnish a large amount of information stimulated the rapid evolution of diagnostic techniques.

Multimodal imaging has revolutionized the diagnostic and therapeutic management of fundus diseases. This set of tools provide a detailed morphologic representation of the molecular, pathophysiological, anatomic, and functional changes occurring in retinal and choroidal tissues (Fogel-Levin et al., 2022). The features of multimodal imaging are its rapidity of acquisition, high reproducibility and reliability, slight or no patient distress, and non-invasiveness (Fig. 1). Nowadays, retinal analysis can no longer do without the holistic approach provided by multimodal imaging, referred to probing all relevant information spaces for the same sample. The first analyses of multimodal imaging data were based on the interpretation of retinal specialists. Although this qualitative approach remains the most commonly used in clinical practice, it does have its drawbacks, mainly because it relies on the experience of the operators, whose interpretations of the images are by definition subjective. More recently, the introduction of even more advanced quantitative approaches has considerably reduced the probability of misinterpretation of imaging data, expanded the amount of information that can be obtained by each imaging modality and provided objective methodologies that are easier to reproduce and share. Current non-invasive multimodal imaging techniques include real color or confocal fundus image acquisition, near infrared reflectance (NIR), fundus autofluorescence (FAF), optical coherence tomography (OCT), OCT angiography (OCTA), and adaptive optics (Novais et al., 2016). These are supported by fluorescein angiography (FA) and indocyanine-green angiography (ICGA), which, although older and more invasive than the other multimodal imaging techniques, are still essential retinal diagnostic tools (Novais et al., 2016).

In this survey we provide background information on each non-invasive imaging modality and discuss in detail the current state of quantitative-based approaches and future prospects.

* Corresponding author. Department of Ophthalmology, IRCCS San Raffaele Scientific Institute, via Olgettina 60, Milan, 20132, Italy.
E-mail address: alessandro.arrigo@hotmail.com (A. Arrigo).

https://doi.org/10.1016/j.preteyeres.2022.101111
Received 30 March 2022; Received in revised form 16 July 2022; Accepted 19 July 2022

List of abbreviations

AFI	active flow intensity
AI	artificial intelligence
AMD	age-related macular degeneration
BAF	blue-light fundus autofluorescence
CC	choriocapillaris
CCP	choriocapillaris porosity
cORA	complete outer retinal atrophy
cRORA	complete RPE and outer retinal atrophy
CSI	choroidal stromal index
cSLO	confocal scanning light ophthalmoscope
CT	choroidal thickness
CVI	choroidal vascularity index
DCP	deep capillary plexus
DDAF	definitely decreased autofluorescence
ELM	external limiting membrane
ETDRS	Early Treatment Diabetic Retinopathy Study
EZ	ellipsoid zone
FA	fluorescein angiography
FAF	fundus autofluorescence
FAZ	foveal avascular zone
FD	fractal dimension
FLIM	fluorescence lifetime imaging microscopy
FLIO	fluorescence lifetime imaging ophthalmoscopy
GA	geographic atrophy
GAF	green-light autofluorescence
HF	hyperreflective foci
HLT	Haller layer thickness
ICGA	indocyanine-green angiography
ILM	internal limiting membrane
iORA	incomplete outer retinal atrophy
iRORA	incomplete RPE and outer retinal atrophy
MNV	macular neovascularization
NIR	near infrared reflectance
OCT	optical coherence tomography
OCTA	optical coherence tomography angiography
OPI	optically preserved islet
qAF	quantitative autofluorescence
QDAF	questionable decreased autofluorescence
RPE	retinal pigment epithelium
SCP	superficial capillary plexus
SLT	Sattler layer thickness
TFI	total flow intensity
UWF	ultrawide field
VD	vessel density
VDI	vessel diameter index
Vdisp:	vessel dispersion
VFI	volume-related flow intensity
VLD	vessel length density
VR	vessel rarefaction
VT	vessel tortuosity

2. Background of multimodal imaging techniques

This section provides a brief description of the technical aspects of the main multimodal imaging techniques employed in clinical practice and in research settings.

2.1. Real color and pseudocolor fundus images

Ordinary cameras were used to take the first non-invasive in-vivo pictures in the diagnostic workup of the human retina. The first commercially available fundus camera was produced by Carl Zeiss in 1926 and consisted of a diagnostic instrument based on flood flash illumination. Unfortunately, it was handicapped by a very limited field of view. The introduction of electronic flashlighting in 1953 (Hansell and Beeson, 1953) was an important breakthrough, making it possible to take color pictures with a larger field of view. Later, the development of the digital systems found in modern fundus cameras enabled images to be checked and modified in real time, improving the accuracy of color fundus images. This imaging modality is still used in clinical settings, and it enjoys the undoubted advantage of being an inexpensive, time-saving way of obtaining retinal pictures. However, this technique is hamstrung by several weaknesses, including poor resolution, operator-dependance, and the need for good pupil dilation. In addition, color fundus cameras have remarkably narrow fields of view (30° or 55°), meaning that only structures at the posterior pole can be properly detected. On the other hand, a variety of methods can be used to merge several fundus images, thus effectively expanding the field of view. The standard way is to use Early Treatment Diabetic Retinopathy Study (ETDRS) 7-field images, which reach the mid-retinal periphery (ETDRS research Early Treatment Diabetic Retinopathy Study Research Group, 1991). At the same time, this diagnostic modality is poorly suited to quantitative analyses. The current trend in research is to try to adopt artificial intelligence (AI)-based algorithms to identify retinal alterations in screening campaigns on large populations (Gulshan et al., 2016; Abràmoff et al., 2016, 2018; Gargeya and Leng, 2017; Quellec et al., 2017; Dong et al., 2021).

The traditional fundus camera evolved into confocal scanning light ophthalmoscope (cSLO) laser-based technology, which was introduced at least twenty years ago (Webb and Hughes, 1981; Plesch et al., 1987). This imaging approach uses a range of different wavelengths, thus detecting information coming from different retinal sources. The core components include a laser diode, a scanning unit, optic units, a beam splitter, a pinhole, and a photodiode detector (Webb and Hughes, 1981; Plesch et al., 1987). The level of detail provided by confocally-based technology is considerably higher than that found in previous approaches. For example, confocal SLO red-free imaging is able to detect and quantify the avascular retina region, both in healthy and pathological conditions, with high a level of accuracy and without having to employ dye (Shin et al., 2012).

In color fundus imaging, the picture is the result of the combination of different light wavelengths. Two of the most commonly used confocal devices are the Heidelberg Spectralis (Heidelberg Eng., Heidelberg, Germany) and the NIDEK Mirante (Nidek Co. Ltd., Gamagori, Japan), where the multicolor image is the result of the combination of infrared reflectance (815 nm excitation), green reflectance (518 nm excitation), and blue reflectance (486 nm excitation) images (Li et al., 2018). The software recognizes and interprets the signal coming from each single image and converts it into pseudocolors. The advantage of the multicolor confocal system is that it provides more information from different signals and enables more post-processing to be performed than a traditional fundus camera. For instance, in a recent study Arrigo and colleagues categorized different subtypes of microaneurysm based on reflectance features in a cohort of diabetic retinopathy patients (Arrigo et al., 2021a). The green- and red-reflectance features of microaneurysms were particularly useful in highlighting distinctive characteristics: red microaneurysms in the multicolor image corresponded to lesions displaying a thin hyperreflective margin and unevenly reflective core on structural OCT and full filling on fluorescein angiography, while green microaneurysms in the multicolor image were found to be mainly hyperreflective on structural OCT and poorly filled on fluorescein angiography. In accordance with histological classifications of retinal microaneurysms, Arrigo et al. interpreted the red type as perfused

vascular alterations with intact endothelium, and the green type as lesions sclerosed to a greater or lesser extent (Stitt et al., 1995; Arrigo et al., 2021a). Mixed red-green microaneurysms in the multicolor image were also described, corresponding to lesions displaying a thick hyperreflective margin and a hyporeflective core on structural OCT, and a variable filling on fluorescein angiography (Arrigo et al., 2021a); Arrigo and colleagues interpreted these types of lesions as microaneurysms in the intermediate degenerative stage, as in the histological description (Stitt et al., 1995; Arrigo et al., 2021a). Conversely, multicolor confocal imaging is more affected by artifacts and media opacities than traditional fundus cameras (Tan et al., 2016), although recent post-processing correction tools are trying to reduce the gap between the two techniques. Where multicolor confocal imaging demonstrated a clear superiority compared with traditional fundus cameras was in detecting vitreoretinal interface disorders and in the epiretinal membrane (Kilic Muftuoglu et al., 2018; Song et al., 2019). The green reflex characterizing the epiretinal membrane on multicolor imaging made it easily detectable and more clearly outlined than traditional in color fundus imaging. These are just examples of the potential application of multicolor confocal imaging analysis in fundus diseases. Although multicolor confocal imaging is a relatively recent technique, we believe it is still underused both in clinical and research settings. Further studies might provide new insights into the possible role of multicolor confocal imaging in retinal diagnostics, encouraging its more widespread use.

Ultrawide field (UWF) technology is a relatively recent addition to fundus imaging. This technology achieves a field of view >200° with a

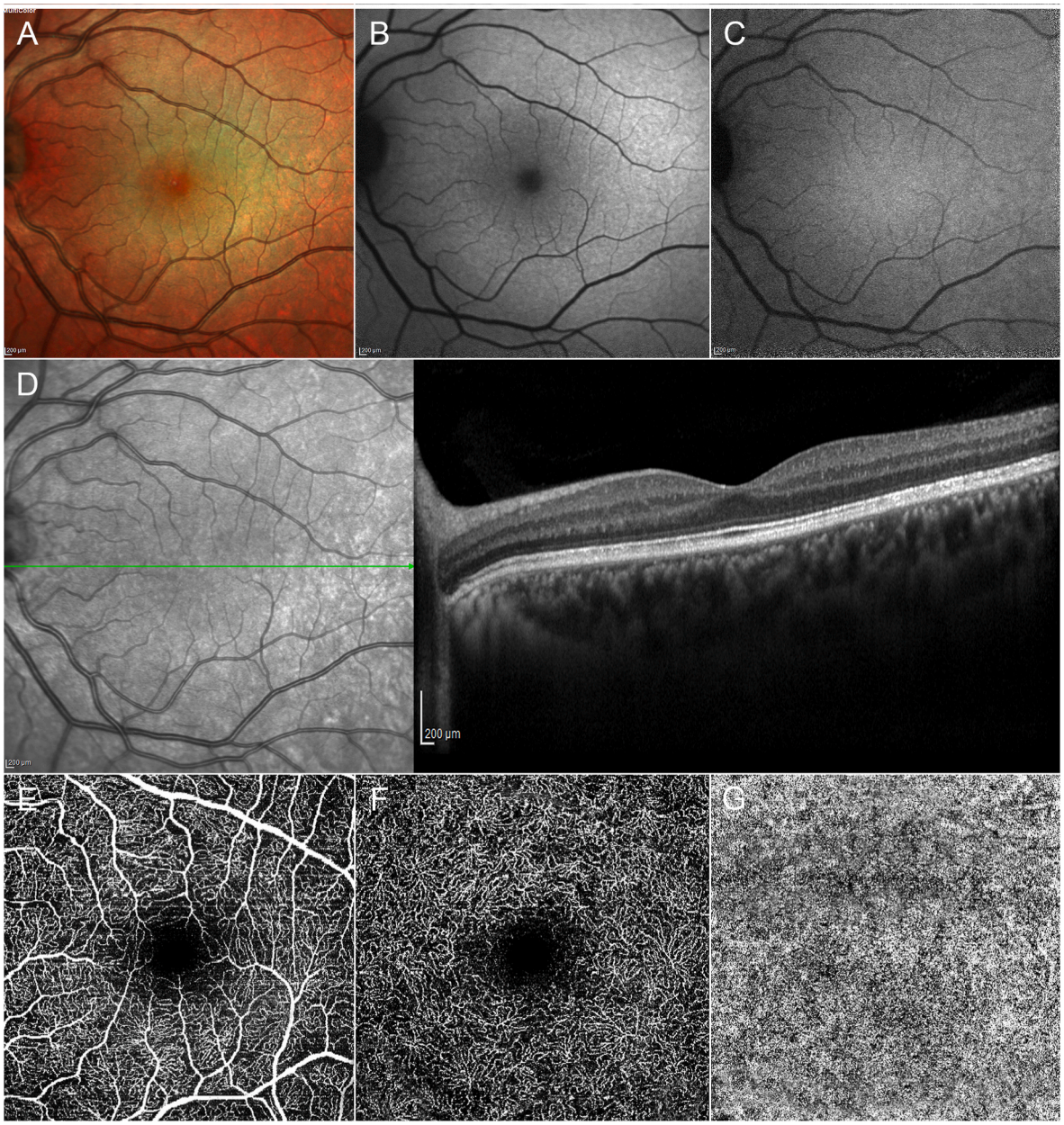

Fig. 1. Multimodal imaging findings in a healthy eye. The confocal multicolor image (A) shows a homogeneous distribution of infrared, green and blue light wavelengths. The BAF image (B) features central hypoautofluorescence secondary to a higher concentration of melanin than lipofuscin, and isofluorescent signal over the entire posterior pole. The NIR image (C) is characterized by central hyperautofluorescence induced by a high concentration of melanin and a diffuse hypoautofluorescent signal in the rest of the posterior pole. Structural OCT (D) provides a histology-like representation of retinal and choroidal layers with very high definition and accuracy. OCTA reconstructions of healthy superficial capillary plexus (E), deep capillary plexus (F), and choriocapillaris (G), with no evident signs of imaging artifacts, are also shown.

single picture, thus exposing to view the entire retina up to the extreme periphery (Oishi et al., 2014). UWF imaging does not require pupil dilation and is highly compatible with conventional techniques, such as ETDRS 7-field images, in grading diabetic retinopathy stages (Silva et al., 2012; Kernt et al., 2012; Rasmussen et al., 2015; Aiello et al., 2019). In essence, it is another confocally-based technology, and as such is subject to pseudocolors and similar artifacts. AI algorithms have also been employed in UWF fundus assessment in screening studies, with good results (Wang et al., 2018; Nagasawa et al., 2019). Other clinically relevant contributions of UWF technology are described in the section on FAF imaging. There is no question that UWF imaging has been a valuable addition to retinal diagnostics. However, the high costs associated with this technique curtail its employment in clinical practice. Combining the benefits of traditional fundus cameras and confocally-based technology will undoubtedly constitute a step forward. From this point of view, the Eidon (CenterVue, Padua, Italy) and Clarus 500 (Carl Zeiss Meditec AG) True-Color wide-field confocal scanners (Olvera-Barrios et al., 2020, 2021; A. Chen et al., 2021), are promising new developments.

1. Infrared and Near-infrared reflectance

Reflectance cameras employ SLO technology with different wavelength excitation filters. Infrared reflectance works with 820 nm excitation, whereas NIR reflectance has 787 nm excitation. Infrared light is greatly absorbed by hemoglobin, whether oxygenated or not, and water (Elsner et al., 1996). These two non-invasive imaging modalities, adopted both in traditional fundus cameras and cSLO devices, are widely used in clinical and research settings. cSLO-based technology is a highly effective way of obtaining good quality and reliable images, especially in view of the very poor resolution and significant effect of media opacities on flash fundus cameras. Thanks to its high penetration, infrared reflectance can pinpoint subretinal structures and provide greater detail than other imaging modalities (Elsner et al., 1996). Infrared reflectance is more successful than color fundus imaging in picking out several deep retinal alterations, including drusen, retinal pigment epithelium (RPE) detachment, and neovascular membranes (Ly et al., 2016a,b), as well as providing a very accurate, non-invasive delineation of large retinal and choroidal vessels. Furthermore, infrared reflectance has been found to be very useful in the field of vitreoretinal alterations, as it is very good at detecting alterations such as retinoschisis, retinal detachment and epiretinal membrane (Banda et al., 2019).

NIR imaging has become increasingly popular in recent years, due to its ability to highlight the distribution of melanin and its alterations (Elsner et al., 1996; Keilhauer and Delori, 2006). Indeed, one of the features of melanin is its considerable capacity to reflect this wavelength (Elsner et al., 1996; Keilhauer and Delori, 2006). NIR imaging provides a very detailed profile of the status of the macula, where melanin is highly concentrated, thus making it possible to carry out a thorough assessment of macular alterations secondary to subretinal debris, atrophy or neovascular complications (Theelen et al., 2009; Grieve et al., 2018; Abdelfattah et al., 2020; Vaz-Pereira et al., 2020). The high concentration of melanin in the foveal and perifoveal regions leads the NIR image to exhibit a central hyperreflectivity, surrounded by overall hyporeflectivity in normal conditions. NIR imaging has proved useful in detecting foveal sparing in retinal diseases involving central degeneration and macular atrophy (Lindner et al., 2017; Bax et al., 2019). In addition, NIR imaging is extremely useful in detecting choroidal nevi, due to the high melanin content in this kind of lesion (Fig. 2). Battaglia Parodi and colleagues previously highlighted the usefulness of NIR imaging in early stages of age-related macular degeneration (AMD) (Battaglia Parodi et al., 2020), as well as in benign foveal depigmentation

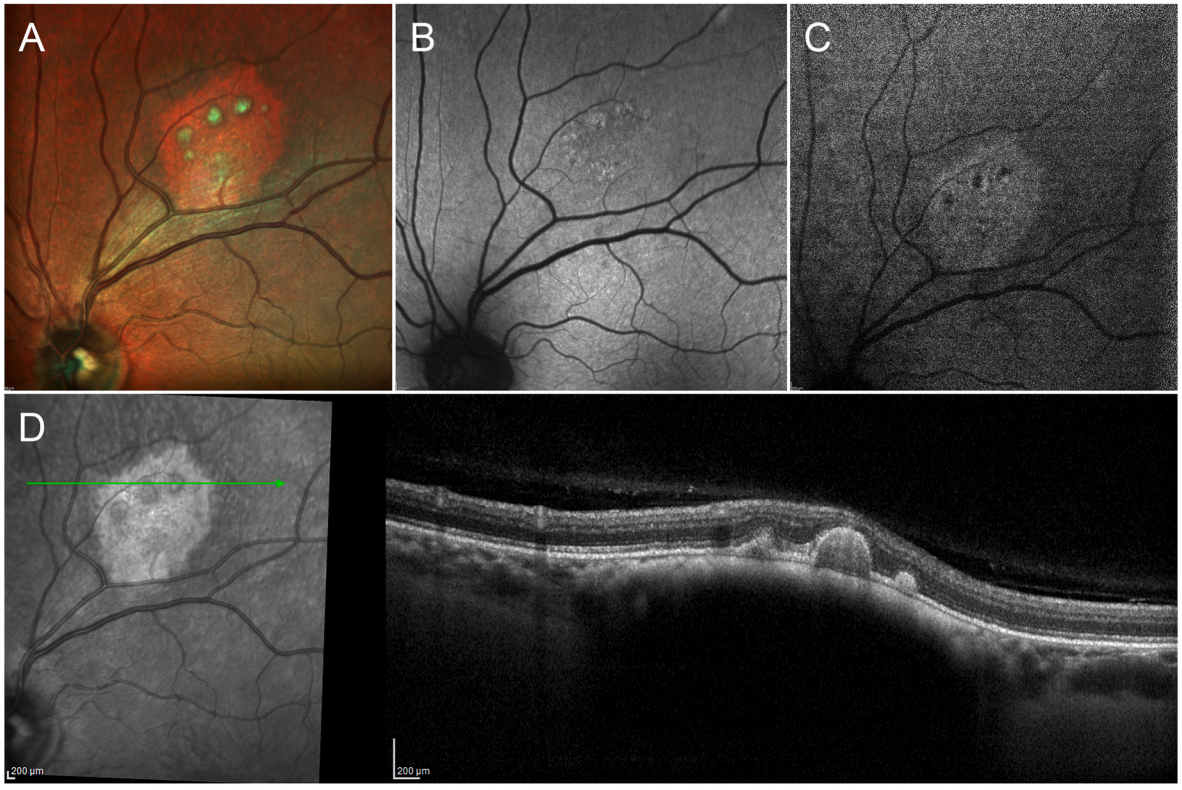

Fig. 2. Multimodal imaging findings in a choroidal nevus. The multicolor image (A) shows a round lesion localized near the superior vascular arcades. The BAF image (B) detects some alterations of the lipofuscin component, with hyperautofluorescent spots localized within the borders of the lesion. Conversely, the NIR image is extremely precise in detecting the increased melanin component characterizing the nevus (C). Interestingly, the hyperautofluorescent regions on BAF correspond to areas of decreased reflectance on NIR. Structural OCT (D) shows a hyporeflective choroidal lesion altering the retinal profile; the altered regions on BAF and NIR correspond to drusen, a relatively common finding in choroidal nevi.

(Parodi et al., 2020a), since it was able to detect more alterations than other imaging modalities. In addition, the modality demonstrated that central, round, NIR hyporeflectivity is the detectable alteration that characterizes the subclinical stage of Best Vitelliform Macular Disease (Parodi et al., 2014, 2020b). NIR imaging has also proved useful in detecting early retinal alterations secondary to pentosan macular toxicity (Wang et al., 2021), neurofibromatosis 1 (Viola et al., 2012), and polypoidal choroidal vasculopathy (Zhang et al., 2015; Simhaee et al., 2020).

Like all the other imaging modalities, infrared reflectance and NIR imaging are potentially affected by artifacts. Furthermore, both continue to be hampered by limited fields of view (up to 100° in the Heidelberg wide-field lens and infrared NIDEK Mirante with wide-field adapter), since these are not available in ultrawide field devices (Banda et al., 2019).

Retromode imaging is a relatively recent development in the field, made possible by the introduction of confocal technology. This approach is based on retro-illumination, in which abnormal fundus features throw a shadow, thus enhancing their contrast and outline (Lee et al., 2014). Retromode imaging has been employed to analyze in detail several disease-related features, including macular edema, retinoschisis, and drusen (Lee et al., 2014).

2. Fundus autofluorescence

The introduction of fundus autofluorescence was a key advance in retinal diagnostics. This imaging modality exploits the capacity of certain retinal structures to act as fluorophores, that is chemical compounds that re-emit light upon light excitation. Like color fundus and infrared imaging, autofluorescence can be obtained by flashlight fundus cameras or by cSLO technology, the latter providing higher quality images. The retina's autofluorescence is used by a detector to generate images reflecting the biochemical integrity of retinal structures. Each fluorophore has its own excitatory wavelength and emitting wavelength. The best known retinal fluorophore is lipofuscin, which has an excitation of 440–470 nm and 510–700 nm emission (Eldred and Katz, 1988; Croce and Bottiroli, 2014; Yung et al., 2016). These optical properties mean lipofuscin is easily detected by blue-light fundus autofluorescence (BAF), which has an excitation of 486 nm. BAF is the most widely used fundus autofluorescence imaging modality in clinical practice. Since lipofuscin characterizes the retinal pigment epithelium, BAF can provide detailed information regarding its structural integrity. In healthy conditions, a BAF image typically displays a central hypoautofluorescence surrounded by overall isoauto fluorescence. The central BAF hypoautofluorescence, perfectly matched with the area of increased NIR reflectance, can be explained if we consider that the foveal and perifoveal regions contain greater concentrations of melanin than lipofuscin. The applications of BAF imaging cover all retinal and choroidal diseases, including AMD, diabetic retinopathy, central serous

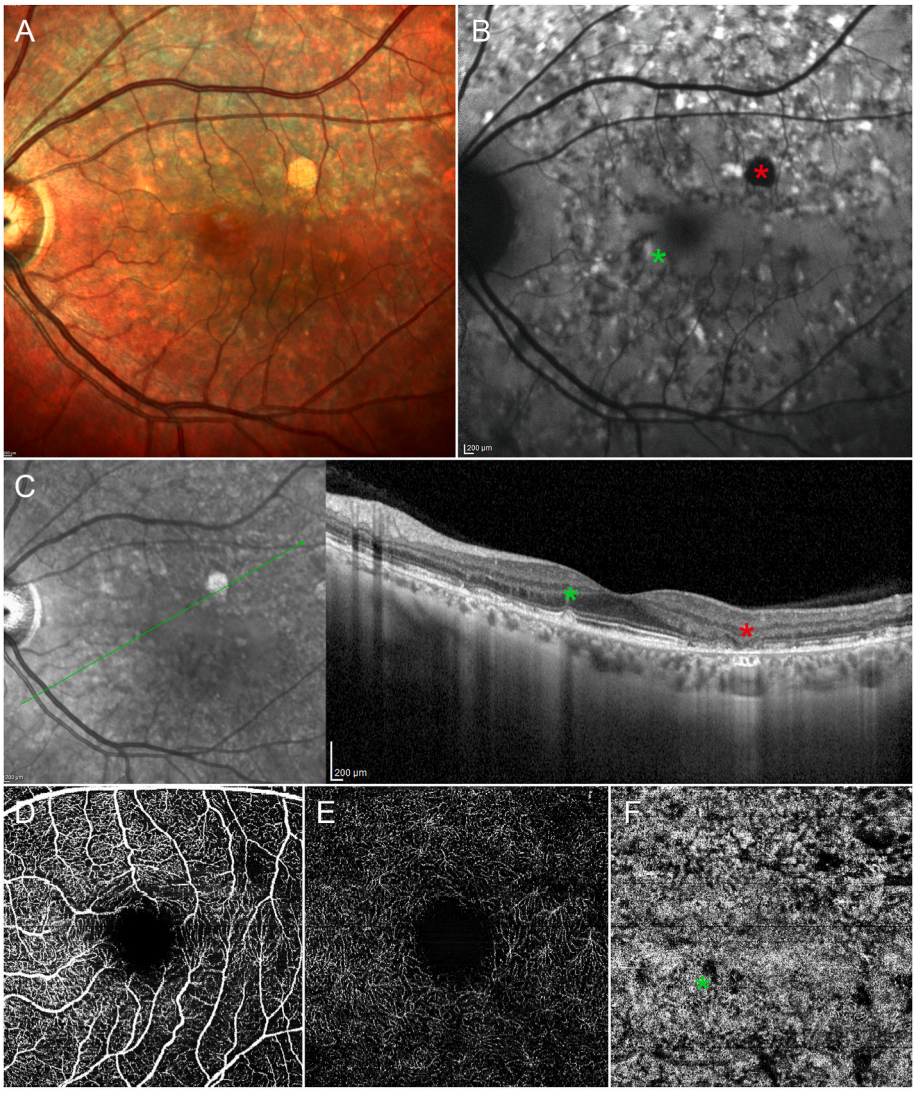

Fig. 3. Multimodal imaging findings in a case of Stargardt cone-rod dystrophy. The confocal multicolor image (A) shows diffuse alterations of posterior pole pigmentation. These are better highlighted by the BAF image (B), where hyperautofluorescent flecks (green asterisk) are clearly visible, together with sparse hypoautofluorescent alterations, corresponding to reabsorbed flecks or complete outer retinal atrophy (red asterisk). Structural OCT (C) shows the outer retinal alterations typical of this early stage of Stargardt disease very effectively. One can see an example of a masking effect with choroidal shadowing next to the bigger subretinal debris (green asterisk), and an evident window effect with choroidal hypertransmission by the complete outer retinal atrophy (red asterisk). OCTA shows a partially spared superficial capillary plexus (D), an impaired deep capillary plexus (E) with FAZ enlargement and regions of reduced perfusion signal. Moreover, the choriocapillaris (F) is considerably impaired, with extensive regions of flow voids. It is worth noting the presence of a masking artifact in the region of the big subretinal debris (green asterisk).

chorioretinopathy and retinal dystrophies (Batıoğlu et al., 2015; L. Chen et al., 2021; Kwan and Fawzi, 2019; Han et al., 2020; Pichi et al., 2018). The importance of BAF imaging in clinical practice is highlighted by the fact that the BAF modality plays a central role in the evaluation of retinal atrophy by detecting partial atrophy, i.e. questionable decreased autofluorescence (QDAF), and complete atrophy, known as definitely decreased autofluorescence (DDAF) (Sadda et al., 2018) (Figs. 3 and 4). In addition, BAF imaging is a valuable tool for monitoring the progression of geographic atrophy (Fig. 5). The combined use of BAF and NIR imaging modalities is also able to reveal changes associated with plaquenil macular toxicity earlier than other imaging techniques (Fig. 6).

BAF imaging has benefitted from the introduction of the ultra-wide field (UWF). The combined use of pseudocolor fundus and BAF imaging modalities expanded the range of alterations occurring in fundus diseases. One of the most impressive examples of this advance was the case of Stargardt disease. Despite the condition being considered just a central degenerative process, UWF-BAF was able to distinguish several distinct patterns, with greater and greater involvement of the mid and extreme retinal periphery (Klufas et al., 2018). In a recent study, Arrigo and colleagues highlighted the correlation between the extension of peripheral alterations and central impairment in Stargardt disease, underlining the usefulness of UWF-based assessment in clinical practice (Arrigo et al., 2020a). Similarly, UWF-BAF imaging has provided new insights regarding peripheral retinal involvement in many other retinal and choroidal diseases, including age-related macular degeneration, diabetic retinopathy, and retinal dystrophies (Guduru et al., 2017; Forshaw et al., 2019; Ashraf et al., 2020b; Hariri et al., 2018).

In central serous chorioretinopathy, UWF imaging has detected regions of hyperpermeability extending outside the retinal vascular arcades, and provided better detailing of the descending tracts typical of the chronic form of the disease (Pang et al., 2014; Lee et al., 2016b). Furthermore, the UWF approach has proved useful in evaluating retinal morphology and posterior staphyloma in high myopia, and in monitoring the progression of the disease (Oh et al., 2022).

Green-light autofluorescence (GAF) is a more recent autofluorescence modality characterized by 518 nm excitation. GAF targets central alterations in particular, since it is less absorbed by lutein, zeaxanthin, and meso-zeaxanthin than BAF (Delori et al., 2001; Wolf--Schnurrbusch et al., 2011). This means that GAF should perform better in detecting small central alterations than BAF. There is high agreement between GAF and BAF, although GAF might be superior in cases where the level of light excitation is lower (Pfau et al., 2017; Müller et al., 2018). However, owing to GAF's relative novelty and its scarcity in commercial devices, its role in clinical practice remains to be defined and more studies are warranted to draw firm conclusions about the features distinguishing BAF and GAF.

3. Optical coherence tomography

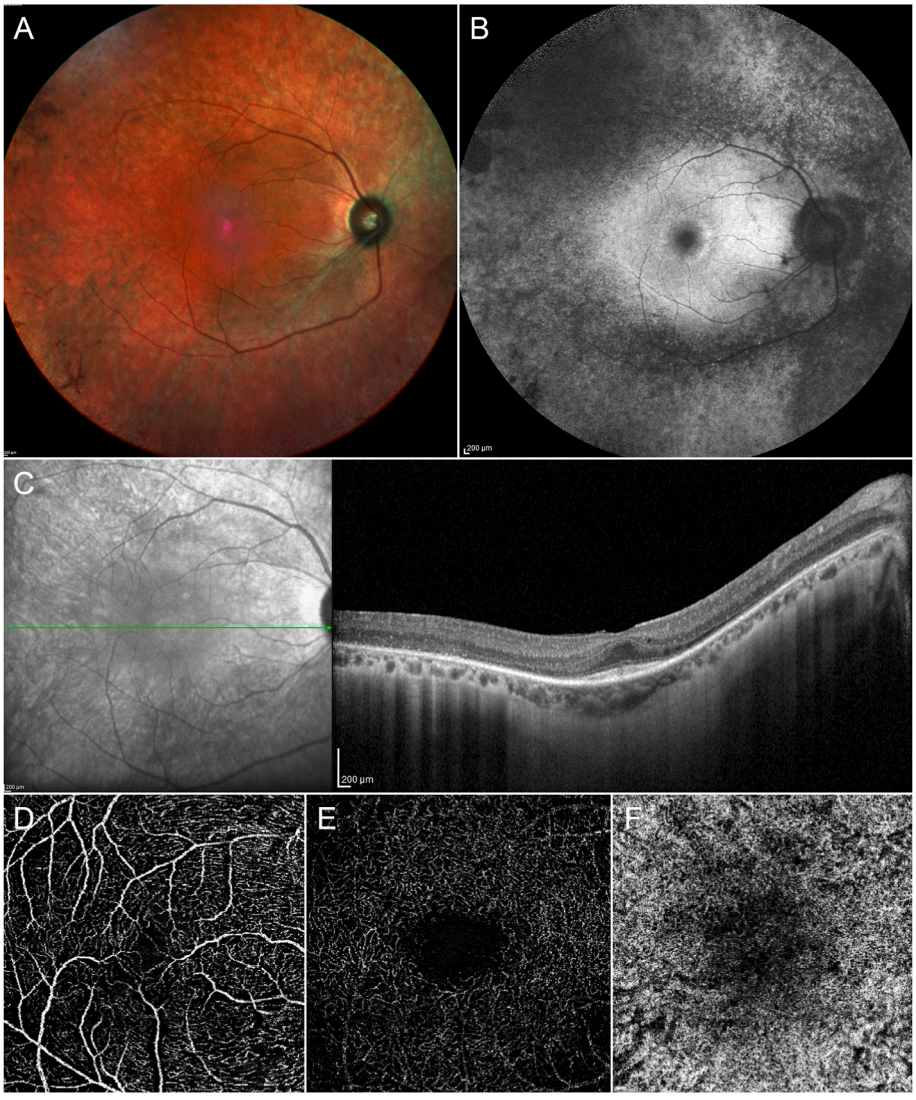

Fig. 4. Multimodal imaging findings in a case of retinitis pigmentosa rod-cone dystrophy. The confocal multicolor image (A) shows diffuse pigmentation changes extending over the vascular arcades, with peripheral pigmented bone spiculae. The BAF image (B) considerably improved the amount of information regarding the peripheral involvement, also pinpointing the typical hyper-autofluorescent perifoveal Hobson Older ring, interpreted as a sign of RPE/photoreceptors complex hyperreactivity. The structural OCT (C) shows the complete disappearance of the outer retinal bands, with central sparing. Increased reflectivity of the choroid can be seen in the peripheral regions – a sign of RPE disruption. Moreover, vitreomacular interface alterations, with early epiretinal membrane and partial loss of the foveal depression, are also visible. OCTA shows a partially spared superficial capillary plexus (D), with evident reduction of the FAZ area, which can be interpreted as the consequence of the tractional force leading to the partial loss of the foveal depression. The deep capillary plexus (E) is impaired, with FAZ enlargement and peripheral projections artifacts. The choriocapillaris (F) is also considerably impaired.

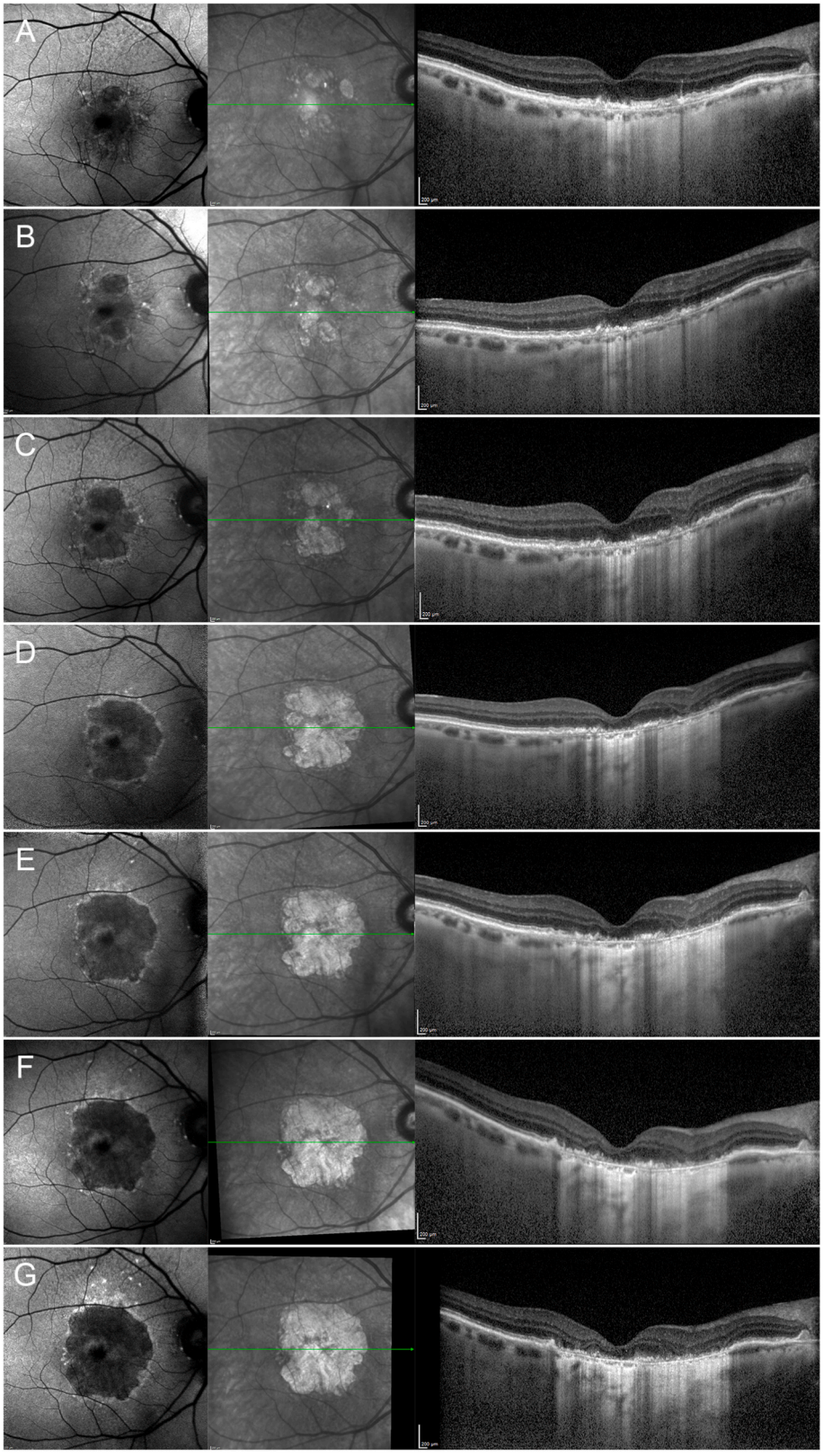

Fig. 5. The role of BAF, IR, and structural OCT on the diagnostic workup of geographic atrophy progression. This is a case of geographic atrophy followed for six years. The baseline image (A) shows a partial macular sparing with choroidal thinning, increased choroidal transmission, pseudodrusen, and attenuation of external retinal bands, together with extramacular atrophic spots. BAF, IR, and structural OCT record the progression of the outer retinal alterations effectively, showing the progressive enlargement of the atrophic area, the involvement of the macula, further choroidal thinning and increased choroidal hypertransmission, on 1-year (B), 2-year (C), 3-year (D), 4-year (E), and 5-year (F) follow-ups. At the 6-year follow-up (G), complete outer retinal atrophy involves almost the entire posterior pole.

OCT technology has revolutionized the diagnostics of fundus diseases (Costa et al., 2006; Drexler and Fujimoto, 2008). Introduced in 1991 (Huang et al., 1991), this non-invasive approach based on the Michelson interferometry principle (Smith and Dobson, 1989) evolved extremely fast and has now reached an almost histological level of accuracy. Various other OCT technologies have been developed, including time domain OCT (Huang et al., 1991), spectral domain OCT (Wojtkowski et al., 2004; Potsaid et al., 2008), and swept source OCT (Marschall et al., 2010; Klein et al., 2011; Laíns et al., 2021). However, whereas Fourier domain OCT performed radically better than time

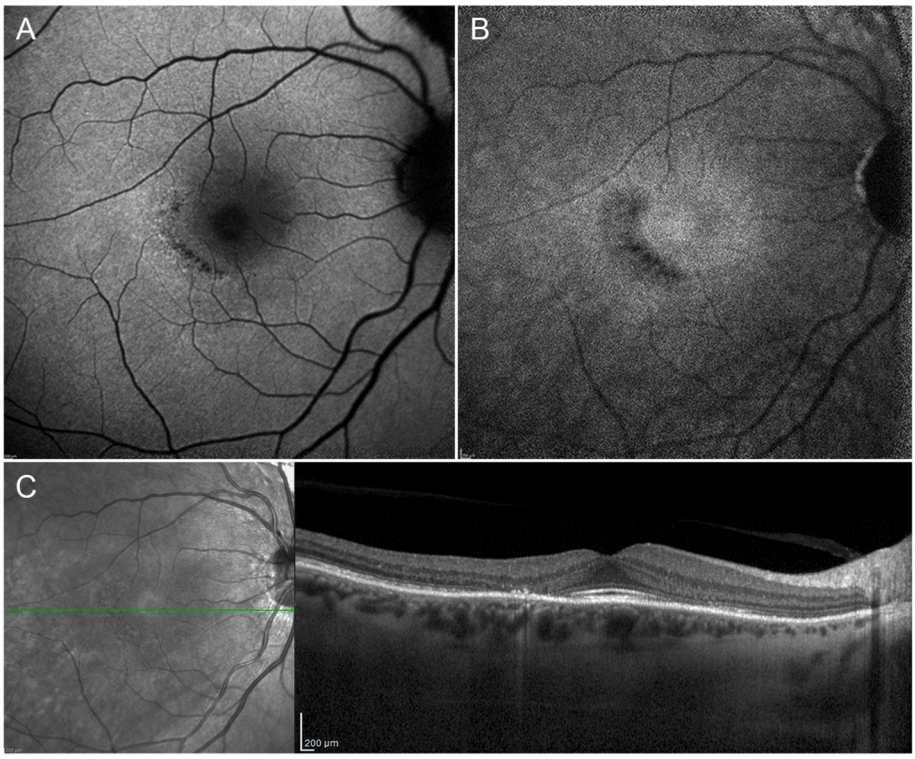

Fig. 6. The role of BAF and NIR imaging in plaquenil retinal toxicity. The plaquenil retinal toxicity is much more evident, with a well-defined region of hypo-autofluorescence in the BAF image (D), and appearing much larger in the NIR image (E). Structural OCT (F) shows evident alterations of the outer retinal bands. Interestingly, both cases highlight the role of NIR imaging in providing much more information than the other imaging modalities.

domain, replacing it, the differences in quality between spectral domain and swept source OCT devices was not so marked, thus rendering both forms of OCT technologies of choice for ocular diagnostics. The most evident limitation of spectral domain technology compared with swept source is the former's inferior choroidal penetration and therefore higher signal attenuation in the imaging of the deeper layers. However, this limitation has been partially reduced by the introduction of "enhanced depth imaging" technology, which is basically a way of obtaining an inverted acquisition of the eye to highlight choroidal structures (Spaide et al., 2008; Margolis and Spaide, 2009). The main technical differences between the above OCT systems are set out in Table 1.

OCT data can be analyzed considering the single transversal OCT image (A-scan), consecutive cross-sectional, transversal A-scans (B-scan), or the axial projection of the B-scan image (enface). The conventional way of analyzing the images is based on the interpretation of the hyperreflective or hyporeflective properties of ocular structures. The main sources of hyperreflective and hyporeflective signals are shown in Table 2.

4. Optical coherence tomography angiography

Table 1
Technical specifications of different optical coherence tomography technologies.

OCT technology	Acquisition Wavelength (nm)	Scanning Speed (A-scans/second)	Axial Resolution (µm)	Transverse Resolution (µm)
Time Domain	800	400	10	20
Spectral Domain	840	27.000–70.000	5–8	14–20
Swept Source	1050	100.000–400.000	5	20

OCTA is a recently developed form of OCT-based technology. Introduced in 2013 (Kim et al., 2013; Choi et al., 2013), it is designed to perform a noninvasive assessment of intraretinal vascular network integrity. OCTA is based on the acquisition of a large number of A-scans (up to 100,000 A-scans/second) to assess the reflectivity changes in small particles by calculating a decorrelation signal. It is believed that the motion of erythrocytes can be captured by very dense, high-speed acquisitions, and in this way the path followed by red blood cells can be reconstructed, reproducing the intraretinal vascular network (Kim et al., 2013; Choi et al., 2013; Schwartz et al., 2014; Kashani et al., 2017). OCTA technology is excellently described in greater technical detail by Tan et al. (2020). OCTA devices are based either on spectral domain or swept source technologies. The resulting signal can be analyzed either by plotting on a structural OCT B-scan or by the enface visualization of the vascular network. OCTA technology has undoubted advantages, especially in terms of offering a detailed visualization of the intraretinal capillaries and of the choriocapillaris. Indeed, the separate analysis of superficial capillary plexus, intermediate capillary plexus, deep capillary plexus, radial peripapillary capillaries and choriocapillaris, which is not possible with conventional fluorescein angiography and indocyanine-green angiography, can be done with OCTA, achieving exceptional detail (Spaide et al., 2018). Moreover, as shown in the chapter dedicated to quantitative analyses, OCTA information can be improved considerably by applying post-processing imaging techniques. The main disadvantages of this technology are the limited field of view, which means it is confined to the posterior pole region, the high number of potential artifacts, and the lack of functional information such as fluorescein leakage (Spaide et al., 2018). The literature is full of well described examples of the utility of OCTA in clinical practice. However, it is essential to keep in mind certain fundamental technical aspects when working with OCTA data. First of all, OCTA cannot by itself provide the full picture of a retina's vascular status. The detection of motion and the subsequent reconstruction of retinal capillaries depends on the blood flow. Indeed, OCTA can capture the signals emitted in a given

Table 2
Main source of hyperreflective and hyporeflective signals detected by structural optical coherence tomography retinal examination.

Hyperreflective		Hyporeflective	
Physiologic Signal	Disease related change	Physiologic Signal	Disease related change
Choroidal stroma	Acute ischemia	Ganglion cell layer	Intraretinal fluid
External limiting membrane	Calcification	Inner nuclear layer	Subretinal fluid
Inner plexiform layer	Cotton wool spot	Outer nuclear layer	Pigment epithelium detachment (serous)
Internal limiting membrane	Drusen	Choroidal vessels	Retinoschisis
Outer plexiform layer	Epiretinal membrane	Vitreous body	
Outer retinal bands	Fibrosis		
Posterior hyaloid membrane	Haemorrhage		
Retinal nerve fiber layer	Hard exudates		
Retinal pigment epithelium	Hyperrefleflective foci		
	Macular neovascularization		
	Microaneurysm		
	Outer retinal tubulation		
	Pigment epithelium detachment (drusenoid, vascolarized, mixed)		
	Pseudodrusen		
	Subretinal hyperreflective material		
	Vitritis		

range of flows, which is a function of the acquisition speed. Moreover, OCTA-based detection is also influenced by the number of particles passing through a given volume. For these reasons, OCTA can only provide part of all the vascular information concerning the retina. This is why OCTA and dye-based angiography are quite substantially mismatched. It is also harder to distinguish arteries and veins with OCTA than with dye-based angiography. Some authors have tried to make this differentiation easier by viewing the veins as originating from vortices within the deep capillary plexus (Xu et al., 2019). However, this matter remains a challenge for OCTA technology.

The main advantages and disadvantages of each angiographic modality are shown in Table 3.

To summarize briefly, OCTA can provide an unprecedented level of morphological detail in vascular structures, although it is less able to provide the same standard of functional information regarding the status of the blood retinal barriers and is more prone to artifacts and blood flow speed than dye-based angiographies. A classic example showing up the divergence between OCTA and fluorescein angiography regards the detection of retinal microaneurysms. Since the blood flow within microaneurysms is highly heterogeneous and includes both laminar and turbulent flows, OCTA-based detection of retinal microaneurysms may be highly variable, and to date cannot be compared with fluorescein angiography (Parrulli et al., 2021). In a previous study, Arrigo et al. tried to assess the factors associated with the different sizes of the neovascular lesions detected by OCTA and FA/ICGA angiography. As measured with FA/ICGA, the area of macular neovascularization is larger than the area measured with OCTA; this is especially evident in type 1 lesions (Costanzo et al., 2016; Haas et al., 2021). Arrigo et al. found that the size

Table 3
The main advantages and disadvantages of retinal angiographic diagnostic modalities.

	PROs	CONs
Fluorescein angiography	Faster acquisition requires less patient collaboration	Scant information about deeper capillaries and choriocapillaris
	Large field of view up to 200° ultrawide field	Scant information regarding neovascular network morphology
	High sensitivity in detecting retinal filling delays	Leakage-related masking effects
	High quality reconstructions of retinal microaneurysms	"Choroidal flush" limiting choroidal network visualization
	Functional information (leakage/staining)	Lower opportunities to use post-processing quantitative approaches
	Full size detection of neovascular membranes	Lower images resolution
	Clinically useful information also in extremely altered retinal morphology	Invasivity
	High sensitivity in detecting vessels alterations (e.g. vasculitis, intraretinal microvascular abnormalities)	
Indocyanine-green angiography	Faster acquisition requires less patient collaboration	Scant information regarding neovascular network morphology
	Large field of view up to 200° ultrawide field	Leakage-related masking effects
	Full size detection of neovascular membranes	Lower opportunities to use post-processing quantitative approaches
	High quality visualization of choroidal vascular network (early-intermediate phases)	Low images resolution
	High quality visualization of choriocapillaris filling (late phase)	Invasivity
	High sensitivity in detecting sub-retinal pigment epithelium neovascular lesions	
	High sensitivity in detecting pachychoroid-related defects	
Optical coherence tomography angiography	Unprecedent level of morphological detail of intraretinal vascular network and choriocapillaris	Slower acquisition requiring high patient collaboration
		No functional information (leakage, staining, filling delay)
	Unprecedent level of morphological detail of neovascular lesions	No discrimination between filling delay and ischemia
	High sensitivity in detecting macular hypoperfusion/ischemia	High number of potential artifacts
	High usage of post-processing quantitative approaches	Limited field of view
	Rapid technological evolution	Limited choroidal network information
	Non-invasivity	Not full-size detection of neovascular membranes
	High images resolution	Poorly reliable in those cases with extremely altered retinal morphology

discrepancy between FA/ICGA angiography and OCTA reconstruction is strongly influenced by the reflective properties of the neovascular lesion (Arrigo et al., 2021a). The divergence in size is related to the low reflectivity signal typical of the neovascular network, which can be explained by the presence of neovascular regions displaying less and slower perfusion (Arrigo et al., 2021a). The delayed filling theory is also

supported by the fact that in all these studies the OCTA-FA/ICGA angiography size divergence was only detected by comparing OCTA size with late-phase angiographic size, thus highlighting OCTA's limited range of sensitivity On the other hand, OCTA can identify morphological features less suited to FA/ICGA angiography. OCTA uses the reflective properties of the neovascular capillaries to distinguish immature lesions from mature, as well as neovascularizations that have already been treated. This is because mature lesions appear thicker and more hyperreflective than immature lesions (Xu et al., 2018). Moreover, OCTA can identify many morphological details, including secondary vascular branching, peripheral vascular arcades, and anastomotic loops (Xu et al., 2018). OCTA sometimes reveals the neovascular network in cases where the neovascular lesion's small size and the widespread presence of leakage make dye-based diagnosis inconclusive (Inoue et al., 2016). Another element to consider is the fact that OCTA is prone to noise-related effects, producing false flow signals (Cole et al., 2017). In addition, OCTA can provide very limited information regarding the choroidal vascular network compared with dye-based angiography, since the choroidal signal is highly attenuated by the presence of the retinal pigment epithelium. For all these reasons, while OCT revolutionized fundus disease diagnostics, OCTA can only be considered a very useful step forwards – not an alternative to FA/ICGA angiography.

3. Quantitative approaches in multimodal imaging

In this section we discuss the main aim of the present survey, namely the role of quantitative post-processing approaches designed to expand the amount of information obtained by non -invasive multimodal imaging techniques.

1. What is a biomarker?

The term "biomarker" is actually a redundant expression in the field of quantitative multimodal imaging and is employed by researchers to indicate a quantitative imaging finding. However, we felt it might be useful to define what a biomarker really is. According to the dictionary definition, a biomarker is "a naturally occurring molecule, gene, or characteristic by which a particular pathological or physiological process, disease, etc. can be identified". At the same time, the term parameter is defined as "a numerical or other measurable factor forming one of a set that defines a system or sets the conditions of its operation". Similarly, the term metric is defined as "a system or standard of measurement". Bearing these in mind, the use of the term biomarker to define a quantitative multimodal imaging finding is inappropriate. Indeed, post-processing quantitative approaches are based on the application of mathematical rules and methods to investigate images' quantitative features. But since the term biomarker is the most frequently encountered in current literature, we will continue to use it in the present survey too. Even so, we feel this confusion might be the first sign of the need to reach a consensus regarding quantitative multimodal imaging terms before more serious misunderstandings occur.

2. Why use multimodal and not unimodal imaging?

While multimodal imaging techniques are the cornerstone of research into retinal and choroidal diseases, they are now also fundamental in clinical practice. As described above, every imaging modality is able to provide highly detailed information regarding retinal and choroidal status by investigating various biophysical properties. Confocally-based fundus images can explore the biochemical properties of the eye and its alterations, assessing the distribution of retinal fluorophores and the nature of a given lesion. OCT-based technology can rightly be considered the de facto in-vivo histology of the eye, characterized as it is by an incomparable level of accuracy. It will surely be further developed in the near future by improving the resolution and acquiring the capacity to perform dedicated analyses of each retinal and choroidal component. OCTA has considerably reduced reliance on dye-based angiography in macular region diagnostics, removing the nuisance of leakage and providing unparalleled detail of the morphology of retinal and choroidal vasculature. This level of performance has not yet been reached in the periphery of the eye, although the next technical improvements are likely to concentrate on reliably increasing the OCTA examination's field of view. Incorporating all this information is making the diagnostic workup of retinal and choroidal diseases faster and more accurate than in the past. The technical demands on ophthalmologists are not so great and the new generation of devices is making multimodal imaging acquisition less time consuming. At all events, the amount of information obtained by a good multimodal imaging assessment more than makes up for the effort required. Furthermore, as discussed in detail below, the introduction of quantitative approaches is opening up a fresh field of investigation that focuses on discovering the functionality of the eye and its components. In this case, at the moment, great technical demands are made of operators intending to perform quantitative multimodal imaging analyses, although the aim is to provide automatic ways to extract multimodal imaging metrics in future. This will make it easier to ensure that quantitative approaches become more widespread.

3. Quantitative metrics in real color and confocal fundus images

Real color and pseudocolor fundus images have seldom been used to perform quantitative analyses so far. Indeed, other techniques such as fundus autofluorescence and OCT-based approaches have proved to be far better at quantifying the size and extension of retinal alterations. On the other hand, as already described above, AI-based approaches to detecting retinal alterations have been tested several times as the possible basis for diagnostic tests and screening campaigns. However, this kind of investigation is still confined to the research context and would require further validation before being considered for widespread use in real-life settings.

4. Quantitative metrics in infrared and near-infrared reflectance

Infrared and NIR reflectance images have not yet been subjected to advanced quantitative analysis. From the qualitative point of view, owing to the penetration achieved by infrared reflectance, this modality is very sensitive to different kinds of alterations in the outer retina, including subretinal debris, atrophy, and exudation (Ly et al., 2016a,b). This is why IR imaging is considered better than color fundus in detecting these kinds of alterations and it can be used to quantify their extensiveness through segmentation tools already included in the software of diagnostic devices. NIR imaging is highly sensitive to melanin changes, which also occur in the absence of other kinds of alterations detectable with different imaging modalities (Parodi et al., 2014, 2020b; Battaglia Parodi et al., 2020). As a result, segmentation tools are used in NIR images to quantify the extent of melanin defects at the posterior pole. NIR imaging can also be useful in detecting choroidal melanosome anomalies (Parrozzani et al., 2015), as well as choroidal nevi (Vallabh et al., 2016).

All the same, there is a sense that these imaging modalities might offer much more information and are currently under exploited. Indeed, confocally-based imaging modalities have the potential to provide a fingerprint of the retina's molecular and metabolic features (Aboualizadeh and Hirschmugl, 2018). Each retinal component is characterized by a specific spectrochemical profile, which can potentially be identified and quantitatively analyzed (Aboualizadeh and Hirschmugl, 2018). Interesting possibilities might arise from considering these imaging modalities as ways of quantifying the specific absorption and scattering of retinal coefficients for each patient, so as to plan the best possible laser or photodynamic treatment (Yust et al., 2012). As for the so-called "photo bio modulation" technique, which is seen as a way of promoting retinal recovery by administering low-energy IR or NIR light (Eells et al., 2016; Rono and Oliver, 2020), quantitative approaches might be

applicable here too in future to optimize the diagnostic workup and treatment strategies for patients. As an example of NIR's hidden potential, a recent study tested the efficacy and safety of retinal photoreceptor-binding upconversion nanoparticles in a rodent model (Ma et al., 2019). These are biocompatible NIR light nanoantennae designed to improve retinal photoreceptor function, expanding the current limits of a patient's visual functions. These advances in the field of nanotechnology may pave the way for future diagnostic and therapeutic biomedical applications (Ma et al., 2019).

5. Quantitative metrics in fundus autofluorescence

BAF and GAF are pivotal multimodal imaging modalities, both in clinical practice and in the research context. Due to its very high sensitivity in detecting lipofuscin changes, BAF is nowadays considered an essential diagnostic methodology, and even more advanced quantitative approaches are being introduced to extend the amount of information it can provide (Schmitz-Valckenberg et al., 2021). The manufacturer's software accompanying BAF devices already includes segmentation tools to measure the extent of the hyperautofluorescent and hypoautofluorescent alterations. Measuring the degree of DDAF and QDAF displayed in a range of retinal and choroidal diseases, including AMD and Stargardt disease, are clinically useful ways of evaluating the rate of a retinal atrophy's progression (Strauss et al., 2017; Fleckenstein et al., 2018). When considering the progression of retinal atrophy, it is important to match quantitative and qualitative BAF imaging information. Indeed, it has been demonstrated that BAF patterns of geographic atrophy are strictly related to the rate of progression (Holz et al., 2007). BAF detects the presence of hyperautofluorescent regions surrounding the atrophy, and the size is directly associated with the atrophy's rate of progression (Schmitz-Valckenberg et al., 2006). The imaging-based interpretation of the hyperautofluorescent perilesional region is a reactive phenomenon of the RPE. Interestingly, a recent histological study revealed that the hyperautofluorescent region displays hypertrophic RPE associated with increased inflammation and microglia activation (Bonilha et al., 2020), thus reinforcing the strict relationship between confocal fundus autofluorescence and the biochemical properties of retinal structures. Moreover, careful attention is paid to the characteristics of the atrophic perimeter. In particular, atrophy circularity, defined as the ratio of area to perimeter squared, is evaluated in close association with the retinal degeneration's varying rate of progression, since the more circular a lesion, the slower the atrophy's rate of progression (Domalpally et al., 2013; Romano et al., 2021a). Artificial intelligence-based approaches are currently being explored as a possible means of performing the automatic recognition and segmentation of retinal alterations revealed by BAF images, as well as of attempting to predict the progression of fundus diseases (Arslan et al., 2020, 2021). A notable boost has been provided by quantitative autofluorescence (qAF), a standardized way of analyzing the quantitative properties of BAF images (Fig. 7). Introduced in 2011, qAF quantitatively analyzes BAF images, taking into account laser power variability and detector sensitivity (Delori et al., 2011). qAF acquisition also includes image calibration, incorporating magnification, refractive errors, and optical media density from normative data on lens transmission spectra. The acquisition software automatically calculates foveal distances, and three rings (inner, middle and outer), each made up of eight segments, are automatically placed at 2.88°, 5.78°, and 8.5° from the fovea. qAF is governed by IGOR (Wavemetrics, Lake Oswego, OR) or HEYEX (Heidelberg Engineering) software, and is nowadays mainly used for research purposes. Applying this approach to healthy subjects revealed increasing qAF values with age, associated with certain differences between ethnic groups and no significant effect on ocular axial length (Greenberg et al., 2013). A recent review article by Sparrow et al. (2020) described in detail the principles underlying qAF and its application in different fundus diseases. Although qAF assessment is still rare in clinical practice, this approach can provide a very thorough quantitative description of pigment changes occurring at the posterior pole, and its use is expected to increase in the near future.

While almost all BAF-related imaging modalities are based on the calculation of the absolute intensity of the images, fluorescence lifetime, defined as the mean time that a fluorophore remains in an excited state, has recently been explored as a novel way of examining the retina.

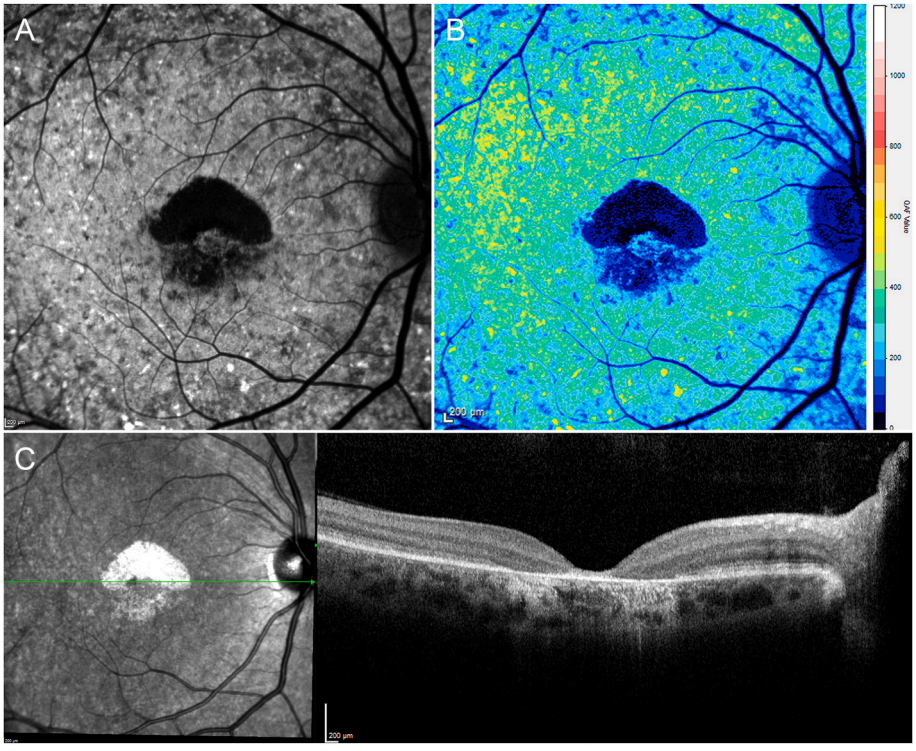

Fig. 7. Blue-light autofluorescence and quantitative autofluorescence imaging. This is a case of Stargardt disease at an advanced stage, with a big central region of definitely decreased fundus autofluorescence, localized above a region of doubtfully decreased fundus autofluorescence, as shown by the BAF image (A). Moreover, multiple hyperautofluorescent and hypoautofluorescent flecks are visible over the entire posterior pole. qAF analysis (B) provides a detailed and normalized map of autofluorescence distribution of the posterior pole, providing the basis for a reliable quantification. Structural OCT (C) records a complete central outer retinal atrophy, including the involvement of the inner retinal layers, and evident choroidal hypertransmission.

Fluorescence lifetime imaging ophthalmoscopy (FLIO) is based on the more general fluorescence lifetime imaging microscopy (FLIM) methodology and consists in calculating the exponential decay of fluorescence over time (Schweitzer et al., 2001). This technique has been implemented in Heidelberg devices and includes a 473-nm pulsed diode laser excitation and two emitted photons in two separate spectral channels, namely a short wavelength channel (498–560 nm) and a long wavelength channel (560–720 nm). FLIM-based approaches have the undoubted advantage of being dye-free techniques. However, when it comes to FLIO images, it is important to bear in mind that excitation and emission wavelengths partially overlap in several retinal fluorophores (Han et al., 2007) (Table 4), thus making it taxing to interpret FLIO data (Dysli et al., 2017). FLIO has been successfully employed in several fundus diseases (Dysli et al., 2017), demonstrating high sensitivity in detecting different patterns of pigment changes.

Current qAF and FLIO approaches rely on high-quality images and the skill of the operators in acquiring them, while the field of view being limited to the posterior pole is a further drawback.

GAF is an imaging modality that is still under-explored, compared with BAF. GAF is less affected by macular pigments' poor light absorption than blue wavelengths (Delori et al., 2001), and thus represents a potentially more sensitive modality for investigating microscopic changes in the macula (Wolf-Schnurrbusch et al., 2011). The segmentation and circularity tools described for BAF analyses can also be applied to GAF images. There have been few studies comparing BAF and GAF imaging approaches to macular atrophy evaluation. GAF has been found to be better than BAF in evaluating geographic atrophy (GA) borders and in assessing central alterations, including foveal sparing (Wolf-Schnurrbusch et al., 2011; Pfau et al., 2017). However, because of the limited data, BAF still represents the technique of choice in the autofluorescence-based evaluation of pigment alterations and atrophy.

6. Quantitative metrics in optical coherence tomography

OCT imaging is certainly the non-invasive approach offering the greatest opportunity to develop and test quantitative parameters, especially considering that not all structural OCT findings can be considered parameters or biomarkers (van Velthoven et al., 2007). Although there have probably been attempts to quantify all structural OCT findings, the literature regards only some of these as having a real clinical application. Indeed, alterations such as drusen and other debris, microaneurysms, choroidal alterations (clefts, hyperreflective columns, and caverns), outer retinal tubulations, hard and soft exudates, and many others should be considered disease-related signs rather than quantitative metrics. Their involvement in analytical processes is often hampered by their being regarded as dichotomic factors (present or absent). Conversely, many other structural OCT characteristics or alterations have improved their clinical impact by adopting quantitative approaches. The manufacturers' software includes segmentation tools to measure retinal and choroidal layers and to create thickness maps. The evaluation of retinal thickness, especially central macular thickness, plays a major role both in clinical practice and in research settings, and is central to retinal therapies. As previously seen in autofluorescence techniques, the border between qualitative and quantitative approaches is not very clearly defined in OCT approaches either. Indeed, in many cases they are treated as dichotomic factors (present or absent) because of the intrinsic difficulty in collecting OCT metrics. This is the case in retinal exudation, for example. However, recent findings have made it impossible to regard retinal fluids as simply present or absent. Nowadays it is very important to distinguish between types of retinal fluid since localization has revealed a prognostic role for the diagnostic workup of exudative retinal diseases (Figs. 8 and 9) (Daruich et al., 2018; Guymer et al., 2019; Spaide et al., 2020) (Table 5). Because of the clinical importance of each type of fluid, the current research is focused on developing an artificial intelligence-based approach to the automatic segmentation and evaluation of retinal fluids (Roberts et al., 2020; Moraes et al., 2021; Schmidt-Erfurth et al., 2022). Although promising, these approaches require very large datasets, high quality data and standardized follow-ups, thus still making them hard to employ extensively in real-life clinical settings.

Similarly, hyperreflective foci (HF) are commonly treated as dichotomic metrics. These lesions, defined as small, round or oval-

Table 4
Main retinal fluorophores, localization, function, and autofluorescence characteristics. Adapted from (Dysli et al., 2017) and expanded.

Fluorophore	Main localization	Main Function	Reference	Excitation, nm	Emission, nm	Lifetime, ns	Reference
Collagen	Connective tissue	Structural	–	280–350	370–440	≤5.3	Maarek et al. (2000); König (2008)
Elastin	Connective tissue	Structural	–	300–370	420–460	≤2.3	Maarek et al. (2000); König (2008)
Flavin adenine dinucleotide (FAD)	Retinal cells mitochondria	Coenzymes of redox reactions	Sinha et al. (2018)	420–500	520–570	2,91	Koziol et al. (2006); König (2008)
Hemoglobin	Retinal and choroidal vessels	Red blood cells composition	–	400–600	non-fluorescent	n/a	–
Lipofuscin	Retinal pigment epithelium	Visual circle	Feeney (1978)	340–500	540,430-460	up to 2.2	Sparrow et al. (2000); Schweitzer et al. (2007)
Lutein	Transretinal localization	Light absorption	Li et al. (2020)	440–540	550	0.03–0.08	Barker et al. (2011)
Melanin	Retinal pigment epithelium	Light absorption	Feeney (1978)	300–800	540 (broad at 785 NIR wavelength)	0.65–1.6	König (2008)
Nicotinamide adenine dinucleotide phosphate hydrate (NADPH)	Retinal cells mitochondria	Coenzymes of redox reactions	Darius et al. (1995)	300–380	450–500	0,3	König (2008)
Phenylalanine	Transretinal localization	Proteins	–	240–270	280	7,5	McGuinness et al. (2006)
Retinal (Shiff base)	Retinal pigment epithelium, photoreceptors	Visual circle	Han et al. (1993)	350	600–650	0.030–0.1	Bachilo and Gillbro (1999)
Tryptophan	Photoreceptors, glial cells	Proteins	Pow and Cook (1997)	250–310	350	2.0–6.0	Guo et al. (2012); Guo et al. (2013)
Tyrosine	Photoreceptors	Proteins	Nag et al. (2019)	250–290	300	2,5	Ashikawa et al. (1982)
Zeaxanthin	Transretinal localization	Light absorption	Li et al. (2020)	440–540	550	0.03–0.08	Barker et al. (2011);

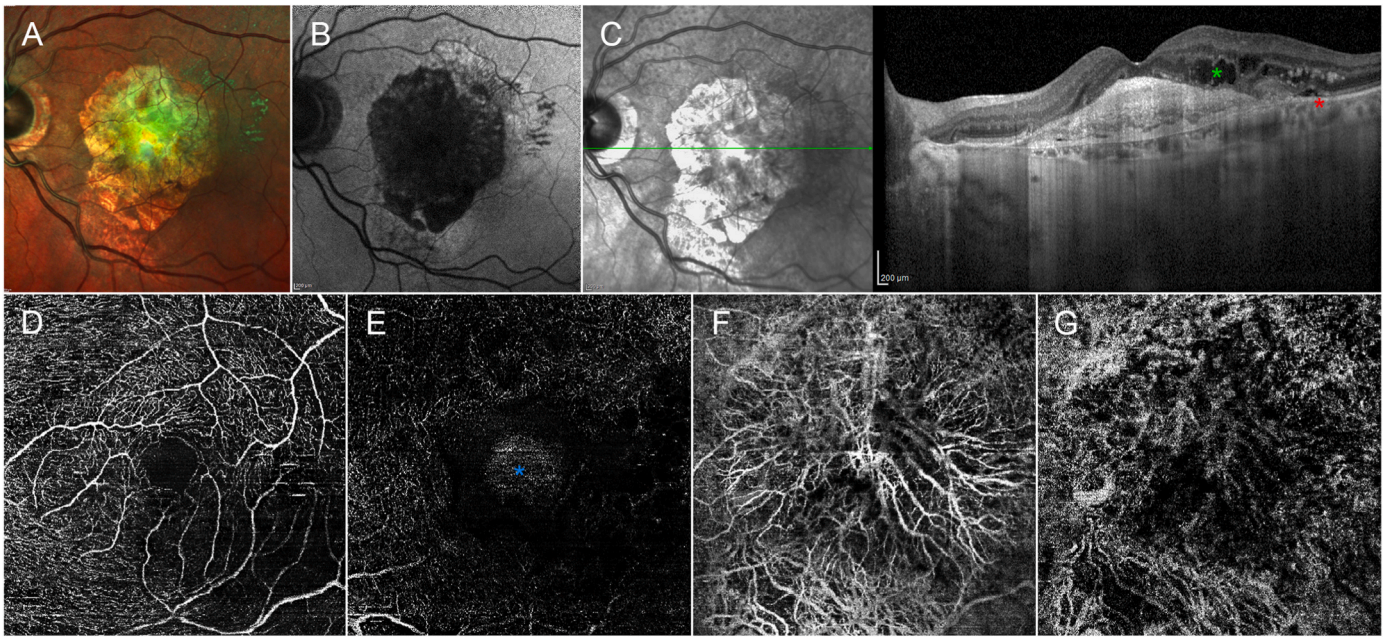

Fig. 8. Multimodal imaging findings in a case of advanced fibro-atrophic stage of age-related macular degeneration. The increased green-reflectance signal seen in multicolor confocal image (A) can be interpreted as extensive fibrosis involving most of the posterior pole. This corresponds to a definitely decreased fundus autofluorescent signal in the BAF image (B). Structural OCT (C) detects the presence of an impressive hyperreflective subretinal lesion, with complete atrophy of the outer retinal bands, and choroidal hypertransmission. Moreover, signs of subretinal (red asterisk) and intraretinal (green asterisk) fluids are also visible. OCTA is considerably affected by segmentation errors, with loss of information regarding the status of the superficial capillary plexus (D). The deep capillary plexus is shown to be almost absent, with projection artifacts and central suspended scattering particles in motion artifact (blue asterisk). The massive neovascular network is clearly visible with OCTA (F). The choriocapillaris (G) is highly impaired in the entire region affected by the fibro-vascular lesion.

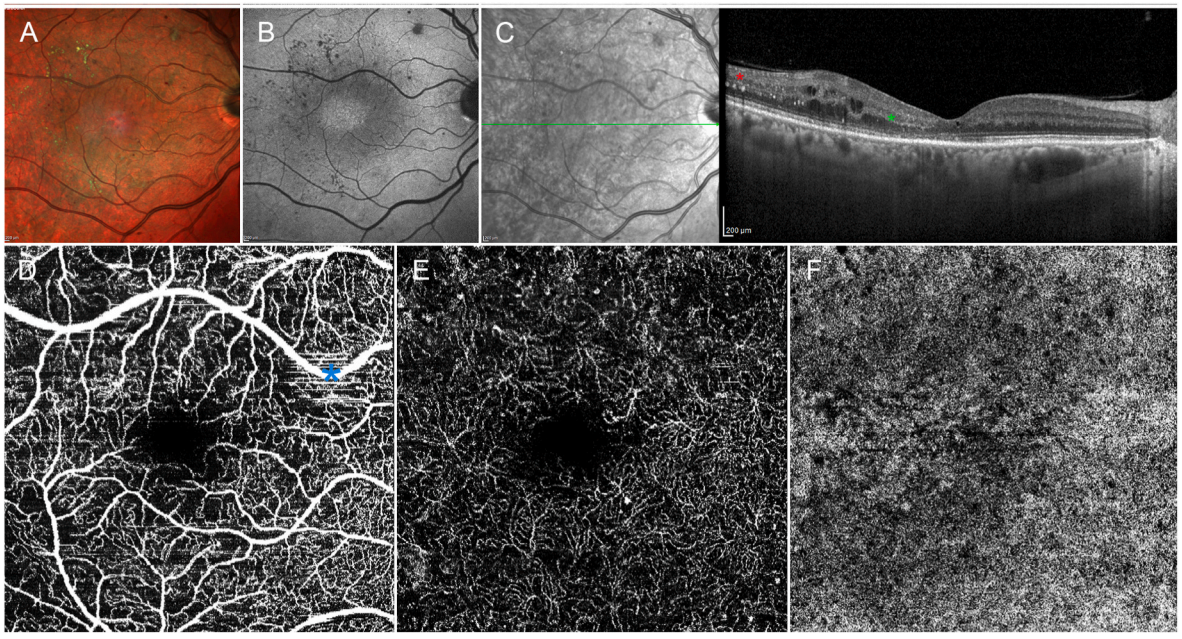

Fig. 9. Multimodal imaging findings in a case affected by diabetic macular edema. The confocal multicolor image (A) shows sparse, hard, exudated micro-hemorrhages, and retinal microaneurysms. These lesions produce the masking effect shown in the BAF image (B). Structural OCT shows the presence of an extra-foveal macular edema, with increased intraretinal hyperreflective foci (green asterisk) and intraretinal hard exudates (red asterisk). This image is useful in drawing attention to the main differences between HF and hard exudates. HF are smaller than hard exudates and not associated with a posterior shadowing effect. OCTA is affected by segmentation and motion artifacts (blue asterisk). The superficial capillary plexus (D) appears tortuous and apparently spared. The deep capillary plexus (E) displays flow signal voids and sparse microaneurysms. It is worth pointing out that the reduced signal might also be the consequence of a deep capillary displacement effect caused by the cystoid arrangement of the intraretinal fluid, thus leading to an artifactual reduction of vessel density. The choriocapillaris (F) is impaired, being also affected by an intraretinal fluid-related masking artifact.

Table 5
Types of retinal fluids. The following abbreviations are used: optical coherence tomography (OCT), retinal pigment epithelium (RPE), outer nuclear layer (ONL).

Type of Fluid	Abbreviation	Localization	Pathogenesis	OCT	Interpretation	Prognosis
Intraretinal fluid	IRF	Within inner retinal layers	Accumulation of fluid in cystoid spaces and/or inner retinal degeneration	Hyporeflective	Excessive leakage secondary to inner blood-retinal barrier breakdown and/or effect of retinal cells degeneration	Negative
Subretinal fluid	SRF	Between RPE and ONL	Accumulation of fluid in the subretinal space	Hyporeflective	Excessive leakage secondary to outer blood-retinal barrier breakdown and/or effect of macular neovascularization	Alone associated with better prognosis
Subretinal hyperreflective material	SHRM	Between RPE and ONL	Accumulation of exudation comprising serum, fibrin, and inflammatory cells in macular neovascularization	Hyperreflective	Deriving from fluid, fibrin, blood, scar or fibrovascular tissue	Negative
Pigment epithelium detachment	PED	Below RPE	Classified as Serous, Drusenoid, Fibrovascular or Mixed	Hyporeflective	Associated with pachychoroid-related disorders, inflammation and/or neovascular diseases	Negative

shaped, well-circumscribed hyperreflective particles localized within retinal layers or in the choroidal space, are commonly interpreted as accumulated activated microglia and inflammatory cells. HF are mainly studied in relation to diabetic macular edema, where a high number of foci is associated with a poor clinical prognosis (Uji et al., 2012; Arrigo et al., 2020b). However, HF have also been extensively described in connection with other fundus diseases, including uveitis (Berasategui et al., 2018), retinal dystrophies (Romano et al., 2020a), and macular neovascularization (Arrigo et al., 2021b). The number of HF and their changes over the follow-up are considered very useful in monitoring the progression of AMD-related geographic atrophy (Fig. 10). Indeed, the Classification of Atrophy Meeting group showed a relationship between HF and both the risk of atrophy onset and its progression (Jaffe et al., 2021). Furthermore, Cao and colleagues recently performed an interesting histological study, showing that HF may be extremely complex in terms of origin and interactions with the other retinal cytotypes, and therefore an important sign of disease activity. Apart from having an inflammatory origin, some HF may arise from the RPE epithelial-mesenchyme transdifferentiation (Cao et al., 2021). HF are also viewed as predictors of macular neovascularization (MNV) onset (Arrigo et al., 2021b) (Fig. 11).

Once again, automatic counting systems based on artificial intelligence have been tested to make HF assessment easier and more reliable (Varga et al., 2019; Schmidt-Erfurth et al., 2020) However, these approaches are not really suitable for real-life settings. As a result, HF assessment is still not properly standardized, both in terms of cutoff numbers and retinal sectors to be included in the investigation (single structural OCT scan, entire macular volume? etc.), which remain arbitrarily established by researchers. For example, in a study that focused on central serous chorioretinopathy, Arrigo et al. found it useful to consider HF cutoff >10, obtained from three consecutive macular slabs, as clinically relevant to evaluate treatment response (Arrigo et al., 2021c). In the same study, RPE and Sattler layer thickness proved clinically useful in providing quantitative cutoffs associated with the risk of MNV onset (in particular, RPE thickness <36 μm and SLT <50 μm) (Arrigo et al., 2021c).

Recently, Arrigo and colleagues proposed a dichotomic structural OCT parameter found in diabetic macular edema known as foveal eversion. This is taken to be OCT evidence of a completely everted foveal profile and was associated with high macular edema persistence and poor visual outcome (Arrigo et al., 2021d). Arrigo and co-workers interpreted foveal eversion as a structural OCT sign of Müller cell impairment, leading to the loss of structural support for the fovea, explaining the eversion of the foveal profile, and the disequilibrium of retinal homeostasis, which in turn would explain the poor absorption of the macular edema secondary to intravitreal treatments (Arrigo et al., 2021d). The interesting aspect of employing foveal eversion as a parameter is that it makes evaluation in a clinical context feasible, since it does not require much technical imaging expertise on the part of the operator. We are now concentrating on distinguishing different patterns of foveal eversion that can be tested in diabetic macular edema as well as in other exudative retinal diseases.

Potentially relevant information can be obtained by the enface visualization of OCT images. Indeed, the borders of a given retinal lesion

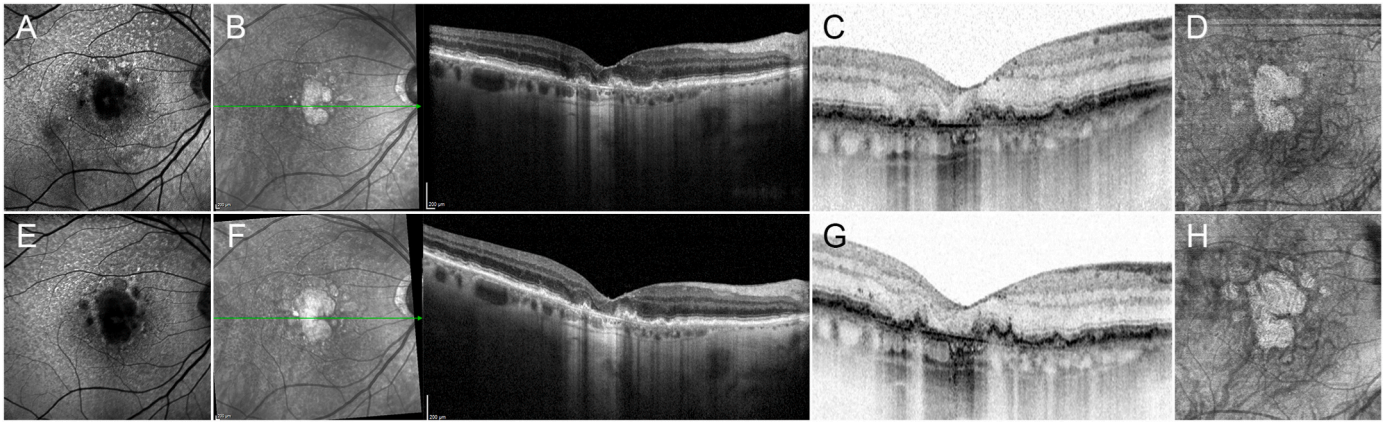

Fig. 10. The role of hyperreflective foci in geographic atrophy. BAF (A) and structural OCT (B) reveal an evident case of geographic atrophy, with a well-marked region of definitely decreased fundus autofluorescence, corresponding to extensive disruption of the outer retinal bands. The inverted colors used in structural OCT (D) help to detect and quantify hyperreflective foci better, which prove to have increased in the altered macular region. Enface OCT visualization (D) enables the borders of the atrophic region to be detected even more precisely. After one year, the BAF (E) and structural OCT (F) images show that the atrophic area has enlarged. The structural inverted color OCT image (G) records modifications in the number and localization of the hyperreflective foci, now more clearly detected at the border of the lesion. Enface OCT (H) precisely highlights the expansion of the atrophic region.

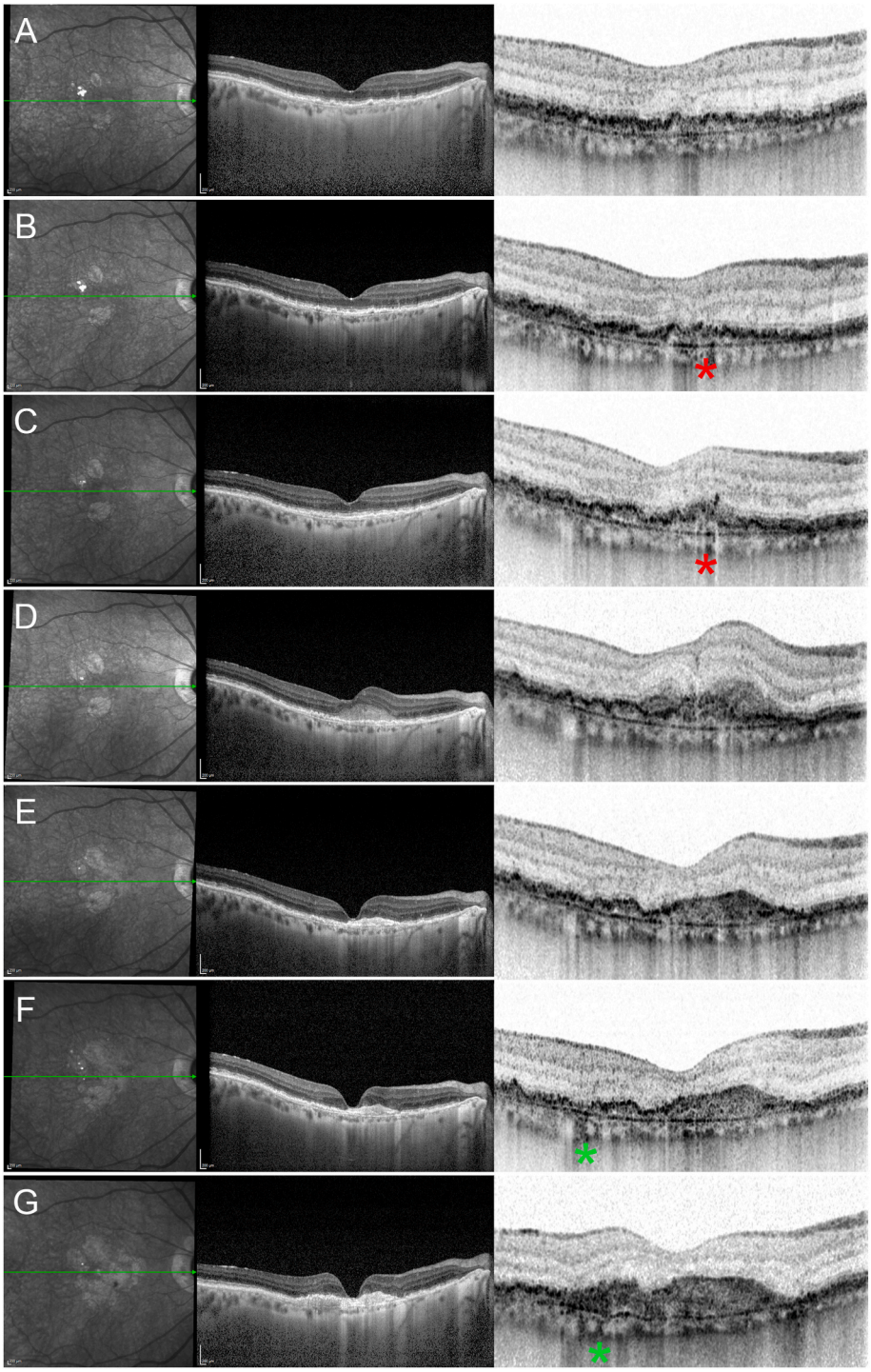

Fig. 11. The role of hyperreflective foci in AMD-related macular neovascularization. The baseline image (A) shows an intermediate case of AMD. The baseline image of the inverted color OCT image is also shown. After six months (B), one notices an increase in the hyperreflective foci (red asterisk), especially in the choroidal side. After a further three months (C), the hyperreflective foci have increased even more (red asterisk), with an evident pigment migration within the outer nuclear layer. At the 12-month follow-up (D) the onset of a macular neovascularization can be seen, with several hyperreflective foci concentrated around the lesion. Anti-VEGF treatments managed the original lesion well, leaving a hyperreflective plaque with no signs of exudation at the 18-month follow-up (E). However, the inverted color OCT shows an increase in choroidal hyperreflective foci near the border of the original lesion (green asterisk) at the 20-month follow-up (F). At the 24-month follow-up (G), we can see the reactivation of the lesion in the same region (green asterisk), with no signs of exudation in the context of the original neovascularization. Hence, the analysis of hyperreflective foci changes may be useful in predicting the onset of macular neovascularization and in assessing the expansion of the neovascular lesion during the follow-up.

can be detected with great precision. In paracentral acute middle maculopathy, enface OCT depicts the ischemic region in great detail, as well as detecting more patterns of the disease associated with different outcomes (Ghasemi Falavarjani et al., 2017; Bakhoum et al., 2018). Furthermore, enface OCT can help to quantify HF (Cao et al., 2021) and to monitor the progression of geographic atrophy in AMD (Thulliez et al., 2019). Other structural OCT metrics have been the object of attempted quantification and are reported in Table 6.

Ever more studies are turning their attention to the clinical relevance of the quantitative assessment of the choroid. This includes measuring choroidal thickness (CT), which can be done in several non-standardized ways. One of the most common approaches concentrates on the subfoveal CT, usually obtained from a single horizontal OCT scan. This metric has been found to have a clinical application in following patients and in predicting disease progression in several conditions, including wet and dry AMD, uveitis and pachychoroid-related disorders (Thorell et al., 2015; Ishikawa et al., 2014; Lee et al., 2016a). Another way to quantitatively investigate CT is to perform multiple measurements to address possible thickness changes throughout the structural OCT line. For example, in several studies Arrigo and colleagues found it useful to take five different choroidal samples by using standardized points (subfoveal, 750 μm on right and left, 1500 μm on right and left) on a high-resolution single horizontal OCT scan, considering three different measurements: CT, Sattler layer thickness (SLT), and Haller layer

Table 6
Description and definition of the main structural OCT metrics, objects of quantification.

Structural OCT Metric	Acronym	Definition	Interpretation	Method of Quantification	Standardization
Central macular thickness	CMT	Macular thickness measurement within 3-mm diameter of the center	Increment associated with exudation, tractional phenomena, debris depositions or proliferations; reduction usually related with atrophic changes	Linear measurement	Standardized if using ETDRS-9 sector grid
Retinal thickness	RT	Macular thickness measurement outside the 3-mm diameter of the center		Linear measurement using multiple samples within the posterior pole	Standardized if using ETDRS-9 sector grid
Retinal nerve fiber layer thickness	RNFL	Measure of the innermost hyperreflective retinal layer at the posterior pole or at the level of the optic nerve head	Thinnings described in several retinal diseases as a sign of inner retinal involvement; mandatory evaluation for glaucoma and other optic nerve diseases	Linear measurement using multiple samples within the posterior pole or in the peripapillary region; often included in the ganglion cell complex, defined as the complex of the nerve fiber layer, the ganglion cell layer, and the inner plexiform layer	Standardized if using ETDRS-9 sector grid or specific glaucoma-related grids
Ganglion cell layer thickness	GCL	Measure of the innermost isoreflective retinal layer at the posterior pole	Thinnings described in several retinal diseases as a sign of inner retinal involvement; mandatory evaluation for glaucoma and other optic nerve diseases	Linear measurement using multiple samples within the posterior pole; often including the macular ganglion cell-inner plexiform layer complex	Standardized if using ETDRS-9 sector grid
Choroidal thickness	CT	Choroidal thickness measurement between the lower margin of the RPE/Bruch membrane complex and the upper margin of the sclera	Increment associated with inflammation, congestion or pachychoroid-related disorders; reduction associated with atrophic changes	Linear measurement using subfoveal thickness or multiple samples within the posterior pole	Not standardized
Hyperreflective foci	HF	Small, round or oval-shaped, well-circumscribed hyperreflective particles localized within retinal layers or in the choroidal space	Increment associated with inflammation, disease progression or retinal degeneration	Counting in one or more (usually horizontal) structural OCT slab or treated as dichotomic factor (present/absent)	Not standardized
Disorganization of inner retinal layers	DRIL	Loss of definition of the boundaries of theinner retinal layers	Associated with neuroretinal degeneration occurring in diabetic retinopathy and intepreted as a negative prognostic factor	Usually dichotomic (present/absent)	Not standardized
Foveal eversion	FE	Structural OCT based detection of completely everted foveal profile in macular edema	Interpreted as a sign of Müller cells impairment leading to the loss of foveal structural support and macular homeostasis	Dichotomic (present/absent)	Not standardized
Ellypsoid zone status	EZ status	Evaluation of the integrity of the second hyperreflective band, intended as the structural OCT layer associated with the junction between the inner and the outer photoreceptors segments	Attenuation, disruption or disappearance associated with degeneration of retinal photoreceptors; more complex classification; EZ reflectivity calculation	Linear measure using multiple thickness samples; qualitative evaluation (present, disrupted, absent)	Not standardized

thickness (HLT). This approach was useful in categorizing several choroidal patterns associated with significantly different subtypes of retinal diseases, including retinitis pigmentosa, Stargardt disease and central serous chorioretinopathy (Arrigo et al., 2019a, 2020c, 2021c).

A separate chapter deals with the choroidal vascularity index (CVI), a parameter derived from the post-processing elaboration of structural OCT data, showing its increasing clinical utility. This metric was introduced in 2016 (Agrawal et al., 2016) as an attempt to apply a similar OCTA-based vessel density methodology on choroidal structural OCT data. In order to calculate the CVI, the structural OCT image needs to be binarized and the black/white ratio ascertained. The inverse calculation can be used to measure the stromal component. Rajabian and colleagues have previously used this approach, extracting the choroidal stromal index (CSI) to quantitatively analyze the stromal contribution to the pathogenesis of focal choroidal excavation, showing that the choroidal region surrounding the site of excavation displayed an altered vessels/stroma ratio (Rajabian et al., 2020a). Although CVI has been successfully applied in different retinal and choroidal diseases, as excellently illustrated by Agrawal and colleagues (Agrawal et al., 2020), we feel it is worth mentioning we employed the parameter ourselves in both retinitis pigmentosa and Stargardt retinal dystrophies. Indeed, the combined use of CVI and choroidal thickness allowed us to distinguish distinct choroidal patterns associated with different progressions and outcomes in both retinal dystrophies. Looking at this in greater detail, Arrigo et al. distinguished a normal-seeming choroid pattern, which was stable, choroid patterns exhibiting a major impairment of the Sattler or Haller choroidal layers, associated with moderate progression, and choroidal patterns showing extensive choroidal degeneration, associated with more severe progression (Arrigo et al., 2019a, 2020c). Studying retinitis pigmentosa, Iovino and colleagues reported a significantly decreased CVI in eyes affected by macular edema, compared with eyes without this complication, suggesting a possible choroidal role in the pathogenesis of macular edema in this retinal dystrophy (Iovino et al., 2019). Using CVI made it possible to detect significant choroidal abnormalities characterizing eyes affected by pentosan polysulfate maculopathy (Wang et al., 2021). Arrigo and co-workers also used CVI to evaluate the effect of inflammation on the clinical course of diabetic macular edema. In the event, lower CVI values, together with a greater number of HF, was found to be associated with a higher pro-inflammatory profile and a better response to intravitreal corticosteroid implants (Arrigo et al., 2020b).

To avoid evaluation bias, it is indispensable to perform the methodological step of excluding choroidal regions showing hypertransmission secondary to the impairment of the overlying RPE/photoreceptor complex.

Another very important structural OCT metric is ellipsoid zone (EZ) status. EZ is not a true anatomical retinal region; the term was introduced in the OCT era to indicate the second hyperreflective outer retinal band, viewed as the site of the inner/outer photoreceptor segment junction (Staurenghi et al., 2014). This is considered the most important structural OCT parameter to evaluate the integrity of retinal photoreceptors. EZ evaluation has undergone various approaches, starting with

mere qualitative evaluation: present, disrupted, or absent (Tao et al., 2016). An international panel of experts has proposed a more complex EZ and outer retinal classification, including complete RPE and outer retinal atrophy (cRORA), incomplete RPE and outer retinal atrophy (iRORA), complete outer retinal atrophy (cORA), and incomplete outer retinal atrophy (iORA) (Sadda et al., 2018). The positive aspect of this classification is that it offers a detailed assessment of which outer retinal structure is involved in the atrophic process (Rajabian et al., 2020b); on the negative side, it requires a considerable level expertise on the part of the operators and it is difficult to apply this time-consuming evaluation in clinical practice. A pure quantitative approach is EZ reflectivity calculation. In this case, it is possible to calculate EZ reflective properties, comparing these to healthy subjects for reference. Romano and colleagues tested this approach in Best disease, assessing EZ reflectivity's relationship with disease progression and identifying a new structural OCT parameter, to be known as optically preserved islet (OPI), in association with better visual outcome (Romano et al., 2020b, 2021b). Many other studies have reinforced the clinical relevance of EZ reflectivity assessment in fundus diseases. However, operators should be aware of the possible influence of OCT signal attenuation sources and keep in mind the need for high-quality images (Lee et al., 2021). Reflectivity quantification could potentially be used to analyze all retinal structures and disease-related alterations. For example, Arrigo and co-workers adopted reflectivity calculation to investigate its predictive role in the administration of ocriplasmin intravitreal injection to resolve vitreomacular traction (Arrigo et al., 2020d).

A recent step forward in the quantitative analysis of structural OCT data concerns the development of a quantitative tool focused on Müller cells. These are fundamental retinal cytotypes that run vertically through the entire thickness of the retina, from the internal limiting membrane (ILM) to the external limiting membrane (ELM), governing the whole structural and functional retinal homeostasis by making the neuroretinal functional unit (Bringmann et al., 2006). A key feature of Müller cells is their ability to concentrate light onto retinal photoreceptors without interfering with the properties of light radiation (Bringmann et al., 2006). On this basis, in a recent study, Arrigo et al. assumed that Müller cells corresponded to the transretinal hyporeflective signal emitted between ILM and ELM (Arrigo et al., 2020e). This tool then selectively isolated this signal from the macular volume, providing a histologically matching representation of extrafoveal Müller cells, while also allowing these cells to be quantified (Fig. 12). As regards foveal Müller cells, these were hard to detect owing to the smaller diameters caused by the greater concentration of foveal cells and by their z-shaped geometrical properties (Arrigo et al., 2020e). However, ours was the first attempt to isolate and quantify retinal Müller cells non-invasively, paving the way for interesting future developments in both the ophthalmological and neurological research fields. We are now working on the optimization of our algorithm to improve the detection of Müller cells in healthy eyes and to test this method in fundus disorders, since they are known to be heavily involved in several fundus diseases (Bringmann et al., 2006). The noninvasive quantitative evaluation of retinal Müller cells is particularly intriguing, since it might lay the groundwork for new kinds of analyses of both ocular and neurological diseases. Indeed, the neuroretina can rightly be considered a direct extension of the central nervous system. Glial cells are often involved earlier in neurodegenerative mechanisms (Gleichman, and Carmichael, 2020), thus making these cytotypes the target of potentially useful diagnostic approaches. This being the case, our method might be tested in neurological disorders such as Alzheimer's disease, Parkinson's disease and many others, with a view to assessing its diagnostic utility and its role in noninvasively detecting early alterations typical of disorders of the central nervous system.

Overall, considering all the structural OCT parameters described above, we can highlight the undoubted advantages offered by

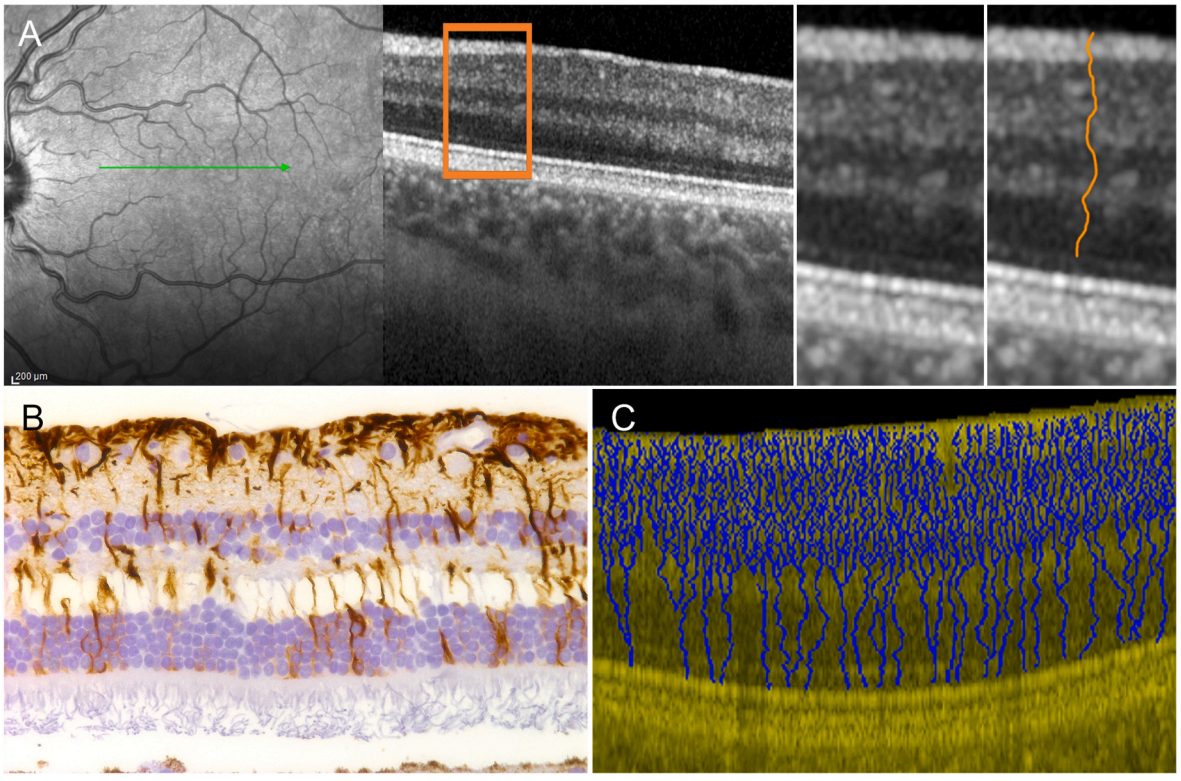

Fig. 12. OCT-based detection of macular Müller cells. Starting from a structural OCT image (A), the theoretical assumption is to selectively analyze the transretinal hyporeflective signal included between the ILM and the ELM, better visible on the magnified OCT image, where a single Müller cell is manually colored orange. Compared with the histology of the same eye, showing Müller cells marked by vimentin and glial fibrillary acidic protein antibodies (B), the OCT-based reconstruction (C) shows a good morphological match, providing a non-invasive way of quantifying macular Müller cells.

quantitative OCT-based approaches in providing new insights into the pathogenesis of fundus diseases and in improving their diagnostic workup. On the other hand, most of these metrics still need to be standardized, and this is why we believe it is essential to establish an international consensus among specialists regarding the most effective way to extract and analyze these parameters.

7. Quantitative metrics in optical coherence tomography angiography

OCTA is another large field in which quantitative approaches have been able to make breakthroughs in the assessment of physiological and pathological retinal characteristics. Compared with OCT, in OCTA the border between qualitative and quantitative approaches is more clearly demarcated. Indeed, most of the OCTA metrics are treated as continuous variables.

Before describing OCTA quantitative parameters, it is important to stress that OCTA is able to provide only part of all the necessary information regarding the perfusion status of the retina. Indeed, OCTA can only detect a blood flow signal within the range covered by a given OCTA device's sensitivity (Spaide et al., 2018). For this reason, perfusion reductions recorded by OCTA can be the result either of blood flow changes outside the range of OCTA sensitivity or a real loss of perfusion. Hence, operators have to bear in mind that OCTA is not able to distinguish between reduced but still present perfusion and totally absent perfusion and must always take care when interpreting OCTA findings. Furthermore, OCTA is a technique prone to several possible artifacts, which are described in a dedicated section, and requires very high-quality images for its findings to be considered reliable.

A crucial step for most OCTA quantitative analyses is image binarization. This involves applying a threshold to isolate retinal capillaries from the background. There are many tools that allow images to be binarized easily; one of the most popular is the ImageJ software package (Schindelin et al., 2012). Binarization might seem a simple operation, but several studies have demonstrated how large the thresholding technique's impact on binarization can be (Mehta et al., 2019, 2020; Borrelli et al., 2021). Arrigo et al. have recently carried out a study including the principal thresholding technique to discover the most reliable binarization thresholds. This took into consideration the following outcomes: detection of retinal capillaries, calculation of overlapping percentages between binarized and original images, impact on quantitative OCTA metrics (Fig. 13) (Arrigo et al., 2021e). Based on their analyses, Arrigo and colleagues found the Huang, Li, Mean and Percentile binarization thresholds to be highly reliable, whereas Intermodes, MaxEntropy, RenylEntropy and Yen were associated with severe errors in detection and inaccurate binarized OCTA reconstructions.

The foveal avascular zone (FAZ) was the first quantitative metric to be adopted. FAZ is a physiological non-perfused retinal area localized within the foveal depression region (Iwasaki and Inomata, 1986). The surrounding capillaries are arranged in a ring, making it possible to segment and measure the FAZ area and perimeter both at the superficial capillary plexus (SCP) and at the deep capillary plexus (DCP). The FAZ area can be analyzed either manually or automatically, with good reproducibility and repeatability (Carpineto et al., 2016; Ishii et al., 2019). The FAZ area is considered a highly sensitive but poorly specific parameter associated with perfusion changes; however, it is subject to remarkably high inter-subject variability, even in healthy eyes (Takase et al., 2015; Linderman et al., 2018). The FAZ area proved to be enlarged in almost all retinal and choroidal diseases, whereas it was found to be smaller in foveal hypoplasia, retinopathy of prematurity and vitreoretinal interface disorders (Yanni et al., 2012; Pakzad-Vaezi et al., 2017; Bacherini et al., 2021). Less frequently used FAZ-related parameters include perimeter, axis ratio, acircularity/circularity index, and major horizontal axis angle (Linderman et al., 2018; Piao et al., 2021).

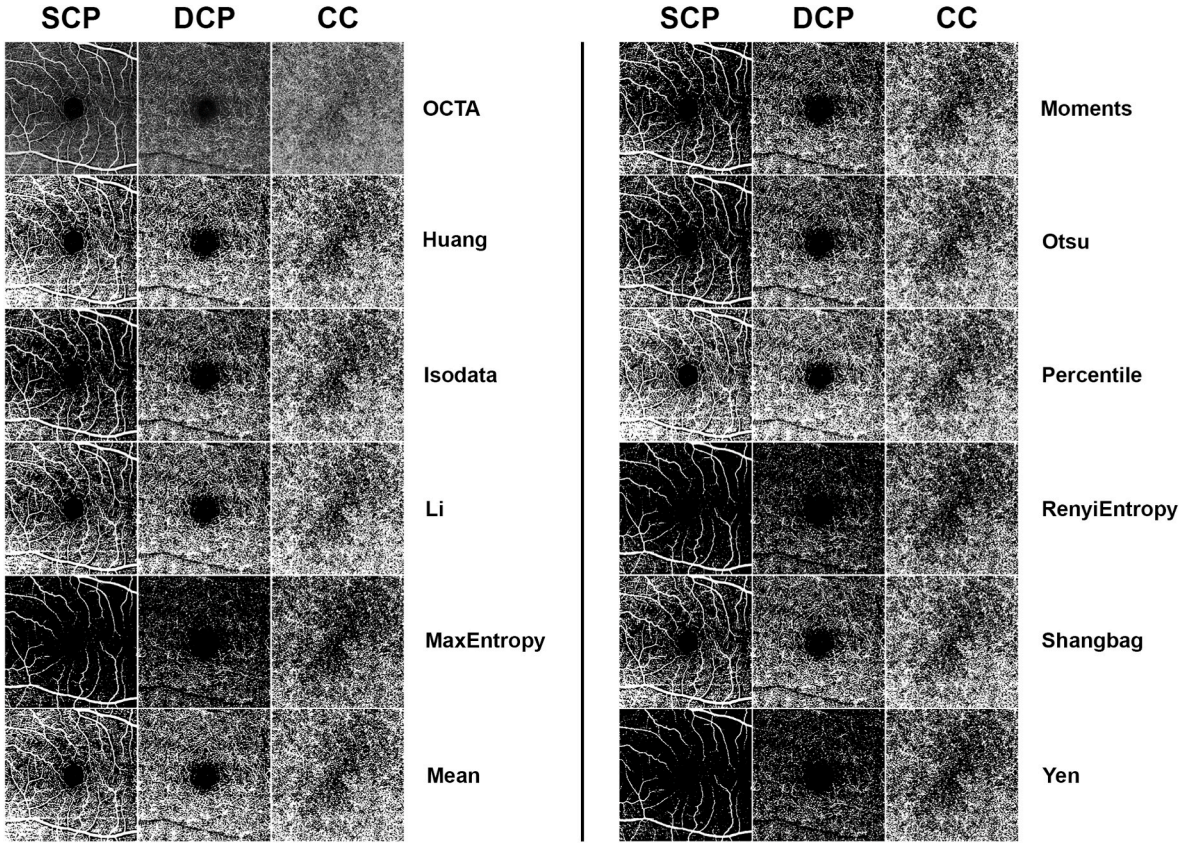

Fig. 13. The impact of different binarization thresholding approaches on OCTA reconstructions. The main thresholding approaches are shown in the figure, with the final outcomes on SCP, DCP and CC reconstructions. The first line corresponds to the original OCTA reconstructions.

Vessel density (VD) is probably the quantitative OCTA metric most often considered. It consists in calculating the ratio between white pixels (retinal capillaries) and black pixels (background) on the binarized OCTA reconstruction. Since FAZ area variability might affect the accuracy of the VD measurement, the segmented FAZ area is usually excluded from VD calculation. On account of its high feasibility and the fact it does not require great technical skill, VD is widely employed in all retinal and choroidal diseases. VD reliability depends on the precise recognition of segmentation boundaries, the absence of artifacts, and the binarization technique selected. Although VD is a very sensitive metric of perfusion, it cannot distinguish hypoperfusion from non-perfusion, thus giving low values in both cases (Spaide et al., 2018; Greig et al., 2020). VD is somehow useful in evaluating the distribution of perfusion within the volume of interest. Vessel length density (VLD) – the ratio between vessel length and unit area calculated on the skeletonized image – is another, similar metric (Lei et al., 2018). Skeletonization of the binarized image is an essential step in this regard. Skeletonization is the process used to reduce the dimension of an object to its medial axis, or skeleton, so as to distinguish its topological and geometrical features better (Saha et al., 2018). Many techniques can be used to obtain skeletonized images automatically; the ImageJ software package includes a reliable way to feasibly skeletonize OCTA images. Overall, the clinical contribution of VLD is similar to that provided by VD, understood as a measure of perfusion distribution. Unlike VD, VLD cannot be applied to the porous structure of the CC.

Another, but less tested OCTA metric is the vessel diameter index (VDI), which refers to the average vessel caliber and is calculated by dividing the total vessel area in the binarized reconstruction by the total vessel length in the skeletonized image (Borrelli et al., 2018a,b).

Many studies have proposed different quantitative methodologies to investigate the complexity of vascular networks. Fractal dimension (FD) is probably the oldest and is a geometrical index of branching complexity that can be applied to vascular microanatomy, calculated on the skeletonized OCTA reconstructions (Zahid et al., 2016). FD has been found to be lower in fundus diseases than in healthy controls and correlated with disease progression (Zahid et al., 2016; Bhardwaj et al., 2018). As in VLD, FD reliability depends on the quality of the binarization and skeletonization steps, and cannot be used to analyze choriocapillaris (CC) features. Moreover, FD requires optimal image resolution to detect objects' borders properly (Napolitano et al., 2012); this might prove challenging in the case of the very small capillaries characterizing the intraretinal vascular networks. Other metrics developed to analyze skeletonized images include the vessel diameter index, vessel perimeter index, and vessel complexity index, proposed by Chu et al. (2016). However, probably due to the high technical complexity of the calculation, to the best of our knowledge these metrics have not been widely reproduced in other studies, thus constituting a low level of evidence.

Our own proposed OCTA metric, namely vessel tortuosity (VT), represents an attempt to overcome the resolution-related limitations of FD. This metric takes as its measure the Euclidean distance between the two furthest points in the skeletonized images of the SCP and DCP (Arrigo et al., 2018). To extract VT, Arrigo et al. used the ImageJ pipeline: Analyze - > Skeleton - > Analyze Skeleton. The theoretical assumption behind the interpretation of VT is the fact that intraretinal capillaries are negligibly affected by the vessel walls, thus establishing a direct relationship between VT values and blood flow perfusion (Arrigo et al., 2018). Arrigo and co-workers also tested the VT metric on AMD-related MNV, proposing a quantitative cutoff value of 8.40 as the dividing line between two clinically different subgroups of patients (Arrigo et al., 2020f; Arrigo et al., 2020g). Eyes exhibiting MNV VT values > 8.40 were associated with a significantly higher onset of outer retinal atrophy and worse outcome than eyes with MNV VT < 8.40. This cutoff proved to be applicable in type 1, type 2 and mixed type MNV forms, suggesting their closer relationship with MNV blood flow features rather than their anatomical localization. More perfused neovascular networks, as revealed by high MNV VT values, were associated with more aggressive and vision-threatening lesions. This metric has also been successfully tested in MNV secondary to other macular diseases, and was found a useful parameter in monitoring MNV evolution during treatment (Arrigo et al., 2021f). The combined use of OCTA and dye-based angiography revealed completely different pathogenic characteristics of AMD-related MNV, always applying an MNV VT cutoff of 8.40 as the discriminating factor. Indeed, neovascular lesions characterized by MNV VT < 8.40 were more exudative at the baseline but less damaging to the outer retinal structures after a 1-year follow-up, whereas lesions displaying MNV VT > 8.40 proved to be less exudative but more likely to lead to outer retinal atrophy and visual decline (Arrigo et al., 2021g).

Vessel dispersion (Vdisp) was developed as a measure of intraretinal vascular network disorganization – a gauge of the standard deviation of the Gaussian distribution of a given vascular network obtained from the ImageJ pipeline: Analyze - > Directionality - > Fourier components method - > Dispersion calculation (Arrigo et al., 2018). It was interesting to test this metric on OCTA reconstructions obtained from eyes affected by intermediate and advanced AMD stages. Arrigo and colleagues found the Vdisp value increased progressively as the AMD stages advanced (Arrigo et al., 2018).

Vessel rarefaction (VR) was developed to measure how distant vessels are from each other in a given vascular network (Arrigo et al., 2018). Mesh hole analysis, available in ImageJ (Hotaling et al., 2015), was used to automatically detect and count all black pixels in discrete clusters between vessels, then extract a mean area (D'Amore et al., 2010; Tomba et al., 2010). Once again, high VR values were associated with progressively worsening AMD stages (Arrigo et al., 2018).

Compared with the remarkable contribution of VT in analyzing MNV morpho-functional properties, Vdisp and VR turned out to be less useful in providing clinically relevant information regarding the neovascular network (Arrigo et al., 2020f; Arrigo et al., 2020g; Arrigo et al., 2021g; Arrigo et al., 2021h). Conversely, the combined use of VD, VT, Vdisp and VR in analyzing intraretinal vascular network properties proved useful in distinguishing different vascular patterns, both in Stargardt disease and retinitis pigmentosa. More specifically, high VD and VT, together with low Vdisp and VR, were significantly more successful prognostic factors in both retinal dystrophies (Arrigo et al., 2019b, 2019c). The intriguing findings obtained from fundus diseases may act as a stimulus to also test these new OCTA metrics in systemic vascular disorders, to assess their potential diagnostic role in evaluating the risk of disease progression, as well as the onset of cardiovascular and cerebrovascular complications.

In addition to the standard OCTA-related limitations, these new metrics also experience the drawbacks associated with their application in biplanar OCTA reconstructions. From this point of view, it would be interesting to test these metrics in tridimensional OCTA reconstructions (Spaide et al., 2015; Borrelli et al., 2020). Although these approaches do not provide sufficiently high-resolution reconstructions yet, the future optimization of the tridimensional rendering algorithms would enable even more detailed quantitative OCTA studies to be carried out. It is worth pointing out, in addition, that VT, Vdisp and VR cannot be applied to the sponge-like structure of the CC.

Fewer quantitative metrics have been developed for the CC plexus; VD thus remains the gold-standard quantitative OCTA parameter (Ferrara et al., 2016). Flow voids are a very interesting form of early CC alteration (Choi et al., 2015; Spaide, 2017; Lejoyeux et al., 2022). These are early-appearing spots of lack of blood flow signal in the sponge-like structure of the CC, occurring earlier than the extensive CC disruption (Choi et al., 2015; Spaide, 2017; Lejoyeux et al., 2022). CC flow voids were the object of the quantitative metric known as CC porosity (CCP), previously used to reveal early CC alterations occurring in the subclinical stage of Best vitelliform macular dystrophy (Parodi et al., 2020a).

When applied to the borders of the atrophic lesion, the evaluation of CC flow impairment proved useful in geographic atrophy to assess the

rate of progression (Nassisi et al., 2019a, 2019b). Moreover, CCP helped detect CC alterations occurring before the onset of MNV in AMD (Arrigo et al., 2022). CCP is calculated on the binarized CC reconstruction by applying a threshold selectively highlighting the black signal of the image, and the percentage area of flow voids is then calculated (Parodi et al., 2020a; Arrigo et al., 2022). It is very important to segment and exclude from the calculation all the possible sources of masking artifacts, including retinal vessels, drusen, and other retinal debris. This step is potentially prone to calculation bias secondary to the remaining presence of possible masking factors. Interestingly, CCP proved statistically significant without a concomitant significant reduction of CC VD; this suggests CCP has a higher sensitivity in detecting very early CC impairment than CC VD, which requires more extensive damage. However, CCP's potential as an OCTA quantitative metric is relatively unexplored, and thus requires more extensive studies to assess its role in retinal diagnostics. All the above-mentioned papers highlighted how important the evaluation of inner choroidal impairment in fundus diseases is. The quantitative evaluation of choroidal and CC interfaces may reveal useful earlier alterations that can be used in the diagnostic workup of fundus disorders. However, as excellently highlighted by Borrelli and colleagues, it can prove difficult to evaluate both the inner choroid and CC because of the presence of segmentation errors, projection artifacts and shadowing artifacts (Borrelli et al., 2018a,b). Indeed, the probability of encountering biases increases as the analyzed structures are deeper and the number of disease-related fundus alterations greater. For this reason, it is to be hoped that further technical advances will provide improved reliability when analyzing deeper structures, and that specialists will agree on a standardized analysis. An intriguing approach to compensate for the shadowed CC signal has been proposed by Zhang and colleagues, who adopted the structural information obtained from enface reconstruction of the CC to detect the regions of attenuated signal and to compensate for them in the final OCTA CC reconstruction (Zhang et al., 2018). Although applied in a small cohort of twelve eyes, this approach provided a potentially stable and reliable way to quantify CC flow voids.

In addition, Arrigo et al. have recently proposed a quantitative intensity analysis of the MNV network that focuses on detecting primary and secondary capillary branches in neovascular lesions (Arrigo et al., 2021i). The theoretical assumption was that MNV reflectivity offers an indirect estimate of perfusion. Arrigo and colleagues found a good match between OCTA reconstruction and dye-based angiographic findings in the early phases. However, as already found in previous investigations, the MNV network was found to be larger on late phase FA/ICGA angiography than on OCTA (Told et al., 2018). Interestingly, this size gap involved the regions displaying low reflectivity on OCTA, thus suggesting that this gap affects MNV regions with perfusion profiles outside the range of OCTA sensitivity. Hence, although MNV reflectivity represents a novel quantitative metric, it might have a useful role in assessing perfusion and filling features of OCTA reconstructions.

Aside from the various advantages and potential pitfalls, all the OCTA parameters described above share the same need to work on the final segmented OCTA reconstruction of SCP, DCP and CC. It is therefore essential to work with high-quality images, reliable segmentations of corresponding retinal slabs, and a minimum of artifacts. To investigate quantitative OCTA features from a different point of view, Arrigo and coworkers have recently developed and proposed three quantitative metrics dedicated to the direct analysis of blood flow intensity signal on the b-scan OCTA volume. Arrigo et al. named these parameters total flow intensity (TFI), active flow intensity (AFI) and volume-related flow intensity (VFI) (Arrigo et al., 2021j). Arrigo and colleagues developed the algorithm to extract these parameters, considering SCP and DCP separately. For this reason, it was essential to select and verify the corresponding retinal slabs, although it was not necessary to obtain the SCP and DCP network reconstructions. TFI is defined as the measure of the amount of volumetric blood flow in SCP and DCP, computed as the sum of the squared voxel flow intensity; it is the overall measure of OCTA signal intensity. AFI is the measure of the average blood flow over all "active" voxels in SCP and DCP, computed by also taking into account the number of voxels showing a flow signal. Indeed, AFI can be considered a voxel-specific measure of the intensity of the blood flow signal passing through SCP and DCP. VFI is defined as the measure of the ratio between a retinal layer TFI and the corresponding volume that does not exhibit flow activity in SCP and DCP. Hence, VFI was developed to consider the perfused volume as a factor for assessing the ratio between the amount of blood flow signal and the volume of interest. In healthy eyes, these metrics are able to explain a contradictory finding regarding the VD parameter. For healthy VD values in DCP are often found to be comparable to or higher than in SCP, although SCP is known to have a bigger network, with a greater flow than DCP (Gadde et al., 2016; Campbell et al., 2017). The SCP-DCP VD contradiction might be explained by the fact that VD calculation is based on planar reconstructions, and does not consider the contribution of different retinal volumes in the two plexa, thus causing a potential overestimation of the DCP. In contrast, these novel parameters were found to be higher in SCP than in DCP, suggesting a more reliable assessment of intraretinal vascular status. Furthermore, Arrigo and colleagues tested these metrics in a small cohort of eyes affected by Stargardt disease as proof of concept. Once again, TFI, AFI and VFI over performed the quantitative vascular assessment of VD, providing more likely estimates of vascular impairment occurring in Stargardt disease (Arrigo et al., 2021j). Although promising, TFI, AFI and VFI are anyhow prone to several OCTA-related limitations, especially those that detect only the blood flow signal lying within the OCTA device's sensitivity range. These are novel OCTA quantitative metrics and need further validations to determine their utility in clinical and research contexts. The quantitative OCTA metrics discussed are summarized in Table 7 and in Fig. 14.

4. Imaging artifacts: classification and suitable action

Artifacts constitute an unavoidable challenge for all imaging techniques. Their presence may cause problems in interpreting the images' findings properly and lead to potentially severe quantitative biases. Although artifacts can affect all the imaging methodologies described above, their impact on OCT-based approaches is the most severe. Indeed, compared with fundus imaging, OCT-based techniques require a longer acquisition time and greater patient collaboration. For all these reasons, considerable efforts have been made to reduce or avoid imaging artifacts. The techniques used in addressing the problem of artifacts include tools to apply during image acquisition and others more suited to post-processing acquired data. One of the key factors in successful image acquisition is eye-tracking, which is a way of obtaining reference coordinates, usually from an infrared fundus image, to follow and correct eye movements and fixation loss, and to facilitate the process of co-registration of consecutive acquired images. The introduction and rapid evolution of eye-tracking technology has had an extremely positive impact on the quality of the images (Lauermann et al., 2017). Unfortunately, operators cannot blindly rely on eye-tracking to obtain good images, since it has been demonstrated that the quality of the images is directly related to acquisition time (Obuchowicz et al., 2019). Lengthy acquisition times do not allow eye-tracking to properly compensate for eye movements, thus providing poor quality data.

Although several attempts have been made to investigate the prevalence and impact of artifacts on image quality and quantitative results (Enders et al., 2019; Holmen et al., 2020), no definite conclusions have been drawn as yet. When considering imaging data, we should always assume the presence of at least one artifact in most of the dataset, with variable impact on the reliability of the quantitative approaches. Similarly, various attempts have been made to classify OCT and OCTA imaging artifacts (Spaide et al., 2015, 2018; Anvari et al., 2021), but the list continues to grow and the classification thus requires constant updating.

In view of this, we would like to propose a way of collecting and classifying imaging artifacts based on their primary origin. Let us assume

Table 7
Quantitative OCTA metrics. The following abbreviations are used: superficial capillary plexus (SCP), deep capillary plexus (DCP), choriocapillaris (CC), macular neovascularization (MNV).

OCTA parameter	Acronym	Definition	Interpretation	Sensitivity	Specificity	Pitfalls of measurement
Foveal avascular zone area	FAZ area	Capillary-free region localized at the margin of the fovea both at the level of SCP and DCP	Physiologic finding: FAZ area enlargement interpreted as early sign of reduced macular perfusion	Highly sensitive for detecting perfusion reduction	Not specific; FAZ area enlarged almost in all retinal diseases; FAZ area reduced in vitreoretinal tractions, foveal hypoplasia and retinopathy of prematurity	Poor detection of borders; not standardized manual or automatic segmentation; high inter-subjects variability
Vessel density	VD	Capillaries/background ratio applicable to intraretinal capillary networks and choriocapillaris	Considered a measure of perfusion reduction/non-perfusion	Highly sensitive for detecting perfusion reduction	Not specific; VD reduced almost in all retinal diseases	Errors related to not precise segmentation or artifacts; dependance from the binarization technique
Vessel length density	VLD	Vessel length/unit area ration calculated on the skeletonized image	Considered a measure of perfusion distribution in the volume of interest	Highly sensitive for detecting perfusion reduction	Not specific; VLD reduced almost in all retinal diseases	Errors related to not precise segmentation or artifacts; dependance from the binarization technique
Vessel diameter index	VDI	Obtained by dividing the total vessel area in the binarized image by the total vessel length in the skeletonized image	Considered a measure of the average vessel caliber	Sensitive for detecting vascular network changes	Not specific	Errors related to not precise segmentation or artifacts; dependance from the binarization technique
Fractal dimension	FD	Geometrical index of branching complexity that can be applied to vascular microanatomy, calculated on the skeletonized image	Considered a measure of perfusion disorganization	Sensitive for detecting perfusion reduction	Not specific; FD reduced almost in all retinal diseases	Errors related to not precise segmentation or artifacts; dependance from the binarization and skeletonization techniques; limited resolution for resolving smaller capillaries
Vessel tortuosity	VT	Measure of the Euclidean distance between two extreme points	Considered a measure of amount of perfusion	Highly sensitive for detecting perfusion changes	Not specific; VT reduced almost in all retinal diseases; VT changes resulted associated with MNV activity	Errors related to not precise segmentation or artifacts; dependance from the binarization and skeletonization techniques
Vessel Dispersion	Vdisp	Measure of the standard deviation of the Gaussian distribution of a vascular network	Considered a measure of the space-filling of a given vascular network, providing information about its disorganization	Sensitive for detecting perfusion reduction	Not specific; Vdisp increased almost in all retinal diseases	Errors related to not precise segmentation or artifacts; dependance from the binarization and skeletonization techniques
Vessel Rarefaction	VR	Measure of the mean distance among vessels	Considered a measure of the amount of rarefaction of the vascular network	Sensitive for detecting perfusion reduction	Not specific; VR increased in retinal diseases	Errors related to not precise segmentation or artifacts; dependance from the binarization technique
Choriocapillaris Porosity	CCP	Measure of the flow voids of the CC	Considered a measure of the early impairment of CC	Highly sensitive for detecting perfusion changes	Not specific	Errors related to segmentation or artifacts; possible biases related with masking or attenuation effects
MNV Reflectivity	–	Measure of reflectivity intensity of the MNV network	Considered an indirect assessment of the perfusion distribution interesting the central and the peripheral branches of the MNV network	Sensitive for assessing perfusion and filling features of intraretinal vessels	Not specific	Errors related to segmentation or artifacts; possible biases related with masking or attenuation effects
Total flow intensity	TFI	Measure of the amount of volumetric blood flow in SCP and DCP	Considered a measure of the intensity of blood flow signal passing through SCP and DCP	Only methodological paper available; to be assessed by further studies		
Active flow intensity	AFI	Measure of the average blood flow over all 'active' voxels in SCP and DCP	Considered a voxel-specific measure of the intensity of blood flow signal passing through SCP and DCP	Only methodological paper available; to be assessed by further studies		
Volume-related flow intensity	VFI	Measure of the ratio between a retinal layer TFI and the corresponding volume that does not exhibit flow activity in SCP and DCP	Considered an overall meausre of the perfusions state of SCP and DCP	Only methodological paper available; to be assessed by further studies		

that three types of artifacts are present: those associated with patient collaboration and fixation, those linked to the limitations of current technologies, and those related to disease-related altered retinal morphology. The main artifacts affecting OCT and OCTA images, based on what emerges from the current literature (Spaide et al., 2015, 2018; Pierro et al., 2017; Kashani et al., 2018; Anvari et al., 2021; Hormel et al., 2021a), are set out in Table 8. These three types of artifacts should not be considered separately; they may be intricately interconnected, cumulatively exerting a negative effect on the final quality of the images. A typical case concerns the segmentation artifact; this can be

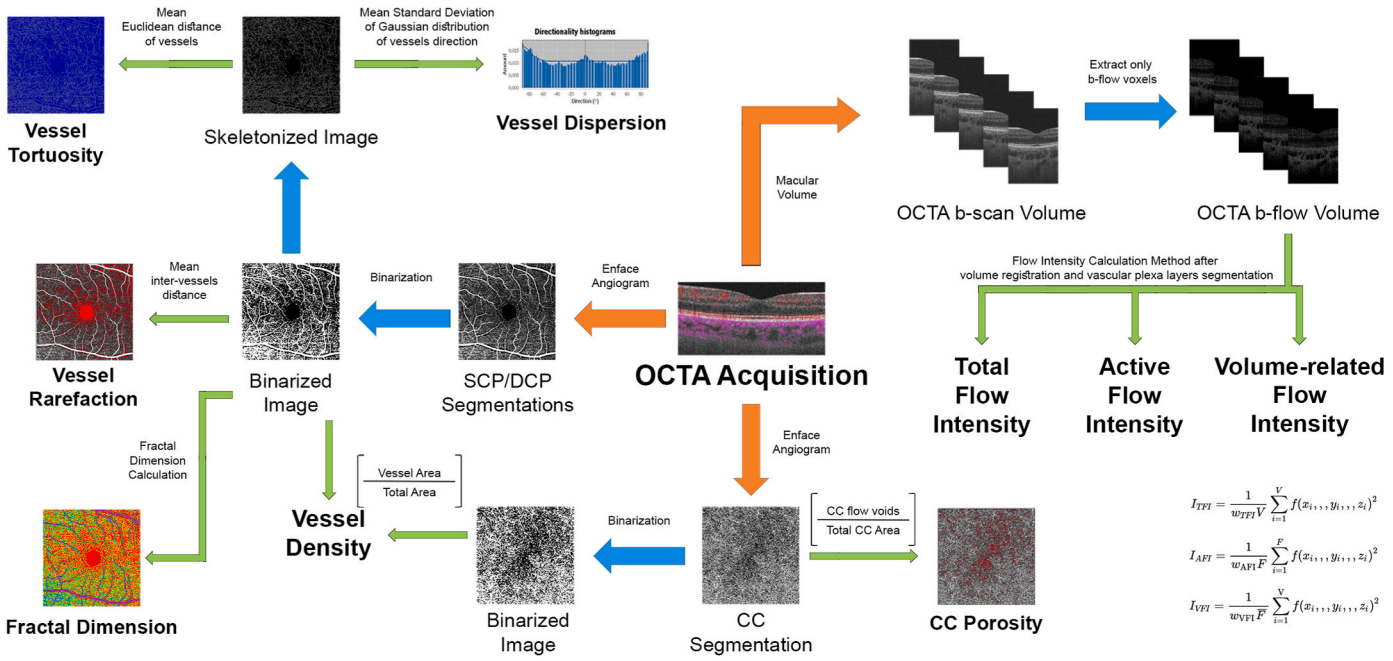

Fig. 14. Schematic representation of the main OCTA quantitative metrics. Orange arrows indicate the approaches used in the analyses, based on enface angiogram reconstructions of the raw macular volume. Blue arrows show the pre-processing steps to be performed before calculating the OCTA metrics. Green arrows lead to the final OCTA metrics (in bold).

caused either by poor fixation or excessive disease-related alterations of retinal morphology. In most cases, the effect of the artifacts can be mitigated, while maintaining a variable influence on the final qualitative and quantitative analyses. When it comes to the manual correction of the segmentations or the images, the outcome will depend on the expertise of the operators. Similarly, several projection removal algorithms designed to eliminate the projected false vessels from deeper OCTA reconstructions have been tested (Zhang et al., 2016; Ashraf et al., 2020a; Hormel et al., 2021c). However, in many cases, the removal of the projections is associated with partial loss of deeper capillaries or regions of flow voids, thus leading to potential underestimations. Artificial intelligence-based approaches designed to automatically recognize and compensate imaging artifacts have also been tested in this field (Lauermann et al., 2019; Hormel et al., 2021b; Le et al., 2021).

Further potentially relevant artifacts include "suspended scattering particles in motion", in other words particles of various origin, such as lipid lobules, which may mimic the flow signal, thus producing a spurious signal on OCTA (Kashani et al., 2018). Similarly, several retinal lesions, including hard exudates and drusen, may be the source of a micro movement signal, wrongly interpreted as blood flow by OCTA (hence known as pseudo flow) (Hou et al., 2019).

At all events, in our opinion once the presence of artifacts has been established, these will inevitably affect the subsequent qualitative and quantitative analyses, quite independently of any kind of image manipulation. This is why we advocate the development of a standardized imaging artifact grading system able to adequately address the problem of artifacts and to apply corrective coefficients to the final result.

5. current limitations and future perspectives in quantitative multimodal imaging

Bearing in mind all the topics discussed above, it is clear that quantitative multimodal imaging is undoubtedly subject to a number of potential limitations. The most important pitfall in quantitative multimodal imaging is the lack of standard rules developed by international experts. As things stand, researchers in the field of quantitative metrics can count only on good practice advice arising from spontaneous studies. This means that in many cases quantitative studies performed in the same field are not easy to compare, owing to the different quantitative methodologies adopted. Similarly, although multimodal imaging techniques are considered highly reproducible, the possible effect of inter-device variability on quantitative metrics has not been fully addressed yet. Any variations in data deriving from different multimodal imaging devices might make quantitative studies poorly comparable to each other.

In addition, the presence of imaging artifacts still represents a major source of potentially severe biases. In this case too it would be useful to develop a standard guide to imaging artifacts. Moreover, most multimodal imaging techniques work very well at the posterior pole, but are not really up to the task of assessing peripheral retinal alterations. The introduction of reliable wide field multimodal imaging technologies would be helpful if bridging this gap. Further advances in multimodal imaging might include optimizing eye-tracking correction algorithms, higher acquisition speeds and image resolution, and the development of entirely new imaging techniques.

As seen in other research contexts, employing artificial intelligence-based approaches will undoubtedly lead to breakthroughs in the field of ophthalmology. In the meantime, artificial intelligence remains a proof-of-concept endeavour, rather than a bid to find a practical solution, and as such inaccessible to most research groups. Artificial intelligence-based approaches require very large datasets, reliable quantitative metrics, and considerable computational power. For this reason, until national and international network databases linked to high performance servers are created, and standard quantitative metrics achieved, artificial intelligence will be unable to attain a meaningful presence in the field of ophthalmology. In any case, there is no denying that ophthalmology has always prided itself on its familiarity with high technology. This is why, now more than ever, it is essential to establish multidisciplinary groups, drawing together ophthalmologists, engineers, mathematicians, physicists, and other specialists, who can use their different perspectives to ensure quantitative approaches reach the next stage in their scientific development.

Table 8
Main artifacts in OCT and OCTA imaging.

Artifact group	Imaging artifact	Definition	Main source	Main effect	Possible correction
Patient-related	Degraded image	Presence of any source of obstacle/disturbance in the proper acquisition of image signal	Media opacities (cataract, corneal defects, floaters, other vitreous anomalies)	In most of the cases a masking effect on the final image or reconstruction; quantitative underestimation	Repeat scan; use the averaged result of multiple scans
	Misregistered scans	Pitfalls in the co-registration process regarding consecutive images of the same slab or consecutive slabs of the same volume	Media opacities, poor fixation, poor collaboaration, no eye-tracking or obsolete technology	Poor quality of the averaged image of the same slab; misregistered retinal volume with misaligned inter-scans boundaries; bias on quantitative analysis	Repeat scan
	Cut edge	Lack of part of the image	Poor fixation, poor collaboaration, no eye-tracking or obsolete technology	Lost of part of the information; bias on quantitative analysis	Repeat scan
	Off center	Decentration of the image	Poor fixation, poor collaboaration, no eye-tracking or obsolete technology, no centration check before acquistion	Unproper representation of the region of interest; bias on quantitative analysis	Repeat scan
	Motion	Image's artifacts related with the excessive motion of the eye during the acquisition	Poor fixation, poor collaboaration, no eye-tracking or obsolete technology	Unproper representation of the region of interest; source of other artifacts (segmentation, vessel doubling, cutted images, etc.); bias on quantitative analysis	Repeat scan; use the averaged result of multiple scans with masking effect correction
	Blinking	Image's artifacts related with the excessive blinking	Dry eye or other sources of excessive blinking	Tipically horizontal bar-like artifact with loss of information; bias on quantitative analysis	Repeat scan trying to reduce patient's distress
Technology-related	Segmentation	No recognition/ misrecognition of segmentation boundaries	Poor fixation, poor collaboration, no eye-tracking or obsolete technology, excessive disease-related morphological disruption of the retina (PED, retinal detachment, extensive fibro-vascular scar, proliferations, fluids, debris, bleeding), masking effects	Unproper recognition of retinal layers, intraretinal vascular network; bias on quantitative analysis	Repeat scan, manual correction of segmentation boundaries
	Projection	False vessels originating from superficial retinal vessels which can appear in deeper retinal layers	OCTA-related artifact related with the misrecognition of superficial motion signal in deeper retinal sectors, obsolete projection artifact removal algorithms	Unproper OCTA reconstructions; bias on quantitative analysis (usually overestimation)	Adoption of projection artifact removal tools included in OCTA manifacturer software, manual correction of segmentation boundaries
	Mirror	Reflection of OCT retinal reconstruction onto itself	Described in high myopia, it represents the misreconstruction of the peripheral part of OCT image caused by the excessive curvature of the eye	Structural OCT inverted image, lack of OCTA reconstruction, bias on quantitative analysis (usually underestimation)	Poor ways to correct it, manual correction of segmentation boundaries might help in limited cases
	Suspended scattering particles in motion	Presence of OCTA motion signal outside retinal capillaries, interpreted by OCTA as blood flow	Presence of suspended particles with light scattering properties	Blurred OCTA signal, bias on quantitative analysis (usually overestimation)	Post-processing approaches to reduce or eliminate spurious signal, preserving intraretinal vascular network reconstructions
	Blood flow speed	Misdetection/no detection of blood flow signal outside the sensitivity range of OCTA devices	Too fast or too slow blood flows not properly detected by OCTA acquisitions	Lack of information, high variability among consecutive OCTA scans, bias on quantitative analysis	Use the averaged result of multiple scans
Disease-related	Window effect	Excessive passage of laser light caused by the disruption/absence of RPE and choroidal hypertransmission	Reduced light absorption from the damaged/lacking RPE	Excessive hyperreflectivity of the choroid with unproper recognition of choroidal vessels, influence of choroidal vessels on OCTA reconstructions, bias on quantitative analysis	Manual correction, exclusion of choroidal hypertransmission area, exclusion of OCTA reconstruction of choroidal vessels
	Shadow effect	Attenuation of the signal/ complete shadowing of the retinal structures situated below the shadowing source	Associated with the following shadowing sources: retinal blood vessels, dense blood deposits, cotton wool exudates, hard exudates, RPE hyperplasia, intraocular foreign body, pigmented scar, choroidal nevi, fibro-vascular membranes, retinal hamartoma, calcium debris, others	Lack of information, bias on quantitative analysis	Poor ways to correct it, manual correction and exclusion of the interested region

6. Future progress in multimodal imaging

There are certain to be further advances in multimodal imaging techniques in the coming years, both in terms of the examination methods and in post-processing techniques. Research efforts are concentrating mainly on developing diagnostic techniques in what amount to functional investigations, rather than on morphological approaches.

We have discussed at length the importance of quantifying melanin in the human retina and the contribution of NIR imaging

(Lapierre-Landry et al., 2018a). Photoacoustic imaging, an ultrasound-based approach to melanin-specific assessment able to detect and quantify melanin within the retina, seems a promising prospect (Liu and Zhang, 2016). When irradiated by a short laser pulse, the optical energy absorbed by melanin is converted into heat, thus generating wideband ultrasonic waves that can be collected by a detector (Liu et al., 2015). This introduces the interesting possibility of combining this imaging modality with fundus cameras, and NIR and OCT technologies, as has been shown in animal models (Liu et al., 2012, 2013, 2015). Similarly, melanin could be quantified by means of polarization-sensitive OCT, which is a non-invasive way of analyzing the birefringence of a retinal sample (Pircher et al., 2011). In this case, the scattering properties of the analyzed samples were found to be related to both the melanin content and the size and shape of the melanin granules (Baumann et al., 2012).

Another promising OCT-based approach is known as photothermal OCT. The theoretical assumption in this diagnostic modality is the observation that the photons absorbed by a given contrast agent are re-emitted as heat due to the photothermal effect (Skala et al., 2008). By combining an amplitude-modulated laser with a phase-sensitive OCT device it is possible to measure the concentration and distribution of melanin in a zebrafish model, by analyzing its absorption peak (Lapierre-Landry et al., 2018b).

When using OCT-based technologies, it should always be borne in mind that backscattered light can provide useful information regarding the properties of retinal tissues. This is what lies behind the development of a technique called directional OCT, which is able to measure the magnitude and directional scattering of the RPE layer, correlating this signal with the concentration of melanin (Meleppat et al., 2019; Ni et al., 2022).

Looking at new technologies for assessing retinal vessels, optical coherence photoacoustic microscopy may represent a promising approach. As described above, optical coherence photoacoustic microscopy is based on the physical principle that the optical energy absorbed by a given sample, in this case hemoglobin, is converted into heat (Liu et al., 2015). It has been shown in animals that it is possible in this way to obtain very detailed reconstructions of retinal vessels (Nguyen et al., 2018). The outcome of this diagnostic modality can be further improved by using colloidal gold nanoparticles as a contrast agent (Nguyen et al., 2019).

These are just a few of the latest techniques, but they give an idea of the sheer speed of technological growth in multimodal imaging. In many cases, the new imaging modalities are based on OCT technology, since it is hard to suppose that other modalities could achieve similar levels of accuracy and resolution. For the moment, these approaches represent solutions that are far from finding an effective clinical application, owing to the considerable technical requirements and the need for validation and artifact assessment. Sometimes, despite the intriguing theoretical principles underlying these novel approaches, they are unable to improve on the performance of current diagnostic technologies, thus bringing development to a halt. Even so, we are likely to witness the introduction of new and potentially interesting multimodal imaging modalities in clinical and research contexts in the coming years.

7. Conclusions

In conclusion, in this survey we have provided what we hope is a comprehensive overview of the current state of the art and the future prospects regarding quantitative multimodal imaging. Multimodal imaging has radically changed the diagnostics of fundus diseases and has enabled morpho-functional retinal features to be investigated from different points of view.

We have good reason to be enthusiastic about the high standard of accuracy and detailing already achieved both in clinical and research contexts. There are sure to be interesting advances in quantitative multimodal imaging in the near future, reinforced by the evolution of imaging technologies and the development of even more sophisticated quantitative metrics. Standardized guidelines, international consensus among experts on the uses of the technologies, and a uniform terminology are urgent needs in the present.

Author statement

The corresponding author (AA) is responsible for ensuring that the descriptions are accurate and agreed by all authors.

AA, EA: manuscript conceptualization, literature review, original draft preparation.

MBP, FB: literature review, reviewing and editing of the draft, supervision.

Funding

This research did not receive any specific grant from funding agencies in the public, commercial, or not-for-profit sectors.

Declaration of competing interest

Prof. Francesco Bandello is consultant for Abbvie, Alimera, Bayer, Boehringer-Ingelheim, Fidia Sooft, Hofmann La Roche, Novartis, Ntc Pharma, Oxurion Nv, Sifi. All other authors have no conflict of interest to declare.

Data availability

Data will be made available on request.

Acknowledgements

The authors wish to acknowledge the long-standing collaboration with Julian Comoy, Alessio Antropoli, Lorenzo Bianco, Andrea Saladino and Cristian Perra.

References

Abdelfattah, N.S., Sadda, J., Wang, Z., Hu, Z., Sadda, S., 2020. Near-infrared reflectance imaging for quantification of atrophy associated with age-related macular degeneration. Am. J. Ophthalmol. 212, 169–174. https://doi.org/10.1016/j.ajo.2020.01.005.

Aboualizadeh, E., Hirschmugl, C.J., 2018. Highlighting IR spectrochemical imaging of the retina. Trends Biochem. Sci. 43 (9), 650–653. https://doi.org/10.1016/j.tibs.2018.04.005.

Abràmoff, M.D., Lavin, P.T., Birch, M., Shah, N., Folk, J.C., 2018. Pivotal trial of an autonomous AI-based diagnostic system for detection of diabetic retinopathy in primary care offices. NPJ Digit Med 1 (1), 39. https://doi.org/10.1038/s41746-018-0040-6.

Abràmoff, M.D., Lou, Y., Erginay, A., Clarida, W., Amelon, R., Folk, J.C., Niemeijer, M., 2016. Improved automated detection of diabetic retinopathy on a publicly available dataset through integration of deep learning. Invest. Ophthalmol. Vis. Sci. 57 (13), 5200–5206. https://doi.org/10.1167/iovs.16-19964.

Agrawal, R., Ding, J., Sen, P., Rousselot, A., Chan, A., Nivison-Smith, L., Wei, X., Mahajan, S., Kim, R., Mishra, C., Agarwal, M., Suh, M.H., Luthra, S., Munk, M.R., Cheung, C.Y., Gupta, V., grid, C.V.I., 2020. Exploring choroidal angioarchitecture in health and disease using choroidal vascularity index. Prog. Retin. Eye Res. 77, 100829 https://doi.org/10.1016/j.preteyeres.2020.100829.

Agrawal, R., Gupta, P., Tan, K.A., Cheung, C.M., Wong, T.Y., Cheng, C.Y., 2016. Choroidal vascularity index as a measure of vascular status of the choroid: measurements in healthy eyes from a population-based study. Sci. Rep. 6, 21090 https://doi.org/10.1038/srep21090.

Aiello, L.P., Odia, I., Glassman, A.R., Melia, M., Jampol, L.M., Bressler, N.M., Kiss, S., Silva, P.S., Wykoff, C.C., Sun, J.K., Diabetic Retinopathy Clinical Research Network, 2019. Comparison of early treatment diabetic retinopathy study standard 7-field imaging with ultrawide-field imaging for determining severity of diabetic retinopathy. JAMA Ophthalmol. 137 (1), 65–73. https://doi.org/10.1001/jamaophthalmol.2018.4982.

Anvari, P., Ashrafkhorasani, M., Habibi, A., Falavarjani, K.G., 2021. Artifacts in optical coherence tomography angiography. J. Ophthalmic Vis. Res. 16 (2), 271–286. https://doi.org/10.18502/jovr.v16i2.9091.

Arrigo, A., Amato, A., Barresi, C., Aragona, E., Saladino, A., Pina, A., Calcagno, F., Bandello, F., Battaglia Parodi, M., 2022. Choroidal modifications preceding the onset

of macular neovascularization in age-related macular degeneration. Ophthalmol Ther. 11 (1), 377–386. https://doi.org/10.1007/s40123-021-00443-1.

Arrigo, A., Antropoli, A., Bianco, L., Rosolia, A., Vuturo, A., Bandello, F., Parodi, M.B., 2021b. Hyperreflective foci precede macular neovascularization formation in angioid streaks. Retin. Cases Brief Rep. https://doi.org/10.1097/ICB.0000000000001201 [Online ahead of print].

Arrigo, A., Aragona, E., Bordato, A., Amato, A., Borghesan, F., Bandello, F., Parodi, M.B., 2021g. Quantitative optical coherence tomography angiography parameter variations after treatment of macular neovascularization secondary to age-related macular degeneration. Retina 41 (7), 1463–1469. https://doi.org/10.1097/IAE.0000000000003065.

Arrigo, A., Aragona, E., Bordato, A., Amato, A., Borghesan, F., Bandello, F., Battaglia Parodi, M., 2021h. Morphological and functional relationship between OCTA and FA/ICGA quantitative features in AMD-related macular neovascularization. Front. Med. 8, 758668 https://doi.org/10.3389/fmed.2021.758668.

Arrigo, A., Aragona, E., Bordato, A., Amato, A., Saladino, A., Bandello, F., Battaglia Parodi, M., 2021aa. High reflectivity and low reflectivity properties on OCTA influence the detection of macular neovascularization in AMD. Front. Phys. 9, 694035 https://doi.org/10.3389/fphy.2021.694035.

Arrigo, A., Aragona, E., Bordato, A., Amato, A., Saladino, A., Bandello, F., Battaglia Parodi, M., 2021i. High reflectivity and low reflectivity properties on OCTA influence the detection of macular neovascularization in AMD. Front. Physiol. https://doi.org/10.3389/fphy.2021.694035 [Online ahead of print].

Arrigo, A., Aragona, E., Capone, L., Lattanzio, R., Zollet, P., Bandello, F., 2021d. Foveal eversion: a possible biomarker of persistent diabetic macular edema. Ophthalmol Ther. 10 (1), 115–126. https://doi.org/10.1007/s40123-020-00324-z, 2021.

Arrigo, A., Aragona, E., Capone, L., Pierro, L., Romano, F., Bandello, F., Parodi, M.B., 2018. Advanced optical coherence tomography angiography analysis of age-related macular degeneration complicated by onset of unilateral choroidal neovascularization. Am. J. Ophthalmol. 195, 233–242. https://doi.org/10.1016/j.ajo.2018.08.001.

Arrigo, A., Aragona, E., Di Nunzio, C., Bandello, F., Parodi, M.B., 2020g. Quantitative optical coherence tomography angiography parameters in type 1 macular neovascularization secondary to age-related macular degeneration. Transl. Vis Sci. Technol. 9 (9), 48. https://doi.org/10.1167/tvst.9.9.48.

Arrigo, A., Aragona, E., Saladino, A., Amato, A., Bandello, F., Battaglia Parodi, M., 2021e. The impact of different thresholds on optical coherence tomography angiography images binarization and quantitative metrics. Sci. Rep. 11 (1), 14758 https://doi.org/10.1038/s41598-021-94333-y.

Arrigo, A., Bordato, A., Aragona, E., Amato, A., Viganò, C., Bandello, F., Battaglia Parodi, M., 2021f. Macular neovascularization in AMD, CSC and best vitelliform macular dystrophy: quantitative OCTA detects distinct clinical entities. Eye 35 (12), 3266–3276. https://doi.org/10.1038/s41433-021-01396-2.

Arrigo, A., Bordato, A., Romano, F., Aragona, E., Grazioli, A., Bandello, F., Battaglia Parodi, M., 2020c. Choroidal patterns in retinitis pigmentosa: correlation with visual acuity and disease progression. Transl. Vis Sci. Technol. 9 (4), 17. https://doi.org/10.1167/tvst.9.4.17.

Arrigo, A., Calamuneri, A., Aragona, E., Bordato, A., Grazioli Moretti, A., Amato, A., Bandello, F., Battaglia Parodi, M., 2021c. Structural OCT parameters associated with treatment response and macular neovascularization onset in central serous chorioretinopathy. Ophthalmol Ther. 10 (2), 289–298. https://doi.org/10.1007/s40123-021-00336-3.

Arrigo, A., Calamuneri, A., Bordato, A., Aragona, E., Pierro, L., Bandello, F., Battaglia Parodi, M., 2020d. Vitreomacular traction quantitative cutoffs for the assessment of resolution after ocriplasmin intravitreal treatment. Sci. Rep. 10 (1), 17583 https://doi.org/10.1038/s41598-020-74472-4.

Arrigo, A., Capone, L., Lattanzio, R., Aragona, E., Zollet, P., Bandello, F., 2020b. Optical coherence tomography biomarkers of inflammation in diabetic macular edema treated by fluocinolone acetonide intravitreal drug-delivery system implant. Ophthalmol Ther. 9 (4), 971–980. https://doi.org/10.1007/s40123-020-00297-z.

Arrigo, A., Grazioli, A., Romano, F., Aragona, E., Bordato, A., di Nunzio, C., Sperti, A., Bandello, F., Battaglia Parodi, M., 2019a. Choroidal patterns in Stargardt disease: correlations with visual acuity and disease progression. J. Clin. Med. 8 (9), 1388. https://doi.org/10.3390/jcm8091388.

Arrigo, A., Grazioli, A., Romano, F., Aragona, E., Marchese, A., Bordato, A., Di Nunzio, C., Sperti, A., Bandello, F., Parodi, M.B., 2020a. Multimodal evaluation of central and peripheral alterations in Stargardt disease: a pilot study. Br. J. Ophthalmol. 104 (9), 1234–1238. https://doi.org/10.1136/bjophthalmol-2019-315148.

Arrigo, A., Perra, C., Aragona, E., Giusto, D., Bandello, F., Battaglia Parodi, M., 2021j. Total flow intensity, active flow intensity and volume related flow intensity as new quantitative metrics in optical coherence tomography angiography. Sci. Rep. 11 (1), 9094. https://doi.org/10.1038/s41598-021-88681-y.

Arrigo, A., Perra, C., Aragona, E., Giusto, D., Doglioni, C., Pierro, L., Giordano Resti, A., Bandello, F., Battaglia Parodi, M., 2020e. Extrafoveal Müller cells detection in vivo in the human retina: a pilot study based on optical coherence tomography. Exp. Eye Res. 199, 108183 https://doi.org/10.1016/j.exer.2020.108183.

Arrigo, A., Romano, F., Albertini, G., Aragona, E., Bandello, F., Battaglia Parodi, M., 2019b. Vascular patterns in retinitis pigmentosa on swept-source optical coherence tomography angiography. J. Clin. Med. 8 (9), 1425. https://doi.org/10.3390/jcm8091425.

Arrigo, A., Romano, F., Aragona, E., Di Nunzio, C., Battista, M., Bandello, F., Battaglia Parodi, M., 2020f. Optical coherence tomography angiography can categorize different subgroups of choroidal neovascularization secondary to age-related macular degeneration. Retina 40 (12), 2263–2269. https://doi.org/10.1097/IAE.0000000000002775.

Arrigo, A., Romano, F., Aragona, E., di Nunzio, C., Sperti, A., Bandello, F., Battaglia Parodi, M., 2019c. OCTA-based identification of different vascular patterns in Stargardt disease. Transl. Vis Sci. Technol. 8 (6), 26. https://doi.org/10.1167/tvst.8.6.26.

Arrigo, A., Teussink, M., Aragona, E., Bandello, F., Battaglia Parodi, M., 2021ba. MultiColor imaging to detect different subtypes of retinal microaneurysms in diabetic retinopathy. Eye 35 (1), 277–281. https://doi.org/10.1038/s41433-020-0811-6.

Arslan, J., Samarasinghe, G., Benke, K.K., Sowmya, A., Wu, Z., Guymer, R.H., Baird, P.N., 2020. Artificial intelligence algorithms for analysis of geographic atrophy: a review and evaluation. Transl. Vis Sci. Technol. 9 (2), 57. https://doi.org/10.1167/tvst.9.2.57.

Arslan, J., Samarasinghe, G., Sowmya, A., Benke, K.K., Hodgson, L.A.B., Guymer, R.H., Baird, P.N., 2021. Deep learning applied to automated segmentation of geographic atrophy in fundus autofluorescence images. Transl. Vis Sci. Technol. 10 (8), 2. https://doi.org/10.1167/tvst.10.8.2, 2021.

Ashikawa, I., Nishimura, Y., Tsuboi, M., Watanabe, K., Iso, K., 1982. Lifetime of tyrosine fluorescence in nucleosome core particles. J. Biochem. 91 (6), 2047–2055. https://doi.org/10.1093/oxfordjournals.jbchem.a133898.

Ashraf, M., Sampani, K., Abu-Qamar, O., Cavallerano, J., Silva, P.S., Aiello, L.P., Sun, J. K., 2020a. Optical coherence tomography angiography projection artifact removal: impact on capillary density and interaction with diabetic retinopathy severity. Transl. Vis Sci. Technol. 9 (7), 10. https://doi.org/10.1167/tvst.9.7.10.

Ashraf, M., Shokrollahi, S., Salongcay, R.P., Aiello, L.P., Silva, P.S., 2020b. Diabetic retinopathy and ultrawide field imaging. Semin. Ophthalmol. 35 (1), 56–65. https://doi.org/10.1080/08820538.2020.1729818.

Bacherini, D., Mastropasqua, R., Borrelli, E., Capuano, V., Iovino, C., Dragotto, F., Caporossi, T., Rizzo, S., Giansanti, F., 2021. OCT-A in the management of vitreoretinal diseases and surgery. Asia Pac. J. Ophthalmol. (Phila). 10 (1), 12–19. https://doi.org/10.1097/APO.0000000000000373.

Bachilo, S.M., Gillbro, T., 1999. Fluorescence of retinal schiff base in alcohols. J. Phys. Chem. A 103 (15), 2481–2488. https://doi.org/10.1021/jp983646a.

Banda, H.K., Shah, A., Shah, G.K., 2019. Application of wide-field infrared reflectance imaging in retinoschisis, retinal detachments, and schisis detachments. Int. J. Retina. Vitreous 5 (Suppl. 1), 42. https://doi.org/10.1186/s40942-019-0188-5.

Barker, F.M. 2nd, Snodderly, D.M., Johnson, E.J., Schalch, W., Koepcke, W., Gerss, J., Neuringer, M., 2011. Nutritional manipulation of primate retinas, V: effects of lutein, zeaxanthin, and n-3 fatty acids on retinal sensitivity to blue-light-induced damage. Invest. Ophthalmol. Vis. Sci. 52 (7), 3934–3942. https://doi.org/10.1167/iovs.10-5898.

Batıoğlu, F., Demirel, S., Özmert, E., 2015. Fundus autofluorescence imaging in age-related macular degeneration. Semin. Ophthalmol. 30 (1), 65–73. https://doi.org/10.3109/08820538.2013.810285.

Battaglia Parodi, M., Iacono, P., Papayannis, A., Alto, G., Buzzotta, A., Arrigo, A., Cicinelli, M.V., Bandello, F., 2020. Near-infrared fundus autofluorescence in early age-related macular degeneration. Eur. J. Ophthalmol. 30 (6), 1448–1453. https://doi.org/10.1177/1120672119885047.

Baumann, B., Baumann, S.O., Konegger, T., Pircher, M., Götzinger, E., Schlanitz, F., Schütze, C., Sattmann, H., Litschauer, M., Schmidt-Erfurth, U., Hitzenberger, C.K., 2012. Polarization sensitive optical coherence tomography of melanin provides intrinsic contrast based on depolarization. Biomed. Opt Express 3 (7), 1670–1683. https://doi.org/10.1364/BOE.3.001670.

Bakhoum, M.F., Freund, K.B., Dolz-Marco, R., Leong, B.C.S., Baumal, C.R., Duker, J.S., Sarraf, D., 2018. Paracentral acute middle maculopathy and the ischemic cascade associated with retinal vascular occlusion. Am. J. Ophthalmol. 195, 143–153. https://doi.org/10.1016/j.ajo.2018.07.031.

Bax, N.M., Valkenburg, D., Lambertus, S., Klevering, B.J., Boon, C.J.F., Holz, F.G., Cremers, F.P.M., Fleckenstein, M., Hoyng, C.B., Lindner, M., Foveal Sparing Atrophy Study Team (FAST), 2019. Foveal sparing in central retinal dystrophies. Invest. Ophthalmol. Vis. Sci. 60 (10), 3456–3467. https://doi.org/10.1167/iovs.18-26533.

Berasategui, B., Fonollosa, A., Artaraz, J., Ruiz-Arruza, I., Ríos, J., Matas, J., Llorenç, V., Diaz-Valle, D., Sastre-Ibañez, M., Arriola-Villalobos, P., Adan, A., 2018. Behavior of hyperreflective foci in non-infectious uveitic macular edema, a 12-month follow-up prospective study. BMC Ophthalmol. 18 (1), 179. https://doi.org/10.1186/s12886-018-0848-5.

Bhardwaj, S., Tsui, E., Zahid, S., Young, E., Mehta, N., Agemy, S., Garcia, P., Rosen, R.B., Young, J.A., 2018. Value of fractal analysis of optical coherence tomography angiography in various stages of diabetic retinopathy. Retina 38 (9), 1816–1823. https://doi.org/10.1097/IAE.0000000000001774.

Bonilha, V.L., Bell, B.A., Hu, J., Milliner, C., Pauer, G.J., Hagstrom, S.A., Radu, R.A., Hollyfield, J.G., 2020. Geographic atrophy: confocal scanning laser ophthalmoscopy, histology, and inflammation in the region of expanding lesions. Invest. Ophthalmol. Vis. Sci. 61 (8), 15. https://doi.org/10.1167/iovs.61.8.15.

Borrelli, E., Balasubramanian, S., Triolo, G., Barboni, P., Sadda, S.R., Sadun, A.A., 2018a. Topographic macular microvascular changes and correlation with visual loss in chronic Leber hereditary optic neuropathy. Am. J. Ophthalmol. 192, 217–228. https://doi.org/10.1016/j.ajo.2018.05.029.

Borrelli, E., Sacconi, R., Parravano, M., Costanzo, E., Querques, L., Battista, M., Grosso, D., Giorno, P., Bandello, F., Querques, G., 2021. Optical coherence tomography angiography assessment of the diabetic macula: a Comparison Study Among Different Algorithms. Retina 41 (9), 1799–1808. https://doi.org/10.1097/IAE.0000000000003145.

Borrelli, E., Sacconi, R., Querques, L., Battista, M., Bandello, F., Querques, G., 2020. Quantification of diabetic macular ischemia using novel three-dimensional optical coherence tomography angiography metrics. J. Biophot. 11, 152. https://doi.org/10.1002/jbio.202000152.

Borrelli, E., Sarraf, D., Freund, K.B., Sadda, S.R., 2018b. OCT angiography and evaluation of the choroid and choroidal vascular disorders. Prog. Retin. Eye Res. 67, 30–55. https://doi.org/10.1016/j.preteyeres.2018.07.002.

Bringmann, A., Pannicke, T., Grosche, J., Francke, M., Wiedemann, P., Skatchkov, S.N., Osborne, N.N., Reichenbach, A., 2006. Müller cells in the healthy and diseased retina. Prog. Retin. Eye Res. 25 (4), 397–424. https://doi.org/10.1016/j.preteyeres.2006.05.003.

Campbell, J.P., Zhang, M., Hwang, T.S., Bailey, S.T., Wilson, D.J., Jia, Y., Huang, D., 2017. Detailed vascular anatomy of the human retina by projection-resolved optical coherence tomography angiography. Sci. Rep. 7, 42201 https://doi.org/10.1038/srep42201.

Cao, D., Leong, B., Messinger, J.D., Kar, D., Ach, T., Yannuzzi, L.A., Freund, K.B., Curcio, C.A., 2021. Hyperreflective foci, optical coherence tomography progression indicators in age-related macular degeneration, include transdifferentiated retinal pigment epithelium. Invest. Ophthalmol. Vis. Sci. 62 (10), 34. https://doi.org/10.1167/iovs.62.10.34.

Carpineto, P., Mastropasqua, R., Marchini, G., Toto, L., Di Nicola, M., Di Antonio, L., 2016. Reproducibility and repeatability of foveal avascular zone measurements in healthy subjects by optical coherence tomography angiography. Br. J. Ophthalmol. 100, 671–676. https://doi.org/10.1136/bjophthalmol-2015-307330.

Chen, A., Dang, S., Chung, M.M., Ramchandran, R.S., Bessette, A.P., DiLoreto, D.A., Kleinman, D.M., Sridhar, J., Wykoff, C.C., Kuriyan, A.E., 2021. Quantitative comparison of fundus images by 2 ultra-widefield fundus cameras. Ophthalmol Retina 5 (5), 450–457.

Chen, L., Messinger, J.D., Ferrara, D., Freund, K.B., Curcio, C.A., 2021. Fundus autofluorescence in neovascular age-related macular degeneration: a clinicopathologic correlation relevant to macular atrophy. Ophthalmol Retina 5 (11), 1085–1096. https://doi.org/10.1016/j.oret.2021.01.012.

Choi, W., Mohler, K.J., Potsaid, B., Lu, C.D., Liu, J.J., Jayaraman, V., Cable, A.E., Duker, J.S., Huber, R., Fujimoto, J.G., 2013. Choriocapillaris and choroidal microvasculature imaging with ultrahigh speed OCT angiography. PLoS One 8 (12), e81499. https://doi.org/10.1371/journal.pone.0081499.

Choi, W., Moult, E.M., Waheed, N.K., Adhi, M., Lee, B., Lu, C.D., de Carlo, T.E., Jayaraman, V., Rosenfeld, P.J., Duker, J.S., Fujimoto, J.G., 2015. Ultrahigh-speed, swept-source optical coherence tomography angiography in nonexudative age-related macular degeneration with geographic atrophy. Ophthalmology 122 (12), 2532–2544. https://doi.org/10.1016/j.ophtha.2015.08.029.

Chu, Z., Lin, J., Gao, C., Xin, C., Zhang, Q., Chen, C.L., Roisman, L., Gregori, G., Rosenfeld, P.J., Wang, R.K., 2016. Quantitative assessment of the retinal microvasculature using optical coherence tomography angiography. J. Biomed. Opt. 21 (6), 66008 https://doi.org/10.1117/1.JBO.21.6.066008.

Cole, E.D., Moult, E.M., Dang, S., Choi, W., Ploner, S.B., Lee, B., Louzada, R., Novais, E., Schottenhamml, J., Husvogt, L., Maier, A., Fujimoto, J.G., Waheed, N.K., Duker, J.S., 2017. The definition, rationale, and effects of thresholding in OCT angiography. Ophthalmol Retina 1 (5), 435–447. https://doi.org/10.1016/j.oret.2017.01.019.

Costa, R.A., Skaf, M., Melo Jr., L.A., Calucci, D., Cardillo, J.A., Castro, J.C., Huang, D., Wojtkowski, M., 2006. Retinal assessment using optical coherence tomography. Prog. Retin. Eye Res. 25 (3), 325–353. https://doi.org/10.1016/j.preteyeres.2006.03.001, 2006 May.

Costanzo, E., Miere, A., Querques, G., Capuano, V., Jung, C., Souied, E.H., 2016. Type 1 choroidal neovascularization lesion size: indocyanine green angiography versus optical coherence tomography angiography. Invest. Ophthalmol. Vis. Sci. 57 (9), OCT307–O313. https://doi.org/10.1167/iovs.15-18830.

Croce, A.C., Bottiroli, G., 2014. Autofluorescence spectroscopy and imaging: a tool for biomedical research and diagnosis. Eur. J. Histochem. 58 (4), 2461. https://doi.org/10.4081/ejh.2014.2461.

D'Amore, A., Stella, J.A., Wagner, W.R., Sacks, M.S., 2010. Characterization of the complete fiber network topology of planar fibrous tissues and scaffolds. Biomaterials 31 (20), 5345–5354. https://doi.org/10.1016/j.biomaterials.2010.03.052.

Darius, S., Wolf, G., Huang, P.L., Fishman, M.C., 1995. Localization of NADPH-diaphorase/nitric oxide synthase in the rat retina: an electron microscopic study. Brain Res. 690 (2), 231–235. https://doi.org/10.1016/0006-8993(95)00559-9.

Daruich, A., Matet, A., Moulin, A., Kowalczuk, L., Nicolas, M., Sellam, A., Rothschild, P. R., Omri, S., Gélizé, E., Jonet, L., Delaunay, K., De Kozak, Y., Berdugo, M., Zhao, M., Crisanti, P., Behar-Cohen, F., 2018. Mechanisms of macular edema: beyond the surface. Prog. Retin. Eye Res. 63, 20–68. https://doi.org/10.1016/j.preteyeres.2017.10.006.

Delori, F., Greenberg, J.P., Woods, R.L., Fischer, J., Duncker, T., Sparrow, J., Smith, R.T., 2011. Quantitative measurements of autofluorescence with the scanning laser ophthalmoscope. Invest. Ophthalmol. Vis. Sci. 52 (13), 9379–9390. https://doi.org/10.1167/iovs.11-8319.

Delori, F.C., Goger, D.G., Hammond, B.R., Snodderly, D.M., Burns, S.A., 2001. Macular pigment density measured by autofluorescence spectrometry: comparison with reflectometry and heterochromatic flicker photometry. J. Opt. Soc. Am. Opt Image Sci. Vis. 18 (6), 1212–1230. https://doi.org/10.1364/josaa.18.001212.

Domalpally, A., Danis, R.P., White, J., Narkar, A., Clemons, T., Ferris, F., Chew, E., 2013. Circularity index as a risk factor for progression of geographic atrophy. Ophthalmology 120 (12), 2666–2671. https://doi.org/10.1016/j.ophtha.2013.07.047.

Dong, L., Yang, Q., Zhang, R.H., Wei, W.B., 2021. Artificial intelligence for the detection of age-related macular degeneration in color fundus photographs: a systematic review and meta-analysis. EClinical Med. 35, 100875 https://doi.org/10.1016/j.eclinm.2021.100875.

Drexler, W., Fujimoto, J.G., 2008. State-of-the-art retinal optical coherence tomography. Prog. Retin. Eye Res. 27 (1), 45–88. https://doi.org/10.1016/j.preteyeres.2007.07.005.

Dysli, C., Wolf, S., Berezin, M.Y., Sauer, L., Hammer, M., Zinkernagel, M.S., 2017. Fluorescence lifetime imaging ophthalmoscopy. Prog. Retin. Eye Res. 60, 120–143. https://doi.org/10.1016/j.preteyeres.2017.06.005.

Early Treatment Diabetic Retinopathy Study Research Group, 1991. Fundus photographic risk factors for progression of diabetic retinopathy. ETDRS report number 12. Ophthalmology 98 (5 Suppl. l), 823–833.

Eells, J.T., Gopalakrishnan, S., Valter, K., 2016. Near-infrared photobiomodulation in retinal injury and disease. Adv. Exp. Med. Biol. 854, 437–441. https://doi.org/10.1007/978-3-319-17121-0_58.

Eldred, G.E., Katz, M.L., 1988. Fluorophores of the human retinal pigment epithelium: separation and spectral characterization. Exp. Eye Res. 47 (1), 71–86. https://doi.org/10.1016/0014-4835(88)90025-5.

Elsner, A.E., Burns, S.A., Weiter, J.J., Delori, F.C., 1996. Infrared imaging of sub-retinal structures in the human ocular fundus. Vis. Res. 36 (1), 191–205. https://doi.org/10.1016/j.oret.2020.08.017.

Enders, C., Lang, G.E., Dreyhaupt, J., Loidl, M., Lang, G.K., Werner, J.U., 2019. Quantity and quality of image artifacts in optical coherence tomography angiography. PLoS One 14 (1), e0210505. https://doi.org/10.1371/journal.pone.0210505.

Feeney, L., 1978. Lipofuscin and melanin of human retinal pigment epithelium. Fluorescence, enzyme cytochemical, and ultrastructural studies. Invest. Ophthalmol. Vis. Sci. 17 (7), 583–600.

Ferrara, D., Waheed, N.K., Duker, J.S., 2016. Investigating the choriocapillaris and choroidal vasculature with new optical coherence tomography technologies. Prog. Retin. Eye Res. 52, 130–155. https://doi.org/10.1016/j.preteyeres.2015.10.002.

Fleckenstein, M., Mitchell, P., Freund, K.B., Sadda, S., Holz, F.G., Brittain, C., Henry, E. C., Ferrara, D., 2018. The progression of geographic atrophy secondary to age-related macular degeneration. Ophthalmology 125 (3), 369–390. https://doi.org/10.1016/j.ophtha.2017.08.038.

Fogel-Levin, M., Sadda, S.R., Rosenfeld, P.J., Waheed, N., Querques, G., Freund, B.K., Sarraf, D., 2022. Advanced retinal imaging and applications for clinical practice: a consensus review. Surv. Ophthalmol. S0039–6257 (22) https://doi.org/10.1016/j.survophthal.2022.02.004, 00035-2.

Forshaw, T.R.J., Minör, Å.S., Subhi, Y., Sørensen, T.L., 2019. Peripheral retinal lesions in eyes with age-related macular degeneration using ultra-widefield imaging: a systematic review with meta-analyses. Ophthalmol Retina 3 (9), 734–743. https://doi.org/10.1016/j.oret.2019.04.014.

Gadde, S.G., Anegondi, N., Bhanushali, D., Chidambara, L., Yadav, N.K., Khurana, A., Sinha Roy, A., 2016. Quantification of vessel density in retinal optical coherence tomography angiography images using local fractal dimension. Invest. Ophthalmol. Vis. Sci. 57 (1), 246–252. https://doi.org/10.1167/iovs.15-18287.

Gargeya, R., Leng, T., 2017. Automated identification of diabetic retinopathy using deep learning. Ophthalmology 124 (7), 962–969. https://doi.org/10.1016/j.ophtha.2017.02.008.

Ghasemi Falavarjani, K., Phasukkijwatana, N., Freund, K.B., Cunningham Jr., E.T., Kalevar, A., McDonald, H.R., Dolz-Marco, R., Roberts, P.K., Tsui, I., Rosen, R., Jampol, L.M., Sadda, S.R., Sarraf, D., 2017. En face optical coherence tomography analysis to assess the spectrum of perivenular ischemia and paracentral acute middle maculopathy in retinal vein occlusion. Am. J. Ophthalmol. 177, 131–138. https://doi.org/10.1016/j.ajo.2017.02.015.

Gleichman, A.J., Carmichael, S.T., 2020. Glia in neurodegeneration: drivers of disease or along for the ride? Neurobiol. Dis. 142, 104957 https://doi.org/10.1016/j.nbd.2020.104957.

Greenberg, J.P., Duncker, T., Woods, R.L., Smith, R.T., Sparrow, J.R., Delori, F.C., 2013. Quantitative fundus autofluorescence in healthy eyes. Invest. Ophthalmol. Vis. Sci. 54 (8), 5684–5693. https://doi.org/10.1167/iovs.13-12445.

Greig, E.C., Duker, J.S., Waheed, N.K., 2020. A practical guide to optical coherence tomography angiography interpretation. Int. J. Retina. Vitreous 6 (1), 55. https://doi.org/10.1186/s40942-020-00262-9.

Grieve, K., Gofas-Salas, E., Ferguson, R.D., Sahel, J.A., Paques, M., Rossi, E.A., 2018. In vivo near-infrared autofluorescence imaging of retinal pigment epithelial cells with 757 nm excitation. Biomed. Opt Express 9 (12), 5946–5961. https://doi.org/10.1364/BOE.9.005946.

Guduru, A., Fleischman, D., Shin, S., Zeng, D., Baldwin, J.B., Houghton, O.M., Say, E.A., 2017. Ultra-widefield fundus autofluorescence in age-related macular degeneration. PLoS One 12 (6), e0177207. https://doi.org/10.1371/journal.pone.0177207.

Gulshan, V., Peng, L., Coram, M., Stumpe, M.C., Wu, D., Narayanaswamy, A., Venugopalan, S., Widner, K., Madams, T., Cuadros, J., Kim, R., Raman, R., Nelson, P. C., Mega, J.L., Webster, D.R., 2016. Development and validation of a deep learning algorithm for detection of diabetic retinopathy in retinal fundus photographs. JAMA 316 (22), 2402–2410. https://doi.org/10.1001/jama.2016.17216.

Guo, K., Achilefu, S., Berezin, M.Y., 2012. Dating bloodstains with fluorescence lifetime measurements. Chem. Eur J. 18 (5), 1303–1305. https://doi.org/10.1002/chem.201102935.

Guo, K., Zhegalova, N., Achilefu, S., Berezin, M.Y., 2013. Bloodstain age analysis: toward solid state fluorescent lifetime measurements. In: Proc. SPIE 8572, Advanced Biomedical and Clinical Diagnostic Systems XI, 857214 (22 March 2013). https://doi.org/10.1117/12.2007756.

Guymer, R.H., Markey, C.M., McAllister, I.L., Gillies, M.C., Hunyor, A.P., Arnold, J.J., FLUID Investigators, 2019. Tolerating subretinal fluid in neovascular age-related macular degeneration treated with ranibizumab using a treat-and-extend regimen: FLUID study 24-month results. Ophthalmology 126 (5), 723–734. https://doi.org/10.1016/j.ophtha.2018.11.025.

Haas, A.M., Ahmed, D., Stattin, M., Graf, A., Krepler, K., Ansari-Shahrezaei, S., 2021. Comparison of macular neovascularization lesion size by the use of spectral-domain optical coherence tomography angiography and swept-source optical coherence

tomography angiography versus indocyanine green angiography. Acta Ophthalmol. 99 (2), e260–e266. https://doi.org/10.1111/aos.14572.
Han, J., Cho, N.S., Kim, K., Kim, E.S., Kim, D.G., Kim, J.M., Yu, S.Y., 2020. Fundus autofluorescence patterns in central serous chorioretinopathy. Retina 40 (7), 1387–1394. https://doi.org/10.1097/IAE.0000000000002580.
Han, M., DeDecker, B.S., Smith, S.O., 1993. Localization of the retinal protonated Schiff base counterion in rhodopsin. Biophys. J. 65 (2), 899–906. https://doi.org/10.1016/S0006-3495(93)81117-2.
Han, M., Giese, G., Schmitz-Valckenberg, S., Bindewald-Wittich, A., Holz, F.G., Yu, J., Bille, J.F., Niemz, M.H., 2007. Age-related structural abnormalities in the human retina-choroid complex revealed by two-photon excited autofluorescence imaging. J. Biomed. Opt. 12 (2), 024012 https://doi.org/10.1117/1.2717522.
Hansell, P., Beeson, E.J.G., 1953. Retinal photography in color. Br. J. Ophthalmol. 37, 65–69. https://doi.org/10.1136/bjo.37.2.65.
Hariri, A.H., Gui, W., Datoo O'Keefe, G.A., Ip, M.S., Sadda, S.R., Gorin, M.B., 2018. Ultra-Widefield fundus autofluorescence imaging of patients with retinitis pigmentosa: a standardized grading system in different genotypes. Ophthalmol Retina 2 (7), 735–745. https://doi.org/10.1016/j.oret.2017.10.018.
Holmen, I.C., Konda, S.M., Pak, J.W., McDaniel, K.W., Blodi, B., Stepien, K.E., Domalpally, A., 2020. Prevalence and severity of artifacts in optical coherence tomographic angiograms. JAMA Ophthalmol. 138 (2), 119–126. https://doi.org/10.1001/jamaophthalmol.2019.4971.
Holz, F.G., Bindewald-Wittich, A., Fleckenstein, M., Dreyhaupt, J., Scholl, H.P., Schmitz-Valckenberg, S., FAM-Study Group, 2007. Progression of geographic atrophy and impact of fundus autofluorescence patterns in age-related macular degeneration. Am. J. Ophthalmol. 143 (3), 463–472. https://doi.org/10.1016/j.ajo.2006.11.041.
Hormel, T.T., Huang, D., Jia, Y., 2021a. Artifacts and artifact removal in optical coherence tomographic angiography. Quant. Imag. Med. Surg. 11 (3), 1120–1133. https://doi.org/10.21037/qims-20-730.
Hormel, T.T., Hwang, T.S., Bailey, S.T., Wilson, D.J., Huang, D., Jia, Y., 2021b. Artificial intelligence in OCT angiography. Prog. Retin. Eye Res. 85, 100965 https://doi.org/10.1016/j.preteyeres.2021.100965.
Hormel, T.T., Jia, Y., Jian, Y., Hwang, T.S., Bailey, S.T., Pennesi, M.E., Wilson, D.J., Morrison, J.C., Huang, D., 2021c. Plexus-specific retinal vascular anatomy and pathologies as seen by projection-resolved optical coherence tomographic angiography. Prog. Retin. Eye Res. 80, 100878 https://doi.org/10.1016/j.preteyeres.2020.100878.
Hotaling, N.A., Bharti, K., Kriel, H., Simon Jr., C.G., 2015. DiameterJ: a validated open source nanofiber diameter measurement tool. Biomaterials 61, 327–338. https://doi.org/10.1016/j.biomaterials.2015.05.015.
Hou, K.K., Au, A., Kashani, A.H., Freund, K.B., Sadda, S.R., Sarraf, D., 2019. Pseudoflow with OCT angiography in eyes with hard exudates and macular drusen. Transl. Vis Sci. Technol. 8 (3), 50. https://doi.org/10.1167/tvst.8.3.50, 2019.
Huang, D., Swanson, E.A., Lin, C.P., Schuman, J.S., Stinson, W.G., Chang, W., Hee, M.R., Flotte, T., Gregory, K., Puliafito, C.A., Fujimoto, J.G., 1991. Optical coherence tomography. Science 254 (5035), 1178–1181. https://doi.org/10.1126/science.1957169.
Inoue, M., Jung, J.J., Balaratnasingam, C., Dansingani, K.K., Dhrami-Gavazi, E., Suzuki, M., de Carlo, T.E., Shahlaee, A., Klufas, M.A., El Maftouhi, A., Duker, J.S., Ho, A.C., Maftouhi, M.Q., Sarraf, D., Freund, K.B., Study Group, C.O.F.T.-1, 2016. A comparison between optical coherence tomography angiography and fluorescein angiography for the imaging of type 1 neovascularization. Invest. Ophthalmol. Vis. Sci. 57 (9), OCT314–O323. https://doi.org/10.1167/iovs.15-18900.
Iovino, C., Au, A., Hilely, A., Violanti, S., Peiretti, E., Gorin, M.B., Sarraf, D., 2019. Evaluation of the choroid in eyes with retinitis pigmentosa and cystoid macular edema. Invest. Ophthalmol. Vis. Sci. 60 (15), 5000–5006. https://doi.org/10.1167/iovs.19-27300.
Ishii, H., Shoji, T., Yoshikawa, Y., Kanno, J., Ibuki, H., Shinoda, K., 2019. Automated measurement of the foveal avascular zone in swept-source optical coherence tomography angiography images. Transl. Vis Sci. Technol. 8 (3), 28. https://doi.org/10.1167/tvst.8.3.28.
Ishikawa, S., Taguchi, M., Muraoka, T., Sakurai, Y., Kanda, T., Takeuchi, M., 2014. Changes in subfoveal choroidal thickness associated with uveitis activity in patients with Behçet's disease. Br. J. Ophthalmol. 98 (11), 1508–1513. https://doi.org/10.1136/bjophthalmol-2014-305333.
Iwasaki, M., Inomata, H., 1986. Relation between superficial capillaries and foveal structures in the human retina. Invest. Ophthalmol. Vis. Sci. 27, 1698–1705.
Jackman, W.T., Webster, J.D., 1886. On photographing the retina of the living human eye. Philadel Photogr 23, 340–341.
Jaffe, G.J., Chakravarthy, U., Freund, K.B., Guymer, R.H., Holz, F.G., Liakopoulos, S., Monés, J.M., Rosenfeld, P.J., Sadda, S.R., Sarraf, D., Schmitz-Valckenberg, S., Spaide, R.F., Staurenghi, G., Tufail, A., Curcio, C.A., 2021. Imaging features associated with progression to geographic atrophy in age-related macular degeneration: classification of atrophy meeting report 5. Ophthalmol Retina 5 (9), 855–867. https://doi.org/10.1016/j.oret.2020.12.009.
Kashani, A.H., Chen, C.L., Gahm, J.K., Zheng, F., Richter, G.M., Rosenfeld, P.J., Shi, Y., Wang, R.K., 2017. Optical coherence tomography angiography: a comprehensive review of current methods and clinical applications. Prog. Retin. Eye Res. 60, 66–100. https://doi.org/10.1016/j.preteyeres.2017.07.002.
Kashani, A.H., Green, K.M., Kwon, J., Chu, Z., Zhang, Q., Wang, R.K., Garrity, S., Sarraf, D., Rebhun, C.B., Waheed, N.K., Schaal, K.B., Munk, M.R., Gattoussi, S., Freund, K.B., Zheng, F., Liu, G., Rosenfeld, P.J., 2018. Suspended scattering particles in motion: a novel feature of OCT angiography in exudative maculopathies. Ophthalmol Retina 2 (7), 694–702. https://doi.org/10.1016/j.oret.2017.11.004.
Keilhauer, C.N., Delori, F.C., 2006. Near-infrared autofluorescence imaging of the fundus: visualization of ocular melanin. Invest. Ophthalmol. Vis. Sci. 47 (8), 3556–3564. https://doi.org/10.1167/iovs.06-0122.
Kernt, M., Hadi, I., Pinter, F., Seidensticker, F., Hirneiss, C., Haritoglou, C., Kampik, A., Ulbig, M.W., Neubauer, A.S., 2012. Assessment of diabetic retinopathy using nonmydriatic ultra-widefield scanning laser ophthalmoscopy (Optomap) compared with ETDRS 7-field stereo photography. Diabetes Care 35 (12), 2459–2463. https://doi.org/10.2337/dc12-0346.
Kilic Muftuoglu, I., Bartsch, D.U., Barteselli, G., Gaber, R., Nezgoda, J., Freeman, W.R., 2018. Visualization of macular pucker by multicolor scanning laser imaging. Retina 38 (2), 352–358. https://doi.org/10.1097/IAE.0000000000001525.
Kim, D.Y., Fingler, J., Zawadzki, R.J., Park, S.S., Morse, L.S., Schwartz, D.M., Fraser, S.E., Werner, J.S., 2013. Optical imaging of the chorioretinal vasculature in the living human eye. Proc. Natl. Acad. Sci. U. S. A. 110 (35), 14354–14359. https://doi.org/10.1073/pnas.1307315110.
Klein, T., Wieser, W., Eigenwillig, C.M., Biedermann, B.R., Huber, R., 2011. Megahertz OCT for ultrawide-field retinal imaging with a 1050 nm Fourier domain mode-locked laser. Opt Express 19 (4), 3044–3062. https://doi.org/10.1364/OE.19.003044.
Klufas, M.A., Tsui, I., Sadda, S.R., Hosseini, H., Schwartz, S.D., 2018. Ultrawidefield autofluoresence in ABCA4 Stargardt disease. Retina 38 (2), 403–415. https://doi.org/10.1097/IAE.0000000000001567.
König, K., 2008. Clinical multiphoton tomography. J. Biophot. 1 (1), 13–23. https://doi.org/10.1002/jbio.200710022.
Koziol, B., Markowicz, M., Kruk, J., Plytycz, B., 2006. Riboflavin as a source of autofluorescence in Eisenia fetida coelomocytes. Photochem. Photobiol. 82 (2), 570–573. https://doi.org/10.1562/2005-11-23-RA-738.
Kwan, C.C., Fawzi, A.A., 2019. Imaging and biomarkers in diabetic macular edema and diabetic retinopathy. Curr. Diabetes Rep. 19 (10), 95. https://doi.org/10.1007/s11892-019-1226-2.
Laíns, I., Wang, J.C., Cui, Y., Katz, R., Vingopoulos, F., Staurenghi, G., Vavvas, D.G., Miller, J.W., Miller, J.B., 2021. Retinal applications of swept source optical coherence tomography (OCT) and optical coherence tomography angiography (OCTA). Prog. Retin. Eye Res. 84, 100951 https://doi.org/10.1016/j.preteyeres.2021.100951.
Lapierre-Landry, M., Carroll, J., Skala, M.C., 2018a. Imaging retinal melanin: a review of current technologies. J. Biol. Eng. 12, 29. https://doi.org/10.1186/s13036-018-0124-5.
Lapierre-Landry, M., Huckenpahler, A.L., Link, B.A., Collery, R.F., Carroll, J., Skala, M.C., 2018b. Imaging melanin distribution in the zebrafish retina using photothermal optical coherence tomography. Transl. Vis Sci. Technol. 7 (5), 4. https://doi.org/10.1167/tvst.7.5.4.
Lauermann, J.L., Treder, M., Alnawaiseh, M., Clemens, C.R., Eter, N., Alten, F., 2019. Automated OCT angiography image quality assessment using a deep learning algorithm. Graefes Arch. Clin. Exp. Ophthalmol. 257 (8), 1641–1648. https://doi.org/10.1007/s00417-019-04338-7.
Lauermann, J.L., Treder, M., Heiduschka, P., Clemens, C.R., Eter, N., Alten, F., 2017. Impact of eye-tracking technology on OCT-angiography imaging quality in age-related macular degeneration. Graefes Arch. Clin. Exp. Ophthalmol. 255 (8), 1535–1542. https://doi.org/10.1007/s00417-017-3684-z.
Le, D., Son, T., Yao, X., 2021. Machine learning in optical coherence tomography angiography. Exp. Biol. Med. (Maywood, NJ, U. S.) 246 (20), 2170–2183. https://doi.org/10.1177/15353702211026581.
Lee, K.E., Heitkotter, H., Carroll, J., 2021. Challenges associated with ellipsoid zone intensity measurements using optical coherence tomography. Transl. Vis Sci. Technol. 10 (12), 27. https://doi.org/10.1167/tvst.10.12.27.
Lee, W.K., Baek, J., Dansingani, K.K., Lee, J.H., Freund, K.B., 2016a. Choroidal morphology in eyes with polypoidal choroidal vasculopathy and normal or subnormal subfoveal choroidal thickness. Retina 36 (Suppl. 1), S73–S82. https://doi.org/10.1097/IAE.0000000000001346.
Lee, W.J., Lee, J.H., Lee, B.R., 2016b. Fundus autofluorescence imaging patterns in central serous chorioretinopathy according to chronicity. Eye 30 (10), 1336–1342. https://doi.org/10.1038/eye.2016.113.
Lee, W.J., Lee, B.R., Shin, Y.U., 2014. Retromode imaging: review and perspectives. Saudi J. Ophthalmol. 28 (2), 88–94. https://doi.org/10.1016/j.sjopt.2014.02.003.
Lei, J., Pei, C., Wen, C., Abdelfattah, N.S., 2018. Repeatability and reproducibility of quantification of superficial peri-papillary capillaries by four different optical coherence tomography angiography devices. Sci. Rep. 8 (1), 17866 https://doi.org/10.1038/s41598-018-36279-2.
Lejoyeux, R., Benillouche, J., Ong, J., Errera, M.H., Rossi, E.A., Singh, S.R., Dansingani, K.K., da Silva, S., Sinha, D., Sahel, J.A., Freund, K.B., Sadda, S.R., Lutty, G.A., Chhablani, J., 2022. Choriocapillaris: fundamentals and advancements. Prog. Retin. Eye Res. 87, 100997 https://doi.org/10.1016/j.preteyeres.2021.100997.
Li, B., George, E.W., Rognon, G.T., Gorusupudi, A., Ranganathan, A., Chang, F.Y., Shi, L., Frederick, J.M., Bernstein, P.S., 2020. Imaging lutein and zeaxanthin in the human retina with confocal resonance Raman microscopy. Proc. Natl. Acad. Sci. U. S. A. 117 (22), 12352–12358. https://doi.org/10.1073/pnas.1922793117.
Li, S., Wang, X., Du, X., Wu, Q., 2018. Clinical application of multicolour scanning laser imaging in diabetic retinopathy. Laser Med. Sci. 33 (6), 1371–1379. https://doi.org/10.1007/s10103-018-2498-5.
Linderman, R.E., Muthiah, M.N., Omoba, S.B., Litts, K., Tarima, S., Visotcky, A., Kim, J.E., Carroll, J., 2018. Variability of foveal avascular zone metrics derived from optical coherence tomography angiography images. Transl. Vis Sci. Technol. 7 (5), 20. https://doi.org/10.1167/tvst.7.5.20.

Lindner, M., Nadal, J., Mauschitz, M.M., Lüning, A., Czauderna, J., Pfau, M., Schmitz-Valckenberg, S., Holz, F.G., Schmid, M., Fleckenstein, M., 2017. Combined fundus autofluorescence and near infrared reflectance as prognostic biomarkers for visual acuity in foveal-sparing geographic atrophy. Invest. Ophthalmol. Vis. Sci. 58 (6), BIO61–BIO67. https://doi.org/10.1167/iovs.16-21210.

Liu, T., Li, H., Song, W., Jiao, S., Zhang, H.F., 2013. Fundus camera guided photoacoustic ophthalmoscopy. Curr. Eye Res. 38 (12), 1229–1234. https://doi.org/10.3109/02713683.2013.815219.

Liu, T., Wei, Q., Song, W., Burke, J.M., Jiao, S., Zhang, H.F., 2012. Near-infrared light photoacoustic ophthalmoscopy. Biomed. Opt Express 3 (4), 792–799. https://doi.org/10.1364/BOE.3.000792.

Liu, X., Liu, T., Wen, R., Li, Y., Puliafito, C.A., Zhang, H.F., Jiao, S., 2015. Optical coherence photoacoustic microscopy for in vivo multimodal retinal imaging. Opt Lett. 40 (7), 1370–1373. https://doi.org/10.1364/OL.40.001370.

Liu, W., Zhang, H.F., 2016. Photoacoustic imaging of the eye: a mini review. Photoacoustics 4 (3), 112–123. https://doi.org/10.1016/j.pacs.2016.05.001.

Ly, A., Nivison-Smith, L., Assaad, N., Kalloniatis, M., 2016a. Infrared reflectance imaging in age-related macular degeneration. Ophthalmic Physiol. Opt. 36 (3), 303–316. https://doi.org/10.1111/opo.12283.

Ly, A., Nivison-Smith, L., Assaad, N., Kalloniatis, M., 2016b. Infrared reflectance imaging in age-related macular degeneration. Ophthalmic Physiol. Opt. 36 (3), 303–316. https://doi.org/10.1111/opo.12283.

Ma, Y., Bao, J., Zhang, Y., Li, Z., Zhou, X., Wan, C., Huang, L., Zhao, Y., Han, G., Xue, T., 2019. Mammalian near-infrared image vision through injectable and self-powered retinal nanoantennae. Cell 177 (2), 243–255. https://doi.org/10.1016/j.cell.2019.01.038 e15.

Maarek, J.M., Marcu, L., Snyder, W.J., Grundfest, W.S., 2000. Time-resolved fluorescence spectra of arterial fluorescent compounds: reconstruction with the Laguerre expansion technique. Photochem. Photobiol. 71 (2), 178–187. https://doi.org/10.1562/0031-8655(2000)071<0178:trfsoa>2.0.co;2.

Margolis, R., Spaide, R.F., 2009. A pilot study of enhanced depth imaging optical coherence tomography of the choroid in normal eyes. Am. J. Ophthalmol. 147 (5), 811–815. https://doi.org/10.1016/j.ajo.2008.12.008.

Marschall, S., Klein, T., Wieser, W., Biedermann, B.R., Hsu, K., Hansen, K.P., Sumpf, B., Hasler, K.H., Erbert, G., Jensen, O.B., Pedersen, C., Huber, R., Andersen, P.E., 2010. Fourier domain mode-locked swept source at 1050 nm based on a tapered amplifier. Opt Express 18 (15), 15820–15831. https://doi.org/10.1364/OE.18.015820.

McGuinness, C.D., Macmillan, A.M., Sagoo, K., McLoskey, D., Birch, D.J.S., 2006. Excitation of fluorescence decay using a 265 nm pulsed light-emitting diode: evidence for aqueous phenylalanine rotamers. Appl. Phys. Lett. 89 (6), 063901 https://doi.org/10.1063/1.2245441.

Mehta, N., Braun, P.X., Gendelman, I., Alibhai, A.Y., Arya, M., Duker, J.S., Waheed, N.K., 2020. Repeatability of binarization thresholding methods for optical coherence tomography angiography image quantification. Sci. Rep. 10 (1), 15368 https://doi.org/10.1038/s41598-020-72358-z.

Mehta, N., Liu, K., Alibhai, A.Y., Gendelman, I., Braun, P.X., Ishibazawa, A., Sorour, O., Duker, J.S., Waheed, N.K., 2019. Impact of binarization thresholding and brightness/contrast adjustment methodology on optical coherence tomography angiography image quantification. Am. J. Ophthalmol. 205, 54–65. https://doi.org/10.1016/j.ajo.2019.03.008.

Meleppat, R.K., Zhang, P., Ju, M.J., Manna, S.K., Jian, Y., Pugh, E.N., Zawadzki, R.J., 2019. Directional optical coherence tomography reveals melanin concentration-dependent scattering properties of retinal pigment epithelium. J. Biomed. Opt. 24 (6), 1–10. https://doi.org/10.1117/1.JBO.24.6.066011.

Moraes, G., Fu, D.J., Wilson, M., Khalid, H., Wagner, S.K., Korot, E., Ferraz, D., Faes, L., Kelly, C.J., Spitz, T., Patel, P.J., Balaskas, K., Keenan, T.D.L., Keane, P.A., Chopra, R., 2021. Quantitative analysis of OCT for neovascular age-related macular degeneration using deep learning. Ophthalmology 128 (5), 693–705. https://doi.org/10.1016/j.ophtha.2020.09.025.

Müller, P.L., Pfau, M., Mauschitz, M.M., Möller, P.T., Birtel, J., Chang, P., Gliem, M., Schmitz-Valckenberg, S., Fleckenstein, M., Holz, F.G., Herrmann, P., 2018. Comparison of green versus blue fundus autofluorescence in ABCA4-related retinopathy. Transl. Vis Sci. Technol. 7 (5), 13. https://doi.org/10.1167/tvst.7.5.13.

Nag, T.C., Kathpalia, P., Gorla, S., Wadhwa, S., 2019. Localization of nitro-tyrosine immunoreactivity in human retina. Ann. Anat. 223, 8–18. https://doi.org/10.1016/j.aanat.2019.01.006.

Nagasawa, T., Tabuchi, H., Masumoto, H., Enno, H., Niki, M., Ohara, Z., Yoshizumi, Y., Ohsugi, H., Mitamura, Y., 2019. Accuracy of ultrawide-field fundus ophthalmoscopy-assisted deep learning for detecting treatment-naïve proliferative diabetic retinopathy. Int. Ophthalmol. 39 (10), 2153–2159. https://doi.org/10.1007/s10792-019-01074-z.

Napolitano, A., Ungania, S., Cannata, V., 2012. Fractal Dimension Estimation Methods for Biomedical Images. Included in: Katsikis V. MATLAB: A Fundamental Tool for Scientific Computing and Engineering Applications, Volume 3. IntechOpen, ISBN 978-953-51-0750-7.

Nassisi, M., Baghdasaryan, E., Borrelli, E., Ip, M., Sadda, S.R., 2019a. Choriocapillaris flow impairment surrounding geographic atrophy correlates with disease progression. PLoS One 14 (2), e0212563. https://doi.org/10.1371/journal.pone.0212563.

Nassisi, M., Shi, Y., Fan, W., Borrelli, E., Uji, A., Ip, M.S., Sadda, S.R., 2019b. Choriocapillaris impairment around the atrophic lesions in patients with geographic atrophy: a swept-source optical coherence tomography angiography study. Br. J. Ophthalmol. 103 (7), 911–917. https://doi.org/10.1136/bjophthalmol-2018-312643.

Nguyen, V.P., Li, Y., Aaberg, M., Zhang, W., Wang, X., Paulus, Y.M., 2018. In vivo 3D imaging of retinal neovascularization using multimodal photoacoustic microscopy and optical coherence tomography imaging. J. Imaging 4 (12), 150. https://doi.org/10.3390/jimaging4120150.

Nguyen, V.P., Li, Y., Qian, W., Liu, B., Tian, C., Zhang, W., Huang, Z., Ponduri, A., Tarnowski, M., Wang, X., Paulus, Y.M., 2019. Contrast agent enhanced multimodal photoacoustic microscopy and optical coherence tomography for imaging of rabbit choroidal and retinal vessels in vivo. Sci. Rep. 9 (1), 5945. https://doi.org/10.1038/s41598-019-42324-5.

Ni, S., Khan, S., Nguyen, T.P., Ng, R., Lujan, B.J., Tan, O., Huang, D., Jian, Y., 2022. Volumetric directional optical coherence tomography. Biomed. Opt Express 13 (2), 950–961. https://doi.org/10.1364/BOE.447882.

Novais, E.A., Baumal, C.R., Sarraf, D., Freund, K.B., Duker, J.S., 2016. Multimodal imaging in retinal disease: a consensus definition. Ophthalmic Surg. Lasers Imaging Retina 47 (3), 201–205. https://doi.org/10.3928/23258160-20160229-01.

Obuchowicz, R., Piórkowski, A., Urbanik, A., Strzelecki, M., 2019. Influence of acquisition time on MR image quality estimated with nonparametric measures based on texture features. BioMed Res. Int. 2019, 3706581 https://doi.org/10.1155/2019/3706581.

Oh, B.L., Park, U.C., Kim, B.H., Lee, E.K., Yoon, C.K., Choe, H.R., Yeon, D.Y., Yu, H.G., 2022. Role of Ultra-widefield Imaging in the evaluation of Long-term change of highly myopic fundus. Acta Ophthalmol. 100 (4), e977–e985. https://doi.org/10.1111/aos.15009.

Oishi, A., Hidaka, J., Yoshimura, N., 2014. Quantification of the image obtained with a wide-field scanning ophthalmoscope. Invest. Ophthalmol. Vis. Sci. 55 (4), 2424–2431. https://doi.org/10.1167/iovs.13-13738.

Olvera-Barrios, A., Heeren, T.F., Balaskas, K., Chambers, R., Bolter, L., Tufail, A., Egan, C., Anderson, J., 2020. Comparison of true-colour wide-field confocal scanner imaging with standard fundus photography for diabetic retinopathy screening. Br. J. Ophthalmol. 104 (11), 1579–1584. https://doi.org/10.1136/bjophthalmol-2019-315269.

Olvera-Barrios, A., Heeren, T.F., Balaskas, K., Chambers, R., Bolter, L., Egan, C., Tufail, A., Anderson, J., 2021. Diagnostic accuracy of diabetic retinopathy grading by an artificial intelligence-enabled algorithm compared with a human standard for wide-field true-colour confocal scanning and standard digital retinal images. Br. J. Ophthalmol. 105 (2), 265–270. https://doi.org/10.1136/bjophthalmol-2019-315394.

Pakzad-Vaezi, K., Keane, P.A., Cardoso, J.N., Egan, C., Tufail, A., 2017. Optical coherence tomography angiography of foveal hypoplasia. Br. J. Ophthalmol. 101 (7), 985–988. https://doi.org/10.1136/bjophthalmol-2016-309200.

Pang, C.E., Shah, V.P., Sarraf, D., Freund, K.B., 2014. Ultra-widefield imaging with autofluorescence and indocyanine green angiography in central serous chorioretinopathy. Am. J. Ophthalmol. 158 (2), 362–371. https://doi.org/10.1016/j.ajo.2014.04.021 e2.

Parodi, M.B., Arrigo, A., Bruschi, E., Manitto, M.P., Martina, E., Bandello, F., 2020a. Benign foveal depigmentation: a multimodal imaging investigation. Retin. Cases Brief Rep. https://doi.org/10.1097/ICB.0000000000001115 [Online ahead of print].

Parodi, M.B., Arrigo, A., Calamuneri, A., Aragona, E., Bandello, F., 2020b. Multimodal imaging in subclinical best vitelliform macular dystrophy. Br. J. Ophthalmol. bjophthalmol-. https://doi.org/10.1136/bjophthalmol-2020-317635, 2020-317635.

Parodi, M.B., Iacono, P., Del Turco, C., Bandello, F., 2014. Near-infrared fundus autofluorescence in subclinical best vitelliform macular dystrophy. Am. J. Ophthalmol. 158 (6), 1247–1252. https://doi.org/10.1016/j.ajo.2014.08.028 e2.

Parrozzani, R., Clementi, M., Frizziero, L., Miglionico, G., Perrini, P., Cavarzeran, F., Kotsafti, O., Comacchio, F., Trevisson, E., Convento, E., Fusetti, S., Midena, E., 2015. In vivo detection of choroidal abnormalities related to NF1: feasibility and comparison with standard NIH diagnostic criteria in pediatric patients. Invest. Ophthalmol. Vis. Sci. 56 (10), 6036–6042. https://doi.org/10.1167/iovs.14-16053.

Parrulli, S., Corvi, F., Cozzi, M., Monteduro, D., Zicarelli, F., Staurenghi, G., 2021. Microaneurysms visualisation using five different optical coherence tomography angiography devices compared to fluorescein angiography. Br. J. Ophthalmol. 105 (4), 526–530. https://doi.org/10.1136/bjophthalmol-2020-316817.

Pfau, M., Goerdt, L., Schmitz-Valckenberg, S., Mauschitz, M.M., Mishra, D.K., Holz, F.G., Lindner, M., Fleckenstein, M., 2017. Green-light autofluorescence versus combined blue-light autofluorescence and near-infrared reflectance imaging in geographic atrophy secondary to age-related macular degeneration. Invest. Ophthalmol. Vis. Sci. 58 (6), BIO121–BIO130. https://doi.org/10.1167/iovs.17-21764.

Piao, H., Guo, Y., Zhang, H., Sung, M.S., Park, S.W., 2021. Acircularity and circularity indexes of the foveal avascular zone in high myopia. Sci. Rep. 11 (1), 16808 https://doi.org/10.1038/s41598-021-96304-9.

Pichi, F., Abboud, E.B., Ghazi, N.G., Khan, A.O., 2018. Fundus autofluorescence imaging in hereditary retinal diseases. Acta Ophthalmol. 96 (5), e549–e561. https://doi.org/10.1111/aos.13602.

Pierro, L., Aragona, E., Arrigo, A., Gagliardi, M., Bandello, F.M., 2017. The mirror artifact effect on OCTA reconstructions of patients with high myopia. Spekt. Augenheilkd. 31, 257–261. https://doi.org/10.1007/s00717-017-0370-9.

Pircher, M., Hitzenberger, C.K., Schmidt-Erfurth, U., 2011. Polarization sensitive optical coherence tomography in the human eye. Prog. Retin. Eye Res. 30 (6), 431–451. https://doi.org/10.1016/j.preteyeres.2011.06.003.

Plesch, A., Klingbeil, U., Bille, J., 1987. Digital laser scanning fundus camera. Appl. Opt. 26 (8), 1480–1486. https://doi.org/10.1364/AO.26.001480.

Potsaid, B., Gorczynska, I., Srinivasan, V.J., Chen, Y., Jiang, J., Cable, A., Fujimoto, J.G., 2008. Ultrahigh speed spectral/Fourier domain OCT ophthalmic imaging at 70,000 to 312,500 axial scans per second. Opt Express 16 (19), 15149–15169. https://doi.org/10.1364/oe.16.015149.

Pow, D.V., Cook, D.K., 1997. Tryptophan is present in glial cells and photoreceptors in the chicken retina. Neuroreport 8 (7), 1767–1770. https://doi.org/10.1097/00001756-199705060-00039.

Quellec, G., Charrière, K., Boudi, Y., Cochener, B., Lamard, M., 2017. Deep image mining for diabetic retinopathy screening. Med. Image Anal. 39, 178–193. https://doi.org/10.1016/j.media.2017.04.012.

Rajabian, F., Arrigo, A., Bordato, A., Mercuri, S., Bandello, F., Battaglia Parodi, M., 2020b. Optical coherence tomography angiography in extensive macular atrophy with pseudodrusen-like appearance. Transl. Vis Sci. Technol. 9 (3), 2. https://doi.org/10.1167/tvst.9.3.2.

Rajabian, F., Arrigo, A., Jampol, L.M., Mercuri, S., Introini, U., Bandello, F., Battaglia Parodi, M., 2020a. Optical coherence tomography angiography features of focal choroidal excavation and the choroidal stroma variations with occurrence of excavation. Retina 40 (12), 2319–2324. https://doi.org/10.1097/IAE.0000000000002765.

Rasmussen, M.L., Broe, R., Frydkjaer-Olsen, U., Olsen, B.S., Mortensen, H.B., Peto, T., Grauslund, J., 2015. Comparison between Early Treatment Diabetic Retinopathy Study 7-field retinal photos and non-mydriatic, mydriatic and mydriatic steered widefield scanning laser ophthalmoscopy for assessment of diabetic retinopathy. J. Diabet. Complicat. 29 (1), 99–104. https://doi.org/10.1016/j.jdiacomp.2014.08.009.

Roberts, P.K., Vogl, W.D., Gerendas, B.S., Glassman, A.R., Bogunovic, H., Jampol, L.M., Schmidt-Erfurth, U.M., 2020. Quantification of fluid resolution and visual acuity gain in patients with diabetic macular edema using deep learning: a post hoc analysis of a randomized clinical trial. JAMA Ophthalmol. 138 (9), 945–953. https://doi.org/10.1001/jamaophthalmol.2020.2457.

Romano, F., Airaldi, M., Cozzi, M., Oldani, M., Riva, E., Bertoni, A.I., Dautaj, A., Bertelli, M., Staurenghi, G., Salvetti, A.P., 2021a. Progression of atrophy and visual outcomes in extensive macular atrophy with pseudodrusen-like appearance. Ophthalmol. Sci. 1, 1. https://doi.org/10.1016/j.xops.2021.100016.

Romano, F., Arrigo, A., Leone, P.P., Bandello, F., Battaglia Parodi, M., 2021b. Short-term modifications of ellipsoid zone in Best vitelliform macular dystrophy. Retina 41 (5), 1010–1017. https://doi.org/10.1097/IAE.0000000000002977.

Romano, F., Arrigo, A., Leone, P.P., Saladino, A., Bandello, F., Battaglia Parodi, M., 2020b. Altered ellipsoid zone reflectivity and deep capillary plexus rarefaction correlate with progression in Best disease. Br. J. Ophthalmol. 104 (4), 461–465. https://doi.org/10.1136/bjophthalmol-2019-313980.

Romano, F., Arrigo, A., MacLaren, R.E., Charbel Issa, P., Birtel, J., Bandello, F., Battaglia Parodi, M., 2020a. Hyperreflective foci as a pathogenetic biomarker in choroideremia. Retina 40 (8), 1634–1640. https://doi.org/10.1097/IAE.0000000000002645.

Rono, C., Oliver, T.R., 2020. Near infrared light exposure is associated with increased mitochondrial membrane potential in retinal pigmented epithelial cells. Photochem. Photobiol. Sci. 19 (10), 1455–1459. https://doi.org/10.1039/d0pp00168f.

Sadda, S.R., Guymer, R., Holz, F.G., Schmitz-Valckenberg, S., Curcio, C.A., Bird, A.C., Blodi, B.A., Bottoni, F., Chakravarthy, U., Chew, E.Y., Csaky, K., Danis, R.P., Fleckenstein, M., Freund, K.B., Grunwald, J., Hoyng, C.B., Jaffe, G.J., Liakopoulos, S., Monés, J.M., Pauleikhoff, D., Rosenfeld, P.J., Sarraf, D., Spaide, R.F., Tadayoni, R., Tufail, A., Wolf, S., Staurenghi, G., 2018. Consensus definition for atrophy associated with age-related macular degeneration on OCT: classification of atrophy report 3. Ophthalmology 125 (4), 537–548. https://doi.org/10.1016/j.ophtha.2017.09.028.

Saha, P.K., Jin, D., Liu, Y., Christensen, G.E., Chen, C., 2018. Fuzzy object skeletonization: theory, algorithms, and applications. IEEE Trans. Visual. Comput. Graph. 24 (8), 2298–2314. https://doi.org/10.1109/TVCG.2017.2738023.

Schindelin, J., Arganda-Carreras, I., Frise, E., Kaynig, V., Longair, M., Pietzsch, T., Preibisch, S., Rueden, C., Saalfeld, S., Schmid, B., Tinevez, J.Y., White, D.J., Hartenstein, V., Eliceiri, K., Tomancak, P., Cardona, A., 2012. Fiji: an open-source platform for biological-image analysis. Nat. Methods 9 (7), 676–682. https://doi.org/10.1038/nmeth.2019.

Schmidt-Erfurth, U., Bogunovic, H., Grechenig, C., Bui, P., Fabianska, M., Waldstein, S., Reiter, G.S., 2020. Role of deep learning-quantified hyperreflective foci for the prediction of geographic atrophy progression. Am. J. Ophthalmol. 216, 257–270. https://doi.org/10.1016/j.ajo.2020.03.042.

Schmidt-Erfurth, U., Reiter, G.S., Riedl, S., Seeböck, P., Vogl, W.D., Blodi, B.A., Domalpally, A., Fawzi, A., Jia, Y., Sarraf, D., Bogunović, H., 2022. AI-based monitoring of retinal fluid in disease activity and under therapy. Prog. Retin. Eye Res. 86, 100972 https://doi.org/10.1016/j.preteyeres.2021.100972.

Schmitz-Valckenberg, S., Bindewald-Wittich, A., Dolar-Szczasny, J., Dreyhaupt, J., Wolf, S., Scholl, H.P., Holz, F.G., Fundus Autofluorescence in Age-Related Macular Degeneration Study Group, 2006. Correlation between the area of increased autofluorescence surrounding geographic atrophy and disease progression in patients with AMD. Invest. Ophthalmol. Vis. Sci. 47 (6), 2648–2654. https://doi.org/10.1167/iovs.05-0892.

Schmitz-Valckenberg, S., Pfau, M., Fleckenstein, M., Staurenghi, G., Sparrow, J.R., Bindewald-Wittich, A., Spaide, R.F., Wolf, S., Sadda, S.R., Holz, F.G., 2021. Fundus autofluorescence imaging. Prog. Retin. Eye Res. 81, 100893 https://doi.org/10.1016/j.preteyeres.2020.100893.

Schwartz, D.M., Fingler, J., Kim, D.Y., Zawadzki, R.J., Morse, L.S., Park, S.S., Fraser, S.E., Werner, J.S., 2014. Phase-variance optical coherence tomography: a technique for noninvasive angiography. Ophthalmology 121 (1), 180–187. https://doi.org/10.1016/j.ophtha.2013.09.002.

Schweitzer, D., Hammer, M., Jentsch, S., Schenke, S., 2007. Interpretation of Measurements of Dynamic Fluorescence of the Eye. SPIE, Boston, MA, USA. https://doi.org/10.1117/12.735815.

Schweitzer, D., Kolb, A., Hammer, M., 2001. Autofluorescence lifetime measurements in images of the human ocular fundus. Proc. SPIE 4432, 29–39.

Shin, Y.U., Kim, S., Lee, B.R., Shin, J.W., Kim, S.I., 2012. Novel. Noninvasive detection of the fovea avascular zone using confocal red-free imaging in diabetic retinopathy and retinal vein occlusion. Invest. Ophthalmol. Vis. Sci. 53 (1), 309–315. https://doi.org/10.1167/iovs.11-8510.

Silva, P.S., Cavallerano, J.D., Sun, J.K., Noble, J., Aiello, L.M., Aiello, L.P., 2012. Nonmydriatic ultrawide field retinal imaging compared with dilated standard 7-field 35-mm photography and retinal specialist examination for evaluation of diabetic retinopathy. Am. J. Ophthalmol. 154 (3) https://doi.org/10.1016/j.ajo.2012.03.019, 549-59e2.

Simhaee, D., Dolz-Marco, R., Freund, K.B., 2020. Choroidal nevi with focal choroidal excavation and polypoidal choroidal neovascularization. Retin. Cases Brief Rep. 14 (1), 39–43. https://doi.org/10.1097/ICB.0000000000000617.

Sinha, T., Makia, M., Du, J., Naash, M.I., Al-Ubaidi, M.R., 2018. Flavin homeostasis in the mouse retina during aging and degeneration. J. Nutr. Biochem. 62, 123–133. https://doi.org/10.1016/j.jnutbio.2018.09.003.

Skala, M.C., Crow, M.J., Wax, A., Izatt, J.A., 2008. Photothermal optical coherence tomography of epidermal growth factor receptor in live cells using immunotargeted gold nanospheres. Nano Lett. 8 (10), 3461–3467. https://doi.org/10.1021/nl802351p.

Smith, L.M., Dobson, C.C., 1989. Absolute displacement measurements using modulation of the spectrum of white light in a Michelson interferometer. Appl. Opt. 28 (16), 3339–3342. https://doi.org/10.1364/AO.28.003339.

Song, J.H., Moon, K.Y., Jang, S., Moon, Y., 2019. Comparison of MultiColor fundus imaging and colour fundus photography in the evaluation of epiretinal membrane. Acta Ophthalmol. 97 (4), e533–e539. https://doi.org/10.1111/aos.13978.

Spaide, R.F., 2017. Choriocapillaris signal voids in maternally inherited diabetes and deafness and in pseudoxanthoma elasticum. Retina 37 (11), 2008–2014. https://doi.org/10.1097/IAE.0000000000001497.

Spaide, R.F., Fujimoto, J.G., Waheed, N.K., 2015. Image artifacts in optical coherence tomography angiography. Retina 35 (11), 2163–2180. https://doi.org/10.1097/IAE.0000000000000765.

Spaide, R.F., Fujimoto, J.G., Waheed, N.K., Sadda, S.R., Staurenghi, G., 2018. Optical coherence tomography angiography. Prog. Retin. Eye Res. 64, 1–55. https://doi.org/10.1016/j.preteyeres.2017.11.003.

Spaide, R.F., Jaffe, G.J., Sarraf, D., Freund, K.B., Sadda, S.R., Staurenghi, G., Waheed, N. K., Chakravarthy, U., Rosenfeld, P.J., Holz, F.G., Souied, E.H., Cohen, S.Y., Querques, G., Ohno-Matsui, K., Boyer, D., Gaudric, A., Blodi, B., Baumal, C.R., Li, X., Coscas, G.J., Brucker, A., Singerman, L., Luthert, P., Schmitz-Valckenberg, S., Schmidt-Erfurth, U., Grossniklaus, H.E., Wilson, D.J., Guymer, R., Yannuzzi, L.A., Chew, E.Y., Csaky, K., Monés, J.M., Pauleikhoff, D., Tadayoni, R., Fujimoto, J., 2020. Consensus nomenclature for reporting neovascular age-related macular degeneration data: consensus on neovascular age-related macular degeneration nomenclature study group. Ophthalmology 127 (5), 616–636. https://doi.org/10.1016/j.ophtha.2019.11.004.

Spaide, R.F., Koizumi, H., Pozzoni, M.C., 2008. Enhanced depth imaging spectral-domain optical coherence tomography. Am. J. Ophthalmol. 146 (4), 496–500. https://doi.org/10.1016/j.ajo.2008.05.032.

Sparrow, J.R., Duncker, T., Schuerch, K., Paavo, M., de Carvalho Jr., J.R.L., 2020. Lessons learned from quantitative fundus autofluorescence. Prog. Retin. Eye Res. 74, 100774 https://doi.org/10.1016/j.preteyeres.2019.100774.

Sparrow, J.R., Nakanishi, K., Parish, C.A., 2000. The lipofuscin fluorophore A2E mediates blue light-induced damage to retinal pigmented epithelial cells. Invest. Ophthalmol. Vis. Sci. 41 (7), 1981–1989.

Staurenghi, G., Sadda, S., Chakravarthy, U., Spaide, R.F., International Nomenclature for Optical Coherence Tomography (IN•OCT) Panel, 2014. Proposed lexicon for anatomic landmarks in normal posterior segment spectral-domain optical coherence tomography: the IN•OCT consensus. Ophthalmology 121 (8), 1572–1578. https://doi.org/10.1016/j.ophtha.2014.02.023.

Stitt, A.W., Gardiner, T.A., Archer, D.B., 1995. Histological and ultrastructural investigation of retinal microaneurysm development in diabetic patients. Br. J. Ophthalmol. 79, 362–367. https://doi.org/10.1136/bjo.79.4.362.

Strauss, R.W., Muñoz, B., Ho, A., Jha, A., Michaelides, M., Cideciyan, A.V., Audo, I., Birch, D.G., Hariri, A.H., Nittala, M.G., Sadda, S., West, S., Scholl, H.P.N., ProgStar Study Group, 2017. Progression of Stargardt disease as determined by fundus autofluorescence in the retrospective progression of Stargardt disease study (ProgStar report No. 9). JAMA Ophthalmol. 135 (11), 1232–1241. https://doi.org/10.1001/jamaophthalmol.2017.4152.

Takase, N., Nozaki, M., Kato, A., Ozeki, H., Yoshida, M., Ogura, Y., 2015. Enlargement of foveal avascular zone in diabetic eyes evaluated by en face optical coherence tomography angiography. Retina 35 (11), 2377–2383. https://doi.org/10.1097/IAE.0000000000000849.

Tan, A.C., Fleckenstein, M., Schmitz-Valckenberg, S., Holz, F.G., 2016. Clinical application of multicolor imaging technology. Ophthalmologica 236 (1), 8–18. https://doi.org/10.1159/000446857.

Tan, B., Sim, R., Chua, J., Wong, D.W.K., Yao, X., Garhöfer, G., Schmidl, D., Werkmeister, R.M., Schmetterer, L., 2020. Approaches to quantify optical coherence tomography angiography metrics. Ann. Transl. Med. 8 (18), 1205. https://doi.org/10.21037/atm-20-3246.

Tao, L.W., Wu, Z., Guymer, R.H., Luu, C.D., 2016. Ellipsoid zone on optical coherence tomography: a review. Clin. Exp. Ophthalmol. 44 (5), 422–430. https://doi.org/10.1111/ceo.12685.

Theelen, T., Berendschot, T.T., Hoyng, C.B., Boon, C.J., Klevering, B.J., 2009. Near-infrared reflectance imaging of neovascular age-related macular degeneration.

Graefes Arch. Clin. Exp. Ophthalmol. 247 (12), 1625–1633. https://doi.org/10.1007/s00417-009-1148-9.

Thorell, M.R., Goldhardt, R., Nunes, R.P., de Amorim Garcia Filho, C.A., Abbey, A.M., Kuriyan, A.E., Modi, Y.S., Gregori, G., Yehoshua, Z., Feuer, W., Sadda, S., Rosenfeld, P.J., 2015. Association between subfoveal choroidal thickness, reticular pseudodrusen, and geographic atrophy in age-related macular degeneration. Ophthalmic Surg. Lasers Imaging Retina 46 (5), 513–521. https://doi.org/10.3928/23258160-20150521-02.

Thulliez, M., Motulsky, E.H., Feuer, W., Gregori, G., Rosenfeld, P.J., 2019. En face imaging of geographic atrophy using different swept-source OCT scan patterns. Ophthalmol Retina 3 (2), 122–132. https://doi.org/10.1016/j.oret.2018.09.004.

Told, R., Sacu, S., Hecht, A., Baratsits, M., Eibenberger, K., Kroh, M.E., Rezar-Dreindl, S., Schlanitz, F.G., Weigert, G., Pollreisz, A., Schmidt-Erfurth, U., 2018. Comparison of SD-optical coherence tomography angiography and indocyanine green angiography in type 1 and 2 neovascular age-related macular degeneration. Invest. Ophthalmol. Vis. Sci. 59 (6), 2393–2400. https://doi.org/10.1167/iovs.17-22902.

Tomba, E., Facco, P., Roso, M., Modesti, M., Bezzo, F., Barolo, M., 2010. Artificial vision system for the automatic measurement of interfiber pore characteristics and fiber diameter distribution in nanofiber assemblies. Ind. Eng. Chem. Res. 49, 2957–2968. https://doi.org/10.1021/ie901179m.

Uji, A., Murakami, T., Nishijima, K., Akagi, T., Horii, T., Arakawa, N., Muraoka, Y., Ellabban, A.A., Yoshimura, N., 2012. Association between hyperreflective foci in the outer retina, status of photoreceptor layer, and visual acuity in diabetic macular edema. Am. J. Ophthalmol. 153 (4), 710–717. https://doi.org/10.1016/j.ajo.2011.08.041, 717.e1.

Vallabh, N.A., Sahni, J.N., Parkes, C.K., Czanner, G., Heimann, H., Damato, B., 2016. Near-infrared reflectance and autofluorescence imaging characteristics of choroidal nevi. Eye 30 (12), 1593–1597. https://doi.org/10.1038/eye.2016.183.

van Velthoven, M.E., Faber, D.J., Verbraak, F.D., van Leeuwen, T.G., de Smet, M.D., 2007. Recent developments in optical coherence tomography for imaging the retina. Prog. Retin. Eye Res. 26 (1), 57–77. https://doi.org/10.1016/j.preteyeres.2006.10.002.

Varga, L., Kovács, A., Grósz, T., Thury, G., Hadarits, F., Dégi, R., Dombi, J., 2019. Automatic segmentation of hyperreflective foci in OCT images. Comput. Methods Progr. Biomed. 178, 91–103. https://doi.org/10.1016/j.cmpb.2019.06.019.E.

Vaz-Pereira, S., Monteiro-Grillo, M., Engelbert, M., 2020. Near-infrared reflectance imaging of neovascularization in proliferative diabetic retinopathy. Int. J. Retina. Vitreous 6 (1), 59. https://doi.org/10.1186/s40942-020-00263-8.

Viola, F., Villani, E., Natacci, F., Selicorni, A., Melloni, G., Vezzola, D., Barteselli, G., Mapelli, C., Pirondini, C., Ratiglia, R., 2012. Choroidal abnormalities detected by near-infrared reflectance imaging as a new diagnostic criterion for neurofibromatosis 1. Ophthalmology 119 (2), 369–375. https://doi.org/10.1016/j.ophtha.2011.07.046.

Wang, K., Jayadev, C., Nittala, M.G., Velaga, S.B., Ramachandra, C.A., Bhaskaranand, M., Bhat, S., Solanki, K., Sadda, S.R., 2018. Automated detection of diabetic retinopathy lesions on ultrawidefield pseudocolour images. Acta Ophthalmol. 96 (2), e168–e173. https://doi.org/10.1111/aos.13528.

Wang, D., Velaga, S.B., Grondin, C., Au, A., Nittala, M., Chhablani, J., Vupparaboina, K. K., Gunnemann, F., Jung, J., Kim, J.H., Ip, M., Sadda, S., Sarraf, D., 2021. Pentosan polysulfate maculopathy: prevalence, spectrum of disease, and choroidal imaging analysis based on prospective screening. Am. J. Ophthalmol. 227, 125–138. https://doi.org/10.1016/j.ajo.2021.02.025.

Webb, R.H., Hughes, G.W., 1981. Scanning laser ophthalmoscope. IEEE Trans. Biomed. Eng. 28 (7), 488–492. https://doi.org/10.1109/TBME.1981.324734.

Wojtkowski, M., Srinivasan, V., Ko, T., Fujimoto, J., Kowalczyk, A., Duker, J., 2004. Ultrahigh-resolution, high-speed, Fourier domain optical coherence tomography and methods for dispersion compensation. Opt Express 12 (11), 2404–2422. https://doi.org/10.1364/opex.12.002404.

Wolf-Schnurrbusch, U.E., Wittwer, V.V., Ghanem, R., Niederhaeuser, M., Enzmann, V., Framme, C., Wolf, S., 2011. Blue-light versus green-light autofluorescence: lesion size of areas of geographic atrophy. Invest. Ophthalmol. Vis. Sci. 52 (13), 9497–9502. https://doi.org/10.1167/iovs.11-8346.

Xu, D., Dávila, J.P., Rahimi, M., Rebhun, C.B., Alibhai, A.Y., Waheed, N.K., Sarraf, D., 2018. Long-term progression of type 1 neovascularization in age-related macular degeneration using optical coherence tomography angiography. Am. J. Ophthalmol. 187, 10–20. https://doi.org/10.1016/j.ajo.2017.12.005.

Xu, X., Yannuzzi, N.A., Fernández-Avellaneda, P., Echegaray, J.J., Tran, K.D., Russell, J. F., Patel, N.A., Hussain, R.M., Sarraf, D., Freund, K.B., 2019. Differentiating veins from arteries on optical coherence tomography angiography by identifying deep capillary plexus vortices. Am. J. Ophthalmol. 207, 363–372. https://doi.org/10.1016/j.ajo.2019.06.009.

Yanni, S.E., Wang, J., Chan, M., 2012. Foveal avascular zone and foveal pit formation after preterm birth. Br. J. Ophthalmol. 96, 961–966. https://doi.org/10.1136/bjophthalmol-2012-301612.

Yung, M., Klufas, M.A., Sarraf, D., 2016. Clinical applications of fundus autofluorescence in retinal disease. Int. J. Retina. Vitreous 2, 12. https://doi.org/10.1186/s40942-016-0035-x.

Yust, B.G., Mimun, L.C., Sardar, D.K., 2012. Optical absorption and scattering of bovine cornea, lens, and retina in the near-infrared region. Laser Med. Sci. 27 (2), 413–422. https://doi.org/10.1007/s10103-011-0927-9.

Zahid, S., Dolz-Marco, R., Freund, K.B., Balaratnasingam, C., Dansingani, K., Gilani, F., Mehta, N., Young, E., Klifto, M.R., Chae, B., Yannuzzi, L.A., Young, J.A., 2016. Fractal dimensional analysis of optical coherence tomography angiography in eyes with diabetic retinopathy. Invest. Ophthalmol. Vis. Sci. 57 (11), 4940–4947. https://doi.org/10.1167/iovs.16-19656.

Zhang, M., Hwang, T.S., Campbell, J.P., Bailey, S.T., Wilson, D.J., Huang, D., Jia, Y., 2016. Projection-resolved optical coherence tomographic angiography. Biomed. Opt Express 7 (3), 816–828. https://doi.org/10.1364/BOE.7.000816.

Zhang, J., Yu, Z., Liu, L., 2015. Multimodality imaging in diagnosing polypoidal choroidal vasculopathy. Optom. Vis. Sci. 92 (1), e21–e26. https://doi.org/10.1097/OPX.0000000000000440.

Zhang, Q., Zheng, F., Motulsky, E.H., Gregori, G., Chu, Z., Chen, C.L., Li, C., de Sisternes, L., Durbin, M., Rosenfeld, P.J., Wang, R.K., 2018. A novel strategy for quantifying choriocapillaris flow voids using swept-source OCT angiography. Invest. Ophthalmol. Vis. Sci. 59 (1), 203–211. https://doi.org/10.1167/iovs.17-22953.